THE EFFECTS OF EMBEDDED PIEZOELECTRIC LAYERS IN COMPOSITE CYLINDERS AND APPLICATIONS

by

John Anthony Mitchell

Thesis submitted to the Faculty of the

Virginia Polytechnic Institute and State University

in partial fulfillment of the requirements

for the degree of

Master of Science

in

Engineering Science and Mechanics

APPROVED

Dr. S. L. Hendricks, Co – Chairperson

Dr. J.N.Reddy, Co – Chairperson

Dr. W. T. Baumann

July 1992

Blacksburg, Virginia

ABSTRACT

An elasticity solution is presented for the static equlibrium equations of an axisymmetric composite cylinder under loadings due to embedded piezoelectric laminae. The solution is used to study both uniform and non-uniform distributions of the piezoelectric effect and results are verified using the finite element method. A cylindrical truss element actuator is developed based upon this analysis and shown to be useful in damping vibrations of truss type structures. It has also been shown that by varying the distribution of the piezoelectric effect spatially, modal actuators capable of actuating specific modes of axial vibrations in a bar can be developed. Finally, the effects of a piezoelectric patch have been investigated. The axial forces generated at the fixed ends of a cylinder are demonstrated to be proportional to the length of patch.

Acknowledgements

I would like to express my appreciation to all those people who have given support to me during my stay at Virginia Tech. These people include students working on the 3rd floor of Femoyer, all students working under Dr. Reddy, and students with whom I studied during course work. The time and effort given by Vanessa in typing this thesis is also greatly appreciated. Thanks also go to my committee members J. N. Reddy, S. L. Hendricks, and W. T. Baumann for their support and efforts on behalf of my thesis. Special thanks go to my personal friends Bala and Sundari and my fiancee Minoti for all of their encouraging support. Finally, thanks to to the people who made this thesis possible, my parents Charles and Carole.

TABLE OF CONTENTS

List of Illustrations

CHAPTER 1

Introduction

1.1 Outline

The individual topics discussed in this thesis are piezoelectricity, elasticity, and vibrations. When taken together, these topics form a new field of study called "smart structures." This is the subject matter for this thesis.

The outline for this thesis is as follows. Chapter 2 presents the basic concepts associated with piezoelectricity and elasticity. A historical note is given on the discovery and first applications of the piezoelectric effect. The so called direct and converse effects of piezoelectric materials is described and a combined linear electromechanical constitutive relationship is given relating stresses, strains and electric effects. This relationship looks very similar to Hooke's law for linear elastic solids. Then the material in Chapter 2 focuses on a particular type of material which exhibits the piezoelectric effect, namely polyvinylidene fluoride (PVDF) a polymer based material. PVDF requires special pre-processing called polarization and this is briefly described. Finally, Chapter 2 points out that the piezoelectric effect is described using a third order tensor, the components of which have some physical meanings which may be described qualitatively.

Based upon the concepts given in Chapter 2, two analytical tools are developed in Chapter 3 to study the effects of embedded PVDF laminae in an axisymmetric composite cylinder. An elasticity solution is presented for the static equilibrium equations and verified using the finite element method. These tools are used to

develop a cylindrical truss element actuator to damp vibrations of a truss type structure. Damping is introduced based upon the knowledge that as the truss deforms members experience a change in length. Fanson and Garba Ref. [17] have proposed damping for truss type structures based upon the same concept but diffferent actuator design. Another application is developed by shaping the piezoelectric effect spatially such that specific modes of axial vibrations for a cylindrical rod may be exclusively excited. Modal actuators as they are called, were presented for plates and beams by Lee and Moon Ref. [8]. Chapter 3 ends with an investigation of the effects of a piezoelectric patch. This topic has been investigated by Crawley and Luis Ref. [22]. They presented an elasticity solution based on the assumption of pure one dimensional shear in bonding layers, used to attach the piezoelectric material to the substructures, and pure extensional strains in the piezoelectric layers. The elasticity solution presented here differs in several respects. First, there are no assumptions on stresses and strains and the solution may be used to model both bonding and piezoelectric layers including shear deformations. Second, the patch in this study is not exactly the same type of patch considered by Crawley and Luis. In the present study the piezoelectric effect is induced in a lamina over a finite area, or like a patch, by varying the polarization profile of the particular piezoelectric layer. Crawley and Luis modeled a piezoelectric layer of finite length bonded to a substructure with the piezoelectric effect uniformly distributed over the patch of piezoelectric. The polarization patch is the last topic discussed in Chapter 3.

Chapter 4 presents a realistic application for the cylindrical truss element actuator. Equations of motion for a truss, being maneuvered much like a truss in space might be, are derived. These maneuvers generate realistic loads and the cylindrical truss element actuator is applied to dampen the associated vibrations. The results may be used to find the optimal placement of such an actuator and indicate that active damping is very effective in reducing the maximum amplitude of transient vibrations.

CHAPTER 2

Piezoelectricity and Elasticity Concepts

2.1 Introduction

There have been many articles written on the use of piezoelectric materials since the discovery of the piezoelectric effect in 1880 by the Curie brothers.[1] They found that by applying pressure to certain types of crystals, an electrification was induced. This relation between pressure and electrification is called the piezoelectric effect. Quartz crystal was one of the first materials discovered to exhibit this behavior. Just prior to World War I, the first sonar device used to sense water depth was developed. By applying a wave of electrical impulses to a piezoelectric quartz crystal, a series of acoustical waves were generated. These waves began at the surface, traveled to and reflected off the ocean floor. The time lapse between wave generation and return was used to calculate the depth of water.

Since then, a new class of materials called ferroelectrics, which exhibit the piezoelectric effect have been developed. Ferroelectrics are more sensitive to electric fields and have a higher electromechanical coupling than a piezoelectric crystal such as quartz.[1] One such ferroelectric is lead zirconate titanate (PZT). This material is in the form of a ceramic and is used as point sensors/actuators or receivers/transmitters. In mechanics, patches of PZT are placed on flexible structures and information such as strain and strain rate are derived based upon the piezoelectric effect for these specific points. One of the most recent advancements in piezoelectricity is the discovery of

the piezoelectric effect in a polymer based material called polyvinylidene fluoride (PVDF).[2] Compared to other materials, PVDF is flexible, rugged, available in thin sheets and easily manufactured in large quantities and at low cost.[3] For these reasons, PVDF is currently being studied for use as distributed sensors/actuators in flexible structures.

The remaining portion of this chapter is devoted to defining terms and equations necessary for an application of piezoelectric materials as sensors/actuators in flexible structures. The second section is a review of Hooke's law and the third section is an introduction to the piezoelectric constitutive equations and associated terminology. The discussion is primarily focused towards the use of PVDF although many of the concepts are applicable to other material types as well.

2.2 Hooke's Law

In this section, constitutive relations relating stresses and strains for a linear elastic solid are given. Since the quantities involved are tensors, the transformation laws for tensors of order three and four are also given. It will become necessary to use this information later on in this and the following chapters.

Solids which have stresses that are linearly related to strains are called linear elastic solids and for materials considered here, it is assumed that this is the case. The relation between stress and strain components, known as generalized Hooke's law,[4] is given by

$$\sigma_{ij} = C_{ijk\ell}\epsilon_{k\ell} \tag{2.1}$$

where $C_{ijk\ell}$ are constants and σ_{ij} and $\epsilon_{k\ell}$ are stresses and strains respectively.

In the actual application of Hooke's law, a simplified notation is used. Since σ_{ij} and ϵ_{ij} are known to be symmetric in i and j, the following matrix relation[5] may be used

$$\sigma = C\epsilon \tag{2.2}$$

where σ and ϵ are (6×1) column vectors of stresses and strains respectively and C is a (6×6) elastic stiffness matrix derived from $C_{ijk\ell}$.

To make use of this equation all the quantities involved must be referred to a common coordinate system. However, in most cases, the constants of proportionality $C_{ijk\ell}$ are given in terms of a set of material axes. Typically these axes do not coincide with the global coordinate system being used in the particular problem and therefore a relation between stresses and strains in a coordinate system different from the material axes is required. As stresses and strains are tensors it follows that $C_{ijk\ell}$ is also a tensor and therefore transforms according to the following transformation law for a fourth order tensor:[4]

$$C'_{mnop} = a_{mi}a_{nj}a_{ok}a_{p\ell}C_{ijk\ell} \tag{2.3}$$

where a_{ij} is the cosine of the angle between the ith primed axis and the jth unprimed axis and $C'_{ijk\ell}$ becomes the constants of proportionality referred to the primed coordinate system. Later in this chapter, it will also become necessary to use the following transformation law for a third order tensor d_{ijk}

$$d'_{mno} = a_{mi}a_{nj}a_{ok}d_{ijk} \tag{2.4}$$

2.3 Piezoelectric Concepts

It is the purpose of this section to review the basic concepts of piezoelectricity so that it is possible to apply piezoelectric materials to the control of flexible structures. There are a number of subsections which describe particular concepts, the last of which focuses on PVDF in particular.

2.3.1 Direct and Converse Effects

The reason that it is possible to sense and control the vibrations of a flexible structure using piezoelectric materials follows from the direct and converse effects. These two phenomena follow from the physical properties of a crystal[6] and can be described using familiar elasticity concepts with the addition of an electrical component. The governing relations that follow are termed the electromechanical constitutive relations.

The direct piezoelectric effect can be best described as "polarization is proportional to applied stress." This definition is easily visualized through a special example.[6] In this case, a piezoelectric material is subjected to a state of uniaxial stress as in Figure 2.1. Due to the direct effect, the material is polarized, meaning that there is charge built up on the specimen, in much the same way as charge is stored in a capacitor. The polarization is represented by D called the electric displacement and the constant of proportionality and applied stress by d and σ respectively. The direct effect is expressed mathematically as

$$D = d\sigma \tag{2.5}$$

Upon inspection of this equation and based on the knowledge that D and σ are

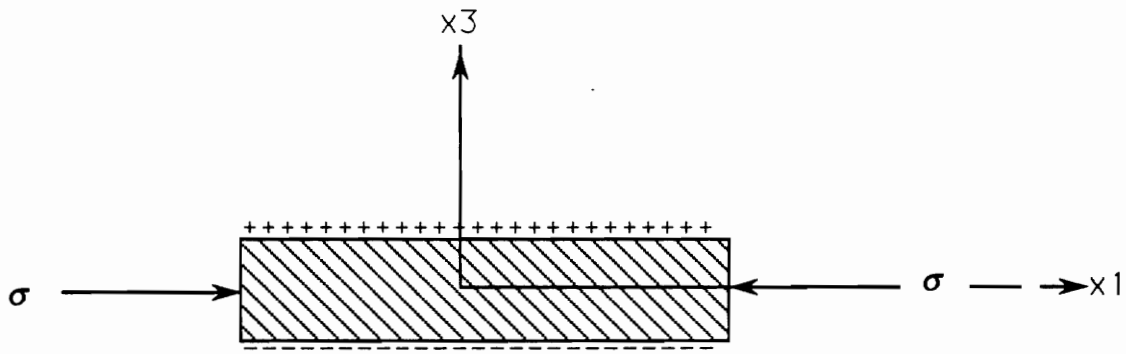

Figure 2.1 Direct Effect

components of first and second order tensors respectively, d is taken as a component of a third order tensor. Stated more precisely, the first order tensor D_i is linearly related to a second order tensor σ_{ij} through a third order tensor d_{ijk} called the piezoelectric tensor.

The reasoning used to describe the direct effect may be applied to the converse effect. In words, the converse effect may be stated as "a change in shape of the piezoelectric is proportional to applied electric field." In this case, the polarization is applied and if the material is unrestrained, deformations will occur. As in the direct effect, the constant of proportionality is the piezoelectric tensor d_{ijk}. The converse effect may be written down in the form of an equation

$$\epsilon_{ij} = d_{ijk} E_k \tag{2.6}$$

where E_k is the kth component of the applied electric field and ϵ_{ij} is the strain tensor representation.

2.3.2 Piezoelectric Tensor

As stated previously, the quantity which linearly relates stresses and strains to polarization in a piezoelectric is the piezoelectric tensor d_{ijk}. As d_{ijk} is a tensor, the components depend upon the coordinate system to which they are referred. Using standard tensor notation, d_{ijk} may be represented in any primed coordinate system through the transformation given in Eq. (2.4). d_{ijk} is a third order tensor and therefore it has $3^3 = 27$ components. However, because of symmetry in j and k, there are only 18 unique components.[6] For this reason the piezoelectric tensor is

often written in matrix notation.

$$[d] = \begin{bmatrix} d_{11} & d_{12} & d_{13} & d_{14} & d_{15} & d_{16} \\ d_{21} & d_{22} & d_{23} & d_{24} & d_{25} & d_{26} \\ d_{31} & d_{32} & d_{33} & d_{34} & d_{35} & d_{36} \end{bmatrix} \tag{2.7}$$

Of course, in this form, the transformation described in Eq. (2.4) may not be directly applied.

2.3.3 Units

To obtain some physical insight into the direct and converse effect, a study of the physical quantities involved is useful. Table 2.1 lists the description and units of these quantities.

2.3.4 Combined Linear Electromechanical Constitutive Relation

In a typical application of piezoelectric materials for control of flexible structures, there is both mechanical as well as electrical loading on the material. Therefore a constitutive relation which incorporates both of these effects is used. This principle is derived based upon the laws of thermodynamics.[6] However, upon inspection, the relation looks like a superposition of the mechanical and electrical effects. In the case of the converse effect, the combined relation is written as

$$\sigma = c^E \epsilon - (dc^E)^T E \tag{2.8}$$

where c^E represents the elastic stiffness matrix with the superscript indicating that the electric field E is held constant. The other variables, ϵ, σ and d are strains, stresses and the components of the piezoelectric tensor in matrix notation. The superscript T indicates matrix transpose.

If the second term on the right hand side of Eq. 2.8 is dropped, the equation reduces to Hooke's law which was given in Section 2.2.

TABLE 2.1

Quantity	Description	Units
E_i	Electric Field	$\frac{volt}{length}$
D_i	Electric Displacement	$\frac{Coulomb}{area}$
σ_{ij}	Stress Tensor	$\frac{force}{area}$
ϵ_{ij}	Strain Tensor	unity
d_{ijk}	Piezoelectric Tensor	$\frac{Coulomb}{force} = \frac{length}{volt}$

2.4 Polyvinylidene Fluoride (PVDF)

At the beginning of this chapter, PVDF was mentioned as a material which exhibits the piezoelectric effect and which has seen some applications in published articles for the control of flexible structures.[7,8,9] However, before actual use is possible, PVDF must be polarized. This process consists of five steps:[3]

1) Uniaxial or biaxial stretching to improve mechanical and electrical properties
2) Annealing at approximately 120° to heal damages due to stretching
3) Application of electrode
4) Application of an electric field of 500-800 kV/cm at $90°C$ to $110°C$ for an hour
5) Cooling under the effect of an electric field

Physical insight into the piezoelectric tensor may be obtained by understanding poling direction. In Figure 2.2 a sample is in stages (4) and (5) of the poling process and poling direction is indicated by the arrows in the diagram. PVDF is classified in terms of crystal structures as class MM2.[6] For this class, the piezoelectric tensors expressed in matrix notation is given as

$$[d] = \begin{bmatrix} 0 & 0 & 0 & 0 & d_{15} & 0 \\ 0 & 0 & 0 & d_{24} & 0 & 0 \\ d_{31} & d_{32} & d_{33} & 0 & 0 & 0 \end{bmatrix} \tag{2.9}$$

The physical interpretation for the components of this tensor is given as follows: d_{31} and d_{32} represent the charge per unit area induced in the x_3-direction due to a uniaxial stress in the x_1 and x_2 directions respectively. Based upon the direct effect and assuming that d_{31} and d_{32} are positive, charge will accumulate in the sense of poling for stresses applied in the positive sense. In Figure 2.1, the sample is subjected to a state of uniaxial stress σ_1. Therefore for $d_{31} > 0$, charge will accumulate as

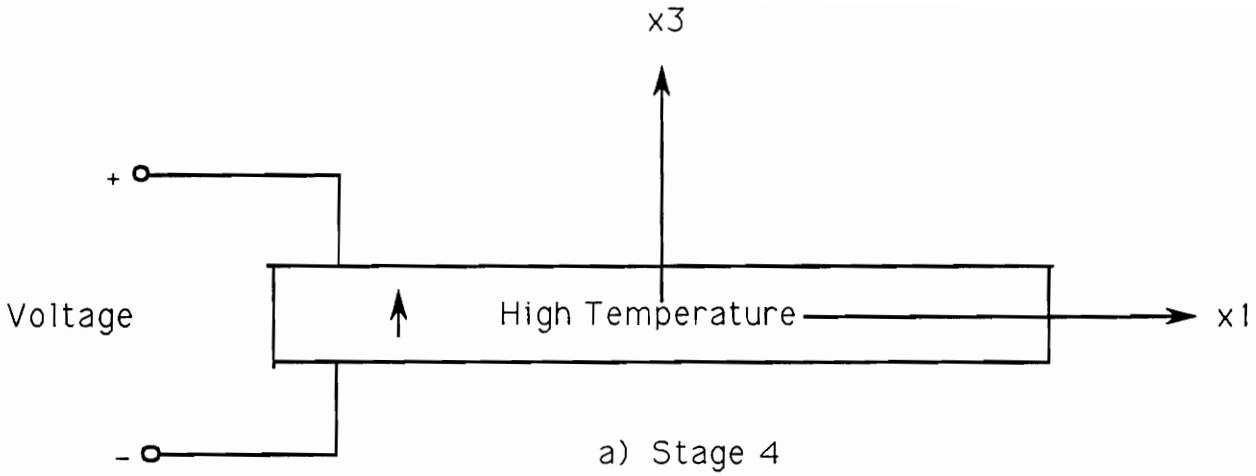

a) Stage 4

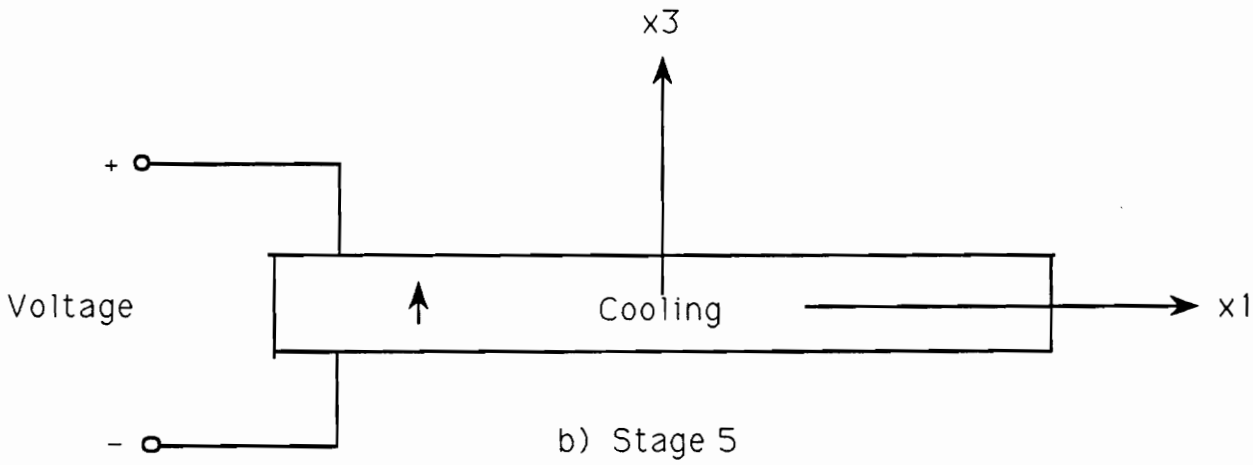

b) Stage 5

Figure 2. 2 Poling Direction

indicated. Alternatively, if d_{33} is negative, charge will accumulate in a sense opposite to the poling direction for a stress σ_3 applied in the positive sense.

Actual values of d_{ijk} for PVDF are determined by experimental methods and they depend strongly on stretch ratio and poling conditions.[3] Table 2.2 lists d_{31}, d_{32} and d_{33} for uniaxially and biaxially stretched films.[10] For both types of film, d_{31} and d_{32} are positive and d_{33} is negative. Based upon the sign of these moduli, the direction of polarization is described using the direct effect. Similarly, it is useful to describe them using the converse effect. Since d_{33} is negative, an application of an electric field in the x_3 direction will cause the film to become thinner.

In addition to d_{ijk}, the elastic moduli for PVDF are also found by experiment. Prior to poling, PVDF is considered to be transversely isotropic in the $x_3 - x_2$ plane, shown in Figure 2.3, and after poling the values change very little. However, some films studied[10] have been shown to be very nearly isotropic in the $x_1 - x_2$ plane as well. For this study, PVDF is assumed to be isotropic. The elastic moduli are given in Table 2.2.[10] Values left blank are not given in the literature.

As mentioned earlier, the polarization process is necessary to induce the piezoelectric effect. This technique may also be used to spatially vary the polarization profile.[8] The profile may be varied in two ways. The first is by applying electrode to portions of the film. Then in stages (4) and (5) of the process only those parts of the film which have electrode become polarized. The second approach is a variation in poling direction. Some portions may have an electric field applied in one direction while others in the opposite direction. Of course, this is only possible by making each

TABLE 2.2 PROPERTIES OF PVDF

Piezoelectric Moduli	Biaxially Stretched Film	Piezo Film
	$10^{12}(C/N)$	$10^{-12}(C/N)$
d_{31}	4.34	21.4
d_{32}	4.36	2.3
d_{33}	-13.5	-31.5

Elastic Material Properties	Values
E_1	$2.5 \times 10^9 Pa$
E_2	$2.5 \times 10^9 Pa$
E_3	
G_{12}	$.898 \times 10^6 Pa$
G_{13}	
G_{23}	
ν_{12}	.392
ν_{13}	
ν_{23}	

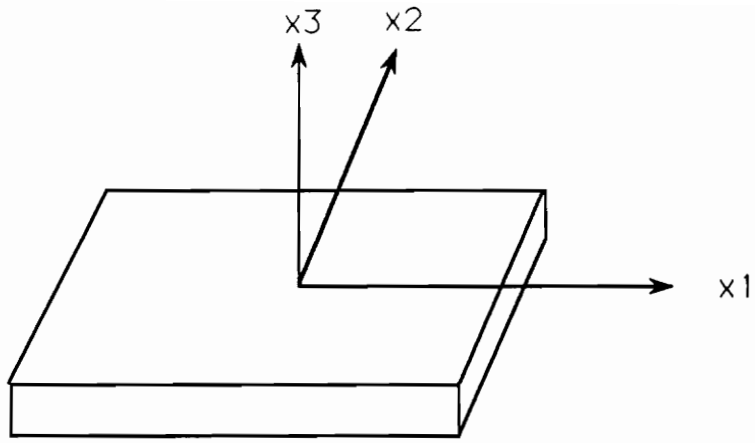

Figure 2.3 Coordinate System for sheet of PVDF

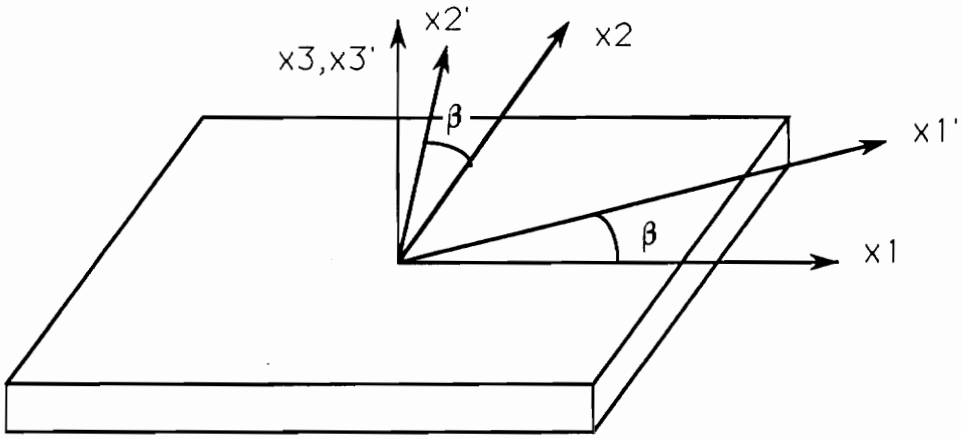

Figure 2.4 Material Coordinate System

electrode electrically disconnected. By varying the polarization profile of the film, it is possible to design spatial modal filters and actuators which can sense or actuate specific modes of a flexible structure.[8]

The final topic for this sub-section is the constitutive relation for PVDF. Using Eq. (2.8) and the form of the piezoelectric tensor for PVDF given in Eq. (2.9), the stress and strain components that PVDF is capable of inducing can be determined. This is possible by expanding the second term on the right hand side of Eq. (2.8). In Figure 2.4, the coordinate system for the film is given where β represents the angle in the $x_1 - x_2$ plane that the material axes make with global coordinates x_1, x_2, x_3. Assuming β is zero, the term $(dc)^T E$ is written as

$$(dc)^T E = \begin{bmatrix} 0 & 0 & H_1 \\ 0 & 0 & H_2 \\ 0 & 0 & H_3 \\ 0 & C_{44}d_{24} & 0 \\ d_{15}C_{55} & 0 & 0 \\ 0 & 0 & 0 \end{bmatrix} \begin{bmatrix} E_1 \\ E_2 \\ E_3 \end{bmatrix} \tag{2.10}$$

where

$$H_1 = d_{31}C_{11} + d_{32}C_{12} + d_{33}C_{13}$$

$$H_2 = d_{31}C_{12} + d_{32}C_{22} + d_{33}C_{23}$$

$$H_3 = d_{31}C_{13} + d_{32}C_{23} + d_{33}C_{33}$$

As previously described, the film is polarized and thus prepared for application of an electric field in the thickness direction. Therefore, the only applicable component of electric field is E_3. Based upon this, it is seen that only normal strains or stresses are induced when the material axes coincide with the global coordinates. In the more general case, when β is not equal to zero, it is possible to induce shear. Using

equation (2.4) components of the piezoelectric tensor may be computed for any angle β. For PVDF, d_{24} and d_{15} are invariant under this transformation, however, the transformation does introduce d_{36}. Figure 2.5 gives the variation of these components with respect to β. In addition to the variation in d_{ijk}, the elastic moduli also change under this transformation if the material is not isotropic. However, for both the isotropic and orthotropic cases, only ϵ_{12} or σ_{12} is induced for application of an electric field in the x_3-direction when β is not zero. For a stress free sample of PVDF, Figure 2.6 indicates the mode of shear strain introduced in this case.

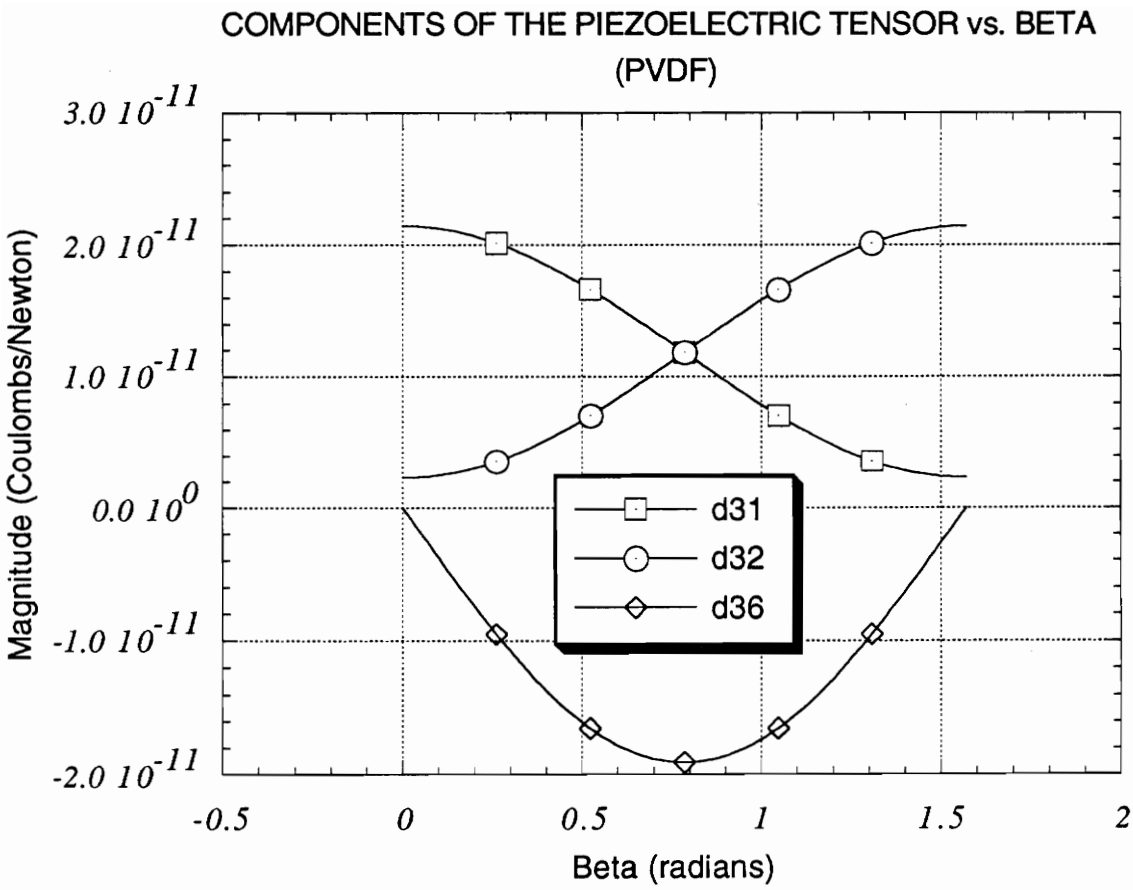
COMPONENTS OF THE PIEZOELECTRIC TENSOR vs. BETA
(PVDF)
3.0 10^-11
2.0 10^-11
1.0 10^-11
0.0 10^0
-1.0 10^-11
-2.0 10^-11
Magnitude (Coulombs/Newton)
-0.5
0
0.5
1
1.5
2
Beta (radians)
d31
d32
d36

Figure 2.5

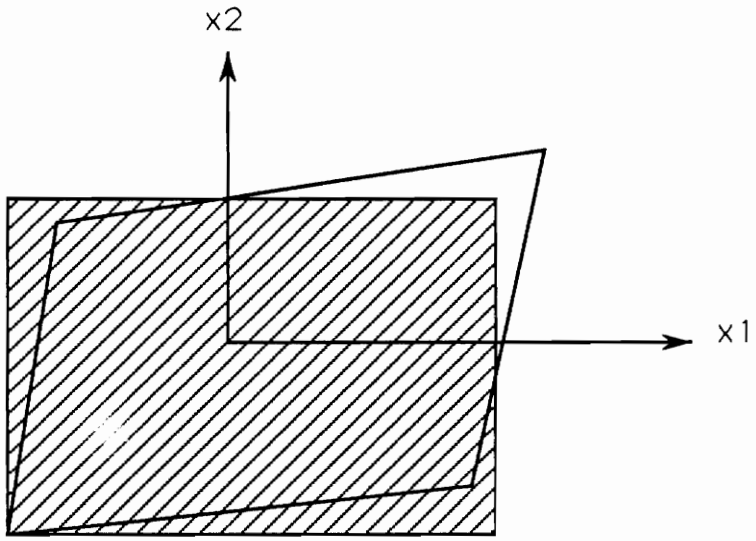

Figure 2.6 Shear Strain due to Piezoelectric Effect (beta = 0)

CHAPTER 3

Elasticity Solution and Actuator Models

3.1 Introduction

In this chapter, a static analysis of an axisymmetric composite cylinder under the action of loads generated by embedded piezoelectric layers is given. PVDF, being available in thin sheets, is particularly suitable for introduction into laminated type structures as an embedded actuator. Therefore, the model is developed based upon a laminate construction built up with composite cross-ply type material layers and PVDF layers. Various polarization profiles are studied via an analytical solution and the Finite Element Method (FEM). One such profile is developed to produce a modal actuator for axial vibrations of a bar. Another actuator is proposed for use in vibration control of a truss structure.

3.2 Equilibrium Equations

The cylinder analyzed in this study is taken to be axisymmetric and therefore the static equilibrium equations [12] are

$$\frac{\partial \sigma_r}{\partial r} + \frac{\partial \sigma_{rz}}{\partial z} + \frac{\sigma_r - \sigma_\theta}{r} = 0 \tag{3.1a}$$

$$\frac{\partial \sigma_{rz}}{\partial r} + \frac{\partial \sigma_z}{\partial z} + \frac{\sigma_{rz}}{r} = 0. \tag{3.1b}$$

The coordinate system associated with these equations is given in Figure 3.1. For the case of an axisymmetric and orthotropic piezoelectric cylinder where the material axes are coincident or at a 90° angle with the cylinder axes, the constitutive relation

from Eqs. (2.8) and (2.10) is

$$\begin{Bmatrix} \sigma_z \\ \sigma_\theta \\ \sigma_r \\ \sigma_{rz} \end{Bmatrix} = \begin{bmatrix} c_{11} & c_{12} & c_{13} & 0 \\ c_{12} & c_{22} & c_{23} & 0 \\ c_{13} & c_{23} & c_{33} & 0 \\ 0 & 0 & 0 & c_{55} \end{bmatrix} \begin{Bmatrix} \epsilon_z \\ \epsilon_\theta \\ \epsilon_r \\ \epsilon_{rz} \end{Bmatrix} + \begin{Bmatrix} H_z \\ H_\theta \\ H_r \\ 0 \end{Bmatrix} E_r \tag{3.2}$$

where

$$\epsilon_z = \frac{\partial w}{\partial z}$$

$$\epsilon_\theta = \frac{u}{r}$$

$$\epsilon_r = \frac{\partial u}{\partial r}$$

$$\epsilon_{rz} = \frac{\partial u}{\partial z} + \frac{\partial w}{\partial r}.$$

Due to the axisymmetry assumption and the fact that this is a specially orthotropic cylinder, the shearing strains and stresses $\epsilon_{r\theta}$, $\epsilon_{z\theta}$, $\sigma_{r\theta}$, and $\sigma_{z\theta}$ are zero.[12] E_r, u and w are the electric field applied in the radial direction, and radial and axial displacements respectively. As mentioned in Section 2.4, if the material axes are not oriented along the axes of the cylinder, the piezoelectric effect induces shearing strains. In this case, it becomes possible to actuate a torsional effect on the cylinder although this is not considered here.

Substituting the constitutive relations (3.2) into Eqs. (3.1), the equilibrium equations expressed in terms of displacements become

$$\begin{aligned} r^2\frac{\partial^2 u}{\partial r^2} + r\frac{\partial u}{\partial r} - \frac{c_{22}}{c_{33}}u + \frac{c_{55}}{c_{33}}r^2\frac{\partial^2 u}{\partial z^2} \\ + \left(\frac{c_{13}+c_{55}}{c_{33}}\right) r^2\frac{\partial^2 w}{\partial r \partial z} + \left(\frac{c_{13}-c_{12}}{c_{33}}\right) r\frac{\partial w}{\partial z} = \left(\frac{H_r - H_\theta}{c_{33}}\right) rE_r \end{aligned} \tag{3.3a}$$

$$\begin{aligned} r\frac{\partial^2 w}{\partial r^2} + \frac{\partial w}{\partial r} + \frac{c_{11}}{c_{55}}r\frac{\partial^2 w}{\partial z^2} + \left(\frac{c_{13}+c_{55}}{c_{55}}\right) r\frac{\partial^2 u}{\partial z \partial r} \\ + \left(\frac{c_{12}+c_{55}}{c_{55}}\right)\frac{\partial u}{\partial z} = \frac{H_z}{c_{55}} r\frac{\partial E_r}{\partial z} \end{aligned} \tag{3.3b}$$

For these equations, it is assumed that the electric field does not vary in the thickness direction r, but may vary in the axial direction z. This variation in the electric field is created in the polarization process as discussed in Section 2.4.

3.3 Composite Cylinder and Boundary Conditions

The cylinder to be analyzed is hollow and composed of n material layers. A cross section is depicted in Figure 3.2. The solution for this problem is found by solving the equilibrium Eqs. (3.1) for each material layer and coupling each layer to adjacent layers through common boundaries. For the analysis, it is assumed that each layer is perfectly bonded to adjacent layers. The boundary conditions and polarization profile for this problem dictate the form of the solution that is obtained, and it is easy to set up cases for which there is no analytical solution. Then it becomes necessary to use computational methods such as the Finite Element Method (FEM) to obtain solutions.

There are two different boundary conditions for this problem, namely, interlaminae and end conditions. The first boundary condition is found by requiring continuity of stresses and displacements through the thickness of the laminate. Continuity of displacements follows directly from the perfectly bonded laminate assumption, whereas continuity of stresses is an equilibrium condition. The second set of boundary conditions are those applied at the ends and these are presented in the next section.

For the kth interface, the interlaminae boundary conditions are

$$u^k|_{r=r_k} = u^{k+1}|_{r=r_k} \tag{3.4a}$$

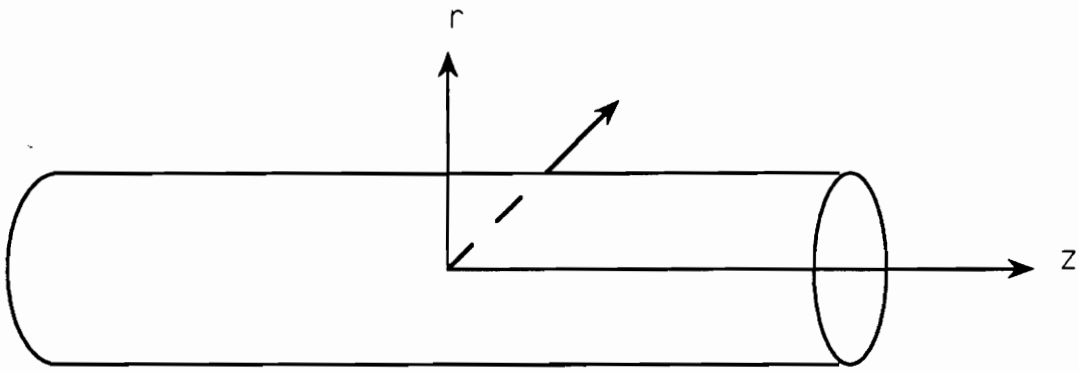

Figure 3.1 Cylindrical Coordinate System

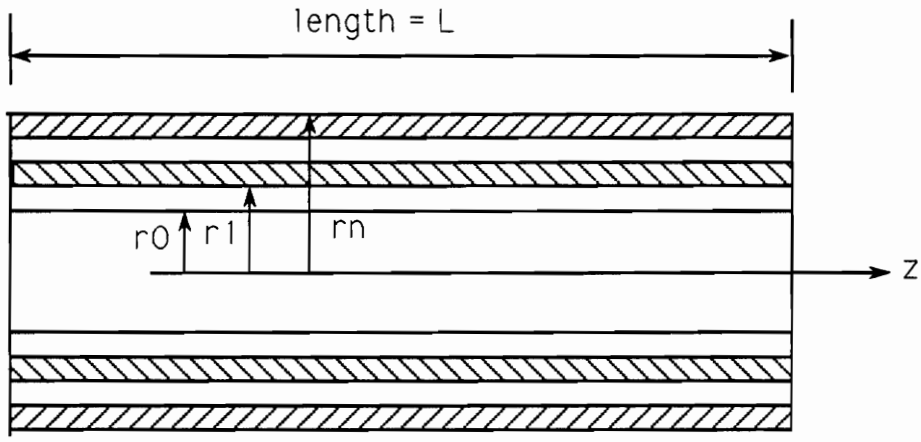

Figure 3.2 Composite Cylinder

$$\omega^k|_{r=r_k} = \omega^{k+1}|_{r=r_k} \tag{3.4b}$$

$$\sigma_r^k|_{r=r_k} = \sigma_r^{k+1}|_{r=r_k} \tag{3.4c}$$

$$\sigma_{rz}^k|_{r=r_k} = \sigma_{rz}^{k+1}|_{r=r_k} \tag{3.4d}$$

$$k = 1, 2, ..., n-1$$

where the superscript k refers to the particular layer and r_k is the radial position of the interface. In addition to this, inner and outer surface tractions are assumed to be homogeneous.

$$\sigma_r^n|_{r=r_n} = 0 \tag{3.5a}$$

$$\sigma_{rz}^n|_{r=r_n} = 0 \tag{3.5b}$$

$$\sigma_r^1|_{r=r_o} = 0 \tag{3.5c}$$

$$\sigma_{rz}^1|_{r=r_o} = 0 \tag{3.5d}$$

3.4 Analytical Solution

Finding an analytical solution to Eqs. (3.1) or (3.3) is a formidable task and is only possible for special loadings and boundary conditions. To this end, the cylinder is taken to be symmetric about the $r-\theta$ plane at $z = 0$. The ends of the cylinder are assumed to be free of shear stress and fixed or have uniform displacement in the z-direction. The end conditions for the composite cylinder are expressed mathematically as

$$\omega^k|_{z=0} = 0 \tag{3.6a}$$

$$\frac{\partial u^k}{\partial z}|_{z=0} = 0 \tag{3.6b}$$

$$\sigma^k_{rz}|_{z=\frac{\ell}{2}} = 0 \tag{3.6c}$$

$$\omega^k|_{z=\frac{\ell}{2}} = z_o \tag{3.6d}$$

where z_o is the applied uniform displacement at the end. Loads are due to the piezoelectric layers and appear on the right hand side of Eqs. (3.3) as body forces. E_r, the polarization profile, can be taken to be uniform or varying with z. For the latter case, it must be possible to express E_r in a Fourier cosine series.

Solutions are taken for u and ω in the following form

$$u(r,z) = \sum_{i=1}^{N} g_i(r) cos\lambda_i z \tag{3.7a}$$

$$\omega(r,z) = \sum_{i=1}^{N} f_i(r) sin\lambda_i z \tag{3.7b}$$

These equations satisfy homogeneous boundary conditions in Eqs. (3.6) if

$$\lambda_i = \frac{2i\pi}{\ell} \tag{3.8}$$

The uniform displacement of the end can be superimposed with the solution for the homogeneous boundary conditions. Substituting Eqs. (3.7) into Eqs. (3.3), and assuming that E_r can be written

$$E_r = \frac{A_o}{2} + \sum_{i=1}^{N} A_i \cos(\lambda_i z) \tag{3.9}$$

then the effect of r and z may be separated out by matching Fourier coefficients of the right hand side with the left hand side of Eqs. (3.3). In doing so, two coupled,

second order, ordinary differential equations in r are left to solve corresponding to the ith term in the Fourier series. These equations are

$$r^2 g'' + rg' - \left[p_1 r^2 + p_2\right] g + p_3 r^2 f' + p_4 r f = H_1 r \tag{3.10a}$$

$$r f'' + f' - p_5 r f - p_6 r g' - p_7 g = H_2 r \tag{3.10b}$$

where

$$p_1 = \frac{c_{55}}{c_{33}}\lambda_i^2 \qquad p_3 = \left(\frac{c_{13} + c_{55}}{c_{33}}\right)\lambda_i$$

$$p_2 = \frac{c_{22}}{c_{33}} \qquad p_4 = \left(\frac{c_{13} - c_{12}}{c_{33}}\right)\lambda_i$$

$$p_5 = \frac{c_{11}}{c_{55}}\lambda_i^2 \qquad p_6 = \left(\frac{c_{13} + c_{55}}{c_{55}}\right)\lambda_i$$

$$p_7 = \left(\frac{c_{12} + c_{55}}{c_{55}}\right)\lambda_i$$

$$H_1 = \left(\frac{H_r - H_\theta}{c_{33}}\right)A_i \qquad H_2 = \frac{-H_z \lambda_i A_i}{c_{55}}$$

A solution to these equations can be found using methods in power series,[13] including both the homogeneous and nonhomogeneous solutions. However, before proceeding it is necessary to consider boundary conditions.

The solution for a given problem is found by solving Eqs. (3.10) for each layer and then coupling layers through common boundaries. Therefore it is convenient to look for solutions for each layer in the form of power series expanding about one of its boundaries. Therefore, solutions for the homogeneous equations are taken as

$$f(r) = \sum_{n=0}^{\infty} a_n (r - r_o)^n \tag{3.11a}$$

$$g(r) = \sum_{n=0}^{\infty} b_n (r - r_o)^n \tag{3.11b}$$

where r_o is the inner radius of a particular layer. Before substituting Eqs. (3.11) into (3.10), a change of variables is necessary. Let

$$R = r - r_o \tag{3.12}$$

then

$$\frac{df}{dr} = \frac{df}{dR}\frac{dR}{dr} = \frac{df}{dR} \tag{3.13a}$$

$$\frac{d^2 f}{dr^2} = \frac{d}{dR}\left(\frac{df}{dR}\right)\frac{dR}{dr} = \frac{d^2 f}{dR^2} \tag{3.13b}$$

Derivatives with respect to g transform identically to those for f.

To proceed, the non-constant coefficients in (3.10) must be expressed as

$$r = R + r_o \tag{3.14a}$$

$$r^2 = R^2 + 2r_oR + r_o^2 \tag{3.14b}$$

Then, using Eqs. (3.13) and (3.14), Eqs. (3.10) become

$$\begin{aligned}\left[R^2 + 2r_oR + r_o^2\right]g'' + \left[R + r_o\right]g' - \left[p_1\left(R^2 + 2r_oR + r_o^2\right) + p_2\right]g \\ + p_3\left[R^2 + 2r_oR + r_o^2\right]f' + p_4\left[R + r_o\right]f \\ = H_1R + H_1r_o\end{aligned} \tag{3.15a}$$

$$\left(R + r_o\right)f'' + f' - p_5\left(R + r_o\right)f - p_6\left(R + r_o\right)g' - p_7g = H_2R + H_2r_o \tag{3.15b}$$

Finally, Eqs. (3.11) can be substituted into Eqs. (3.15). However, because of the obvious algebra associated with this step, a discussion and final result will be presented.

After substitution, the procedure is to find values for a_n and b_n by setting coefficients of powers R^n to zero so that the equations are satisfied. However, because

of the coupled nature of these equations it is necessary to alternate between the equations satisfying each successively. Because these are second order equations there are four arbitrary constants a_o, a_1, b_o, and b_1. These are non-zero unknowns, and the remaining coefficient a_n and b_n for $n \geq 2$ are expressed in terms of these. For example, substituting Eqs. (3.11) into Eq. (3.15a), and considering powers R^o,

$$b_2 = \frac{\left(p_2 + p_1 r_o^2\right) b_o - r_o b_1 - p_4 r_o a_o - p_3 r_o^2 a_1}{2r_o^2} \tag{3.16}$$

Therefore, b_2 is explicitly expressed as a funciton of the arbitrary constants b_o, b_1, a_o, and a_1. Similarly for powers of R^1,

$$\begin{aligned} b_3 = & \frac{-6r_o b_2 - \left(1 - p_2 - p_1 r_o^2\right) b_1 + 2p_1 r_o b_o}{6r_o^2} \\ & + \frac{-2p_3 r_o^2 a_2 - \left(2p_3 r_o + p_4 r_o\right) a_1 - p_4 a_o}{6r_o^2} \end{aligned} \tag{3.17}$$

In this case however, a_2 must be known. Therefore equation (3.15b) must be used to find a_2. Doing so for powers of R^o,

$$a_2 = \frac{-a_1 + p_5 r_o a_o + p_6 r_o b_1 + p_7 b_o}{2r_o} \tag{3.18}$$

Here a_2 is explicitly expressed as a function of the arbitrary constants a_o, a_1, b_o and b_1 and can be substituted into 3.17 for calculation of b_3. This process of alternating between the two equations to find the power series coefficients is necessary for all terms. However, it is only necessary to do this by hand to compute b_2, b_3, a_2 and a_3, after which a general recursion relation can be found. These results are

$$a_3 = \frac{-4a_2 + p_5 r_o a_1 + p_5 a_o + 2p_6 r_o b_2 + (p_6 + p_7) b_1}{6r_o} \tag{3.19}$$

$$
\begin{aligned}
b_{n+2} = & \frac{-[r_o(n+1)(2n+1)]b_{n+1} - [n^2 - p_2 - p_1 r_o^2]b_n}{r_o^2(n+2)(n+1)} \\
& + \frac{2p_1 r_o b_{n-1} + p_1 b_{n-2} - p_3 r_o^2(n+1)a_{n+1}}{r_o^2(n+2)(n+1)} \\
& + \frac{-[2p_3 r_o n + p_4 r_o]a_n - [p_3(n-1) + p_4]a_{n-1}}{r_o^2(n+2)(n+1)}
\end{aligned} \tag{3.20}
$$

$$
\begin{aligned}
a_{n+2} = & \frac{-(n+1)(n+1)a_{n+1} + p_5 r_o a_n + p_5 a_{n-1}}{r_o(n+2)(n+1)} \\
& + \frac{(np_6 + p_7)b_n + p_6 r_o(n+1)b_{n+1}}{r_o(n+2)(n+1)}
\end{aligned} \tag{3.21}
$$

Eqs. (3.20) and (3.21) are for $n \geq 2$. This finishes the solution to the homogeneous equations (3.10). However, a method for finding a_o, a_1, b_o, and b_1 is needed because these are embedded in the recursion relations (3.20) and (3.21). To circumvent this problem the solutions are taken in the following way:

$$
\begin{aligned}
f(r) &= d_o f_o(r) + d_1 f_1(r) + d_2 f_2(r) + d_3 f_3(r) \\
g(r) &= d_o g_o(r) + d_1 g_1(r) + d_2 g_2(r) + d_3 g_3(r)
\end{aligned} \tag{3.22}
$$

where the arbitrary constants a_o, a_1, b_o, and b_1 have been replaced by d_o, d_1, d_2, and d_3. Each function f_o, f_1, f_2, f_3, g_o, g_1, g_2, and g_3 has recursion relations based upon Eqs. (3.20) and (3.21), but in a special way. For example, by taking $a_1 = b_o = b_1 = 0$ and using the recursion relations for $f(r)$ and $g(r)$, the recursion relations for $f_o(r)$ and $g_o(r)$, are found giving functions that look like

$$
f_o(r) = d_o \left[1 + \sum_{n=2}^{\infty} a_n R^n \right] \tag{3.23a}
$$

$$
g_o(r) = d_o \sum_{n=2}^{\infty} b_n R^n \tag{3.23b}
$$

This approach isolates a_o in a way such that it may be calculated by a straightforward application of boundary conditions. Similarly by taking $a_o = b_o = b_1 = 0$, $f_1(r)$ and $g_1(r)$ look like

$$f_1(r) = d_1 \sum_{n=1}^{\infty} a_n R^n \tag{3.24a}$$

$$g_1(r) = d_1 \sum_{n=2}^{\infty} b_n R^n \tag{3.24b}$$

The remaining functions are given by

$$f_2(r) = d_2 \sum_{n=2}^{\infty} a_n R^n \tag{3.25a}$$

$$g_2(r) = d_2 \left[1 + \sum_{n=2}^{\infty} b_n R^n\right] \tag{3.25b}$$

for $a_o = a_1 = b_1 = 0$, and

$$f_3(r) = d_3 \sum_{n=2}^{\infty} a_n R^n \tag{3.26a}$$

$$g_3(r) = d_3 \sum_{n=1}^{\infty} b_n R^n \tag{3.26b}$$

for $a_o = a_1 = b_o = 0$.

The solution to the non-homogeneous Eqs. (3.15) is found in the same way as that for the homogeneous equations. However, the form of the power series is taken as[20]

$$f_4(r) = R^2 \sum_{n=0}^{\infty} a_n R^n \tag{3.27a}$$

$$g_4(r) = R^2 \sum_{n=0}^{\infty} b_n R^n \tag{3.27b}$$

Substituting Eqs. (3.27) into Eqs. (3.15) and setting coefficients for each power of R^n to zero gives the recursion relation for the particular solutions. The first four terms

for each are calculated in the same way as described before, by alternating between each equation satisfying them successively. These terms are given by

$$b_o = \frac{H_1}{2r_o} \tag{3.28a}$$

$$a_o = \frac{H_2}{2} \tag{3.28b}$$

$$b_1 = \frac{H_1 - 6r_o b_o - 2p_3 r_o^2 a_o}{6r_o^2} \tag{3.28c}$$

$$a_1 = \frac{H_2 - 4a_o + 2p_6 r_o b_o}{6r_o} \tag{3.28d}$$

$$\begin{aligned} b_2 =& \frac{-15r_o b_1 - (4 - p_1 r_o^2 - p_2) b_o}{12r_o^2} \\ &+ \frac{-3p_3 r_o^2 a_1 - (4p_3 r_o + p_4 r_o) a_o}{12r_o^2} \end{aligned} \tag{3.28e}$$

$$a_2 = \frac{-9a_1 + p_5 r_o a_o + 3p_6 r_o b_1 + (2p_6 + p_7) b_o}{12r_o} \tag{3.28f}$$

$$\begin{aligned} b_3 =& \frac{-28r_o b_2 - (9 - p_1 r_o^2 - p_2) b_1 + 2p_1 r_o b_o}{20r_o^2} \\ &+ \frac{-4p_3 r_o^2 a_2 - (6p_3 r_o + p_4 r_o) a_1 - (2p_3 + p_4) a_o}{20r_o^2} \end{aligned} \tag{3.28g}$$

$$\begin{aligned} a_3 =& \frac{-16a_2 + p_5 r_o a_1 + p_5 a_o}{20r_0} \\ &+ \frac{(3p_6 + p_7) b_1 + 4p_6 r_o b_2}{20r_o} \end{aligned} \tag{3.28h}$$

The general recursion relation for a_n and b_n for $n \geq 4$ are given by

$$\begin{aligned} b_n =& \frac{p_1 b_{n-4} + 2p_1 r_o b_{n-3} - [n^2 - p_1 r_o^2 - p_2] b_{n-2}}{r_o^2 (n+2)(n+1)} \\ &+ \frac{-r_o (2n+1)(n+1) b_{n-1} - [p_3 (n-1) + p_4] a_{n-3}}{r_o^2 (n+2)(n+1)} \\ &+ \frac{-[2p_3 r_o n + p_4 r_o] a_{n-2} - p_3 r_o^2 (n+1) a_{n-1}}{r_o^2 (n+2)(n+1)} \end{aligned} \tag{3.30a}$$

$$a_n = \frac{-(n+1)^2 a_{n-1} + p_5 r_o a_{n-2} + p_5 a_{n-3}}{(n+2)(n+1)r_o} + \frac{(np_6 + p_7)b_{n-2} + p_6 r_o (n+1) b_{n-1}}{(n+2)(n+1)r_o} \tag{3.30b}$$

So far, solutions for $f(r)$ and $g(r)$ have been found for each λ_i, $i = 1, 2, ..., N$. Substituting the form of these solutions back into Eqs. (3.7) gives

$$u(r,z) = \sum_{i=1}^{N} \{d_{oi} g_{oi}(r) + d_{1i} g_{1i}(r) + d_{2i} g_{2i}(r) + d_{3i} g_{3i}(r) + g_{4i}(r)\} \cos\lambda_i z \tag{3.31a}$$

$$\omega(r,z) = \sum_{i=1}^{N} \{d_{oi} f_{oi}(r) + d_{1i} f_{1i}(r) + d_{2i} f_{2i}(r) + d_{3i} f_{3i}(r) + f_{4i}(r)\} \sin\lambda_i z \tag{3.31b}$$

Now it is necessary to consider the constant term in the Fourier cosine series for E_r given in Eq. (3.9). This represents the case where $\lambda_i = 0$, and thus, because of the form the solution taken, the second equilibrium equation given in (3.3b) is automatically satisfied. However, to include the displacement condition for the end, it is necessary to look for solutions in the following form

$$u = u^*(r) \tag{3.32a}$$

$$\omega = \omega^*(z) \tag{3.32b}$$

Using Eqs. (3.32), the equilibrium equations (3.3), which include the constant term from the Fourier cosine series expansion for E_r, are given by

$$r^2 \frac{d^2 u^*}{dr^2} + r\frac{du^*}{dr} - \frac{c_{22}}{c_{33}} u^* + \left(\frac{c_{13} - c_{12}}{c_{33}}\right) r \frac{d\omega^*}{dz} = \left(\frac{H_r - H_\theta}{c_{33}}\right) r \frac{A_o}{2} \tag{3.33a}$$

$$\frac{d^2\omega^*}{dz^2} = 0 \tag{3.33b}$$

The solution to equation (3.33b) is given as

$$\omega^*(z) = c_3 z + c_4 \tag{3.34}$$

To satisfy the boundary conditions

$$c_4 = 0 \tag{3.35a}$$

$$c_3 = \frac{2z_o}{\ell} \tag{3.35b}$$

Now the solution for $\omega^*(z)$ can be substituted into Eq. (3.33a). For isotropic cylinders, Eq. (3.33a) reduces to

$$r^2\frac{d^2u^*}{dr^2} + r\frac{du^*}{dr} - u^* = q_1 r \tag{3.36}$$

and for orthotropic cylinders it becomes

$$r^2\frac{d^2u^*}{dr^2} + r\frac{du^*}{dr} - \beta^2 u^* = (q_1 + q_2 c_3)r \tag{3.37}$$

where

$$\beta^2 = \frac{c_{22}}{c_{33}}$$

$$q_1 = \left(\frac{H_r - H_\theta}{c_{33}}\right)\frac{A_o}{2}$$

$$q_2 = \frac{c_{12} - c_{13}}{c_{33}}$$

Equations (3.36) and (3.37) are Euler equations[13] for which the homogeneous solutions can be found by taking $u^* = r^x$. This gives a quadratic polynomial in x. For the isotropic case, the homogeneous solution is given by

$$u_h^* = c_1 r + \frac{c_2}{r} \tag{3.38}$$

and for the orthotropic case, the solution is

$$u_h^* = c_1 r^{\beta} + c_2 r^{-\beta} \tag{3.39}$$

The particular solution, for the isotropic case, is found by taking

$$u_p^* = Arlnr \tag{3.40}$$

and using the method of undetermined coefficients,[13] A is found to be

$$A = \frac{q_1}{2} \tag{3.41}$$

while for the orthotropic case the particular solution takes the form

$$u_p^* = Br \tag{3.42}$$

where B is given by

$$B = \frac{q_1 + q_2 c_3}{1 - \beta^2} \tag{3.43}$$

Using the fact that the final solutions are a superposition of the homogeneous and particular solutions, the non-harmonic components of displacements for isotropic and orthotropic cylinders respectively are given by

$$u^*(r) = \frac{c_1}{r} + c_2 r + Arlnr \tag{3.44a}$$

$$\omega^*(z) = c_3 z \tag{3.44b}$$

$$u^*(r) = c_1 r^{\beta} + c_2 r^{-\beta} + Br \tag{3.45a}$$

$$\omega^*(z) = c_3 z \tag{3.45b}$$

where c_3, β, A and B are defined above in Eqs. (3.35b), (3.37), (3.41) and (3.43) respectively. c_1 and c_2 are arbitrary constants chosen to satisfy boundary conditions.

This ends the derivation of the analytical solution. However, for implementation, further manipulations are required to set up a system of algebraic equations which can be solved for the unknown arbitrary constants that satisfy boundary conditions. To clarify the procedure, the solution for each layer is written here again.

$$u(r,z) = \sum_{i=1}^{N} g_i(r) \cos \lambda_i z + u^*(r) \tag{3.46}$$

$$\omega(r,z) = \sum_{i=1}^{N} f_i(r) \sin \lambda_i z + \omega^*(z) \tag{3.47}$$

Since each layer has the same harmonic content as all other layers, the boundary conditions are satisfied for each λ_i in the above equations. This is equivalent to matching Fourier coefficients. The end conditions in (3.6) have been satisfied by the selection of λ_i and by the solution for $\omega^*(z)$. Therefore the only conditions remaining to be satisfied are the interlamina conditions given in Eqs. (3.4) and (3.5). Boundary conditions for harmonic and non-harmonic terms are satisfied separately. The harmonic solution has four unknowns for each layer in the cylinder which corresponds exactly to the number of boundary conditions given in (3.4) and (3.5). The non-harmonic components of the solution $u^*(r)$ and $\omega^*(z)$ have two unknowns for each layer. These solutions satisfy half the boundary conditions in (3.4) and (3.5) automatically, leaving $2n$ boundary conditions with $2n$ unknowns.

First, the algebraic equations that must be solved for the ith mode are derived. The harmonic portion of the expanded solutions are written again for clarity.

$$u(r,z) = \sum_{i=1}^{N} [d_{oi}g_{oi}(r) + d_{1i}g_{1i}(r) + d_{2i}g_{2i}(r) + d_{3i}g_{3i}(r) + g_{4i}(r)] \cos \lambda_i z \qquad (3.48a)$$

$$\omega(r,z) = \sum_{i=1}^{N} [d_{oi}f_{oi}(r) + d_{1i}f_{1i}(r) + d_{2i}f_{2i}(r) + d_{3i}f_{3i}(r) + f_{4i}(r)] \sin \lambda_i z \qquad (3.48b)$$

Applying the first boundary condition in Eq. (3.4) for the kth interface yields

$$u^k|_{r=r_k} = u^{k+1}|_{r=r_k} \qquad (3.4a)$$

$$g_{oi}^k(r_k)d_{oi}^k + g_{1i}^k(r_k)d_{1i}^k + g_{2i}^k(r_k)d_{2i}^k + g_{3i}^k(r_k)d_{3i}^k - d_{2i}^{k+1} = -g_{4i}^k(r_k) \qquad (3.49)$$

where superscripts indicate the particular lamina. At this point a reminder is helpful. Since all power series for each layer were expanded about the inner surface of the particular layer, all terms on the right hand side of Eq. (3.4a) are zero except one. For example,

$$g_{oi}^{k+1}(r_k) = \sum_{n=2}^{\infty} b_n^o (r_k - r_k)^n = 0. \qquad (3.50)$$

$$g_{1i}^{k+1}(r_k) = \sum_{n=2}^{\infty} b_n^1 (r_k - r_k)^n = 0. \qquad (3.51)$$

$$g_{2i}^{k+1}(r_k) = 1 + \sum_{n=2}^{\infty} b_n^2 (r_k - r_k)^n = 1. \qquad (3.52)$$

$$g_{3i}^{k+1}(r_k) = \sum_{n=1}^{\infty} b_n^3 (r_k - r_k)^n = 0 \qquad (3.53)$$

$$g_{4i}^{k+1}(r_k) = \sum_{n=0}^{\infty} b_n^4 (r_k - r_k)^{n+2} = 0. \qquad (3.54)$$

Similarly for the second condition in (3.4)

$$\omega^k|_{r=r_k} = \omega^{k+1}|_{r=r_k} \qquad (3.4b)$$

$$f_{oi}^k(r_k)d_{oi}^k + f_{1i}^k(r_k)d_{1i}^k + f_{2i}^k(r_k)d_{2i}^k + f_{3i}^k(r_k)d_{3i}^k - d_{oi}^{k+1} = -f_{4i}^k(r_k) \tag{3.55}$$

As in the previous case, all terms on the right hand side of equation (3.4b) are zero except one. Similar situations arise for the remaining two boundary conditions in 3.4 therefore the results are given here.

$$\sigma_r^k|_{r=r_k} = \sigma_r^{k+1}|_{r=r_k} \tag{3.4c}$$

$$\begin{aligned}
&\sum_{j=0}^{3}\left[c_{13}^k\lambda_i f_{ji}^k(r_k) + \frac{c_{23}^k}{r_k}g_{ji}^k(r_k) + c_{33}^k\frac{dg_{ji}^k}{dr}|_{r=r_k}\right]d_{ji}^k \\
&\quad - c_{13}^{k+1}\lambda_i d_{oi}^{k+1} - \frac{c_{23}^{k+1}}{r_k}d_{2i}^{k+1} - c_{33}^{k+1}d_{3i}^{k+1} \\
&\quad = H_r^k A_i^k - H_r^{k+1}A_i^{k+1} - c_{13}^k\lambda_i f_{4i}^k(r_k) - c_{23}^k\frac{g_{4i}^k}{r_k}(r_k) - c_{33}^k\frac{dg_{4i}^k}{dr}|_{r=r_k}
\end{aligned} \tag{3.56}$$

$$\sigma_{rz}^k|_{r=r_k} = \sigma_{rz}^{k+1}|_{r=r_k} \tag{3.4d}$$

$$\begin{aligned}
&c_{55}^k\sum_{j=0}^{3}\left[\frac{df_{ji}^k}{dr}|_{r=r_k} - \lambda_i g_{ji}^k(r_k)\right]d_{ji}^k - c_{55}^{k+1}d_{1i}^{k+1} + c_{55}^{k+1}\lambda_i d_{2i}^{k+1} \\
&\quad = c_{55}^k\left[\lambda_i g_{4i}^k(r_k) - \frac{df_{4i}^k}{dr}|_{r=r_k}\right]
\end{aligned} \tag{3.57}$$

Finally, the inner and outer surface boundary conditions given in (3.5) are derived in the same way and are as follows:

$$\sigma_r^k|_{r=r_n} = 0. \tag{3.5a}$$

$$\begin{aligned}
&\sum_{j=0}^{3}\left[c_{13}^n\lambda_i f_{ji}^n(r_n) + \frac{c_{23}^n}{r_n}g_{ji}^n(r_n) + c_{33}^n\frac{dg_{ji}^n}{dr}|_{r=r_n}\right]d_{ji}^n \\
&\quad = H_r^n A_i^n - c_{13}^n\lambda_i f_{4i}^n(r_n) - c_{23}^n\frac{g_{4i}^n(r_n)}{r_n} - c_{33}^n\frac{dg_{4i}^n}{dr}|_{r=r_n}
\end{aligned} \tag{3.58}$$

$$\sigma_{rz}^n|_{r=r_n} = 0 \tag{3.5b}$$

$$\sum_{j=0}^{3}\left[\frac{df_{ji}^{n}}{dr}|_{r=r_n} - \lambda_i g_{ji}^{n}(r_n)\right] d_{ji}^{n}$$
$$= \lambda_i g_{4i}^{n}(r_n) - \frac{df_{4i}^{n}}{dr}|_{r=r_n}. \tag{3.59}$$

$$\sigma_r^1|_{r=r_o} = 0 \tag{3.5c}$$

$$c_{13}^1 \lambda_i d_{oi}^1 + \frac{c_{23}^1}{r_o} d_{2i}^1 + c_{33}^1 d_{3i}^1 = H_r^1 A_i^1 \tag{3.60}$$

$$\sigma_{rz}^1|_{r=r_o} = 0 \tag{3.5d}$$

$$d_{1i}^1 - \lambda_i d_{2i}^1 = 0 \tag{3.61}$$

This finishes the boundary conditions for the harmonic components of the solution. Equations (3.49) and (3.55) through (3.61) yield $4n$ unknowns d_{oi}^k, d_{1i}^k, d_{2i}^k, d_{3i}^k for the ith mode and $k = 1, 2, ..., n$. The system is banded with a bandwidth of eight since each layer is coupled to adjacent layers through common boundaries. A solution is given using Gauss elimination.

Similar derivatives are required for the non-harmonic components $u^*(r)$ and $\omega^*(z)$. Due to the form of these solutions, all shear and axial displacement boundary conditions are automatically satisfied. These solutions yield no shear stress or strain and all layers have the same axial displacement. Therefore, the boundary conditions in (3.4) and (3.5) reduce to

$$\sigma_r^k|_{r=r_k} = \sigma_r^{k+1}|_{r=r_k} \tag{3.62a}$$

$$u^k|_{r=r_k} = u^{k+1}|_{r=r_k} \tag{3.62b}$$

$$k = 1, 2, ..., n-1$$

$$\sigma_r^1|_{r=r_o} = 0 \tag{3.62c}$$

$$\sigma_r^n|_{r=r_n} = 0 \tag{3.62d}$$

This leaves $2n$ equations (3.62) in $2n$ unknowns c_1^k and c_2^k for $k = 1, 2, ..., n$. The solution to this set of equations is straightforward using Gauss elimination. Although not symmetric, the system is banded with a bandwidth of four and size directly proportional to the number of layers involved.

3.5 Solution by the Finite Element Method

Using the finite element method (FEM), the cylinder in Figure 3.2 is modeled using Eqs. (3.1) and (3.2). The displacement formulation presented here follows the methodology given in Ref. [14].

The first step in the finite element analysis is to discretize the domain. Due to the axisymmetry assumption only domain in the $r - z$ plane is modeled as indicated in Figure 3.3. There is no approximation in modeling of the domain because it is modeled exactly with rectangular type elements.

The weak form is developed next and to this end Eqs. (3.1) are written as

$$\frac{1}{r}\frac{\partial}{\partial r}(r\sigma_r) + \frac{\partial \sigma_{rz}}{\partial z} - \frac{\sigma_\theta}{r} = 0 \tag{3.63a}$$

$$\frac{1}{r}\frac{\partial}{\partial r}(r\sigma_{rz}) + \frac{\partial \sigma_z}{\partial z} = 0 \tag{3.63b}$$

Equations (3.63) are multiplied by two arbitrary functions, ϕ_1 and ϕ_2 respectively, and then integrated over the domain Ω of an arbitrary element.

$$\int_\Omega \left[\frac{\phi_1}{r}\frac{\partial}{\partial r}(r\sigma_r) + \phi_1\frac{\partial \sigma_{rz}}{\partial z} - \phi_1\frac{\sigma_\theta}{r}\right] r dr dz = 0 \tag{3.64a}$$

$$\int_\Omega \left[\frac{\phi_2}{r}\frac{\partial}{\partial r}(r\sigma_{rz}) + \phi_2\frac{\partial \sigma_z}{\partial z}\right] r dr dz = 0 \tag{3.64b}$$

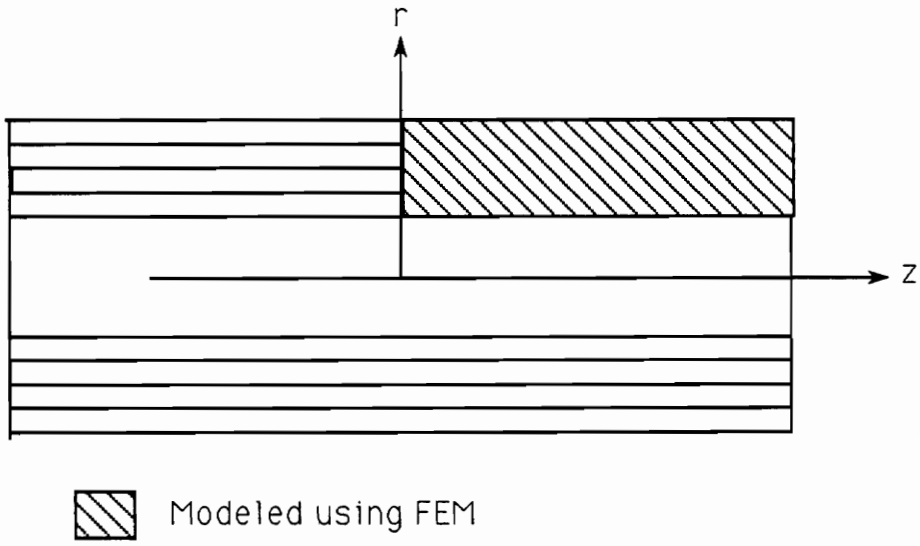

Figure 3.3 Finite Element Modeling of Cylinder

These equations may be integrated by parts if ϕ_1 and ϕ_2 are differentiable at least once with respect to r and z. Upon integration the following weak form for Eqs. (3.63) is obtained

$$\oint (n_r\sigma_r + n_z\sigma_{rz})\phi_1 r ds - \int_\Omega \left\{ \frac{\partial \phi_1}{\partial r}\sigma_r + \frac{\partial \phi_1}{\partial z}\sigma_{rz} + \phi_1 \frac{\sigma_\theta}{r} \right\} r dr dz = 0 \qquad (3.65a)$$

$$\oint (n_r\sigma_{rz} + n_z\sigma_z)\phi_2 r ds - \int_\Omega \left\{ \frac{\partial \phi_2}{\partial r}\sigma_{rz} + \frac{\partial \phi_2}{\partial z}\sigma_z \right\} r dr dz = 0 \qquad (3.65b)$$

where n_r and n_z represent components of the normal vector to the boundary of the element. The first integral in both of Eqs. (3.65) is a boundary integral. The terms inside the parentheses are components of the stress vector acting on the surface of the element. If the element boundary is not coincident with the boundary of the domain, then the stress vectors acting on an adjacent element with a common boundary are equal and opposite. Therefore, the boundary terms cancel in an equilibrium sense, throughout the domain except on the domain boundary and here the boundary conditions are known.

To simplify the expressions, the following definitions for the element surface tractions are made

$$t_r = n_r\sigma_r + n_z\sigma_{rz} \qquad (3.66a)$$

$$t_z = n_r\sigma_{rz} + n_z\sigma_z \qquad (3.66b)$$

To proceed further, it is necessary to substitute the constitutive relations (3.2) into Eqs. (3.65), where it is assumed that u and w can be approximated by

$$u = \sum_{j=1}^{n} u_j \psi_j \qquad (3.67a)$$

$$w = \sum_{j=1}^{n} w_j \psi_j \tag{3.67b}$$

where $\psi_j = \psi_j(r, z)$ and n is the number of nodes in an element and u_j and w_j are nodal displacements of the element. From the beginning, ϕ_1 and ϕ_2 were taken as arbitrary but differentiable at least once. If the interpolation functions ψ_j are taken to be differentiable at least once with respect to r and z, then ϕ_1 and ϕ_2 can be taken as

$$\phi_2 = \phi_1 = \psi_i \tag{3.68}$$

Using Eqs. (3.66), (3.67) and (3.68), Eqs. (3.65) can be written in terms of ψ_j and the unknown nodal displacements u_j and w_j. This is given as:

$$\begin{bmatrix} k_{ij}^{11} & k_{ij}^{12} \\ k_{ij}^{21} & k_{ij}^{22} \end{bmatrix} \begin{Bmatrix} u_j \\ w_j \end{Bmatrix} = \begin{Bmatrix} f_i^1 \\ f_i^2 \end{Bmatrix} + \begin{Bmatrix} q_i^1 \\ q_i^2 \end{Bmatrix} \tag{3.70}$$

where

$$\begin{aligned} k_{ij}^{11} = & \int_{\Omega_e} \left\{ c_{33} \frac{\partial \psi_i}{\partial r} \frac{\partial \psi_j}{\partial r} + c_{55} \frac{\partial \psi_i}{\partial z} \frac{\partial \psi_j}{\partial z} r dr dz \right\} \\ & + \int_{\Omega_e} \left\{ c_{23} \left[\frac{\partial \psi_i}{\partial r} \psi_j + \psi_i \frac{\partial \psi_j}{\partial r} \right] \right\} dr dz \\ & + \int_{\Omega_e} c_{22} \frac{\psi_i \psi_j}{r} dr dz \end{aligned}$$

$$\begin{aligned} k_{ij}^{12} = & \int_{\Omega_e} \left\{ c_{13} \frac{\partial \psi_i}{\partial r} \frac{\partial \psi_j}{\partial z} + c_{55} \frac{\partial \psi_i}{\partial z} \frac{\partial \psi_j}{\partial r} \right\} r dr dz \\ & + \int_{\Omega_e} \left\{ c_{12} \psi_i \frac{\partial \psi_j}{\partial z} \right\} dr dz \end{aligned}$$

$$k_{ij}^{21} = (k_{ij}^{12})^T$$

$$k_{ij}^{22} = \int_{\Omega_e} \left\{ c_{55} \frac{\partial \psi_i}{\partial r} \frac{\partial \psi_j}{\partial r} + c_{11} \frac{\partial \psi_i}{\partial z} \frac{\partial \psi_j}{\partial z} \right\} r dr dz$$

$$f_i^1 = \int_{\Omega_e} H_r E_r \frac{\partial \psi_i}{\partial r} r dr dz + \int_{\Omega_e} H_\theta E_r \psi_i dr dz$$

$$f_i^2 = \int_{\Omega_e} H_z E_r \frac{\partial \psi_i}{\partial z} r dr dz$$

Equation (3.70) is an algebraic equation in the unknown nodal displacements of an arbitrary element. However, the domain consists of many elements and therefore Eq. (3.70) is computed for each element and coupled to the remaining elements by assembling the element equations. This assembling process is accomplished by enforcing continuity of displacements at inter-element nodes thereby coupling all nodal displacements to each other. The result is a set of linear, algebraic equations with the nodal displacements of the entire domain as unknowns. Due to the banded and symmetric structure of the equations, modified Gauss elimination routines are used to find solutions. This saves both computational time and space on the computer. Computer implementation was done using the program FEM2D.[14]

As stated above, each element is coupled to all other elements in the domain by enforcing continuity of displacements between elements which have a common boundary. This is analogous to the boundary conditions applied in the previous section for the analytical solution. However, for the analytical solution both displacement and stress continuity was enforced along common boundaries of different material types. Herein lies the difference between the analytical solution and the displacement formulation of the finite element method. The analytical solution will necessarily have continuity of displacements and stresses through the thickness of the laminate while the finite element method will yield continuity of displacements automatically but not necessarily of stresses. This raises the question as to whether

or not a solution using the finite element method satisfies the equilibrium equations. The answer is yes, that is equilibrium in an integral sense. The equations satisfied using the finite element method are the weak form of the original governing partial differential equations (3.1). In obtaining the weak form, the equilibrium equations have been integrated once by parts, and therefore, using the finite element method, equilibrium is said to be satisfied in an integral sense.

3.6 Examples

3.6.1 Cylindrical Truss Element Actuator

In this section, a multipurpose cylindrical bar, with embedded PVDF layers, is proposed for use as an active member to control the vibrations of a truss. Such a member would be placed in the load paths of the truss, and thus, serve both as an actuator, to bring transient deformations to zero, as well as a load carrying member. This concept is given in Ref. [17] based upon a different actuator design.

The actuator design consists of adding piezoelectric laminae to a composite cylinder such that axial forces may be generated at the ends based upon the piezoelectric effect. It should generate the largest possible loads while at the same time not excessively sacrificing axial stiffness. Therefore the piezoelectric effect is uniformly distributed along the length of the cylinder in PVDF layers. This is equivalent to having a uniform polarization profile. On the other hand, axial stiffness depends upon ply orientations of the composite laminae. Therefore, various ply orientations are studied to determine their effects on axial stiffness, and upon the forces transmitted to the boundaries.

The technique for calculating the transmitted boundary forces was different from that for axial stiffness computations. For force calculations, the cylinder was constrained from deforming in the axial direction. Since PVDF layers either contract or expand, depending on the polarity of the applied electric field, forces are generated at the boundaries due to this constraint. In contrast, the axial stiffness was calculated by applying a unit displacement to the end of the cylinder. Both the FE solution, given in section 3.5, and the analytical solutions given in Eqs. (3.44), (3.45), and (3.35b) were used for this analysis.

The radial dimensions for the cylinder used in this study are similar to that proposed by NASA for the truss structure of the space station[18] prior to June 1988. It has an inside diameter of 50 mm and a thickness of 1.5 mm. Additional PVDF layers bring the total thickness to 2.1 mm. The passive portion of the cylinder is comprised of the composite material T300/5208, and is made up of three layers. Two PVDF layers are added giving a total of five layers for the cylinder. Properties assumed for T300/5208 are given in Table 3.1. The length of the cylinder used here was .5 m.

Before proceeding, it is necessary to describe exactly how the electric field E_r (volt/length) is applied to PVDF layers. It is the available voltage V divided by the thickness t of the particular layer. For all cases studied here, the PVDF layers were 3×10^{-4} m thick and 1.0 volt was applied, giving an electric field of 3.33×10^3 volts/m. In general, the formula is given by

$$E_r = V/t \tag{3.71}$$

Table 3.1
Properties of T300/5208

Property	Value
E_1	$132 \times 10^9\ Pa$
E_2	$10.8 \times 10^9\ Pa$
E_3	$10.8 \times 10^9\ Pa$
$G_{12} = G_{13}$	$5.65 \times 10^9\ Pa$
G_{23}	$3.38 \times 10^9\ Pa$
$\nu_{12} = \nu_{13}$	.24
ν_{23}	.49
Density	$1389.2 kg/m^3$

A unit voltage was applied here because results may be used to find effects for any other voltage simply by multiplying them by the new voltage.

Results are presented in Table 3.2 and Figures 3.4 through 3.6. In Table 3.2, P represents the axial force generated by PVDF layers and K represents the axial stiffness of the cylinder. Approximately an 8% increase in axial load at the end can be achieved by introducing a 90° lamina. However, this increase in force is at the expense of axial stiffness. Additional 90° layers yield smaller increases in the axial force and likely reduce the axial stiffness below what is acceptable. The effect of placing the PVDF layers on the outside is negligible.

It is worth mentioning the mechanism by which axial forces are transmitted to the boundary. When the electric field is applied to PVDF layers in a positive sense, as described in Chapter 2, the material expands axially. However, this expansion is constrained and therefore compressive forces are generated and transmitted to the boundary via PVDF layers themselves. This is indicated in Figure 3.6. It is also possible to generate tensile forces by applying the electric field in the opposite direction or the negative sense. This is physically realized by simply changing the polarity on the applied voltage.

In addition to axial effects induced by the PVDF laminae, the entire cylinder expands radially as indicated in Figure 3.4. As illustrated, PVDF layers induce this expansion and passive layers simply move along with them. Both Figures 3.4 and 3.5 show that the interlamina boundary conditions, continuity of radial displacements and stresses, are satisfied by both the analytical and FE solutions.

Table 3.2

ID	CASE	STIFFNESS $K(\frac{N}{m})$	ELECTRIC STIFFNESS $P(\frac{N}{V})$
I	0°/*0°/*0°/0°/0°	6.55×10^7	-1.89×10^{-2}
II	0/*0°/90°/*0°/0°	5.38×10^7	-2.07×10^{-2}
III	90°/*0°/90°/*0°/90°	$.587 \times 10^7$	-2.11×10^{-2}
IV	90°/*0°/90°/*0°/0°	3.05×10^7	-2.13×10^{-2}
V	90°/*0°/0°/*0°/0°	4.25×10^7	-2.13×10^{-2}
VI	*0°/0°/0°/0°/*0°	6.55×10^7	-1.89×10^{-2}
VII	*0°/0°/90°/0°/*0°	5.38×10^7	-2.07×10^{-2}
VIII	*0°/90°/90°/90°/*0°	$.586 \times 10^7$	-2.13×10^{-2}
IX	*0°/90°/90°/0°/*0°	3.02×10^7	-2.12×10^{-2}
X	*0°/90°/0°/0°/*0°	4.22×10^7	-2.10×10^{-2}

*indicates PVDF layer

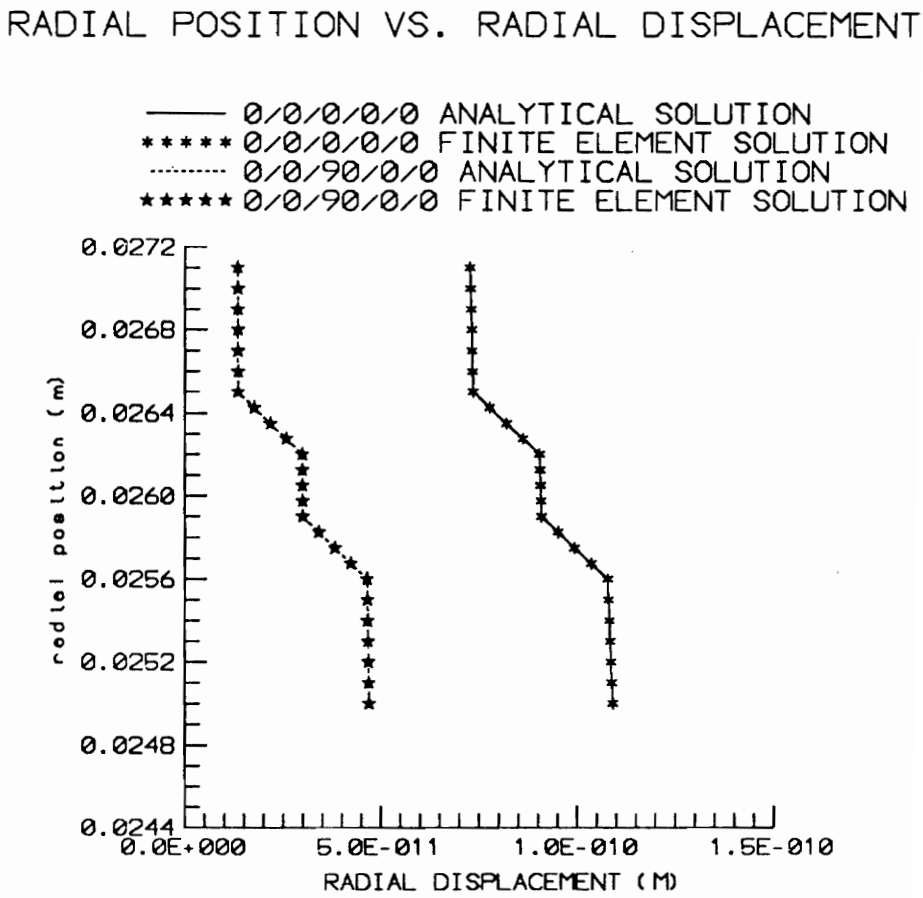
RADIAL POSITION VS. RADIAL DISPLACEMENT
0/0/0/0/0 ANALYTICAL SOLUTION
0/0/0/0/0 FINITE ELEMENT SOLUTION
0/0/90/0/0 ANALYTICAL SOLUTION
0/0/90/0/0 FINITE ELEMENT SOLUTION
0.0272
0.0268
0.0264
0.0260
0.0256
0.0252
0.0248
0.0244
radial position (m)
0.0E+000
5.0E-011
1.0E-010
1.5E-010
RADIAL DISPLACEMENT (M)

Figure 3.4

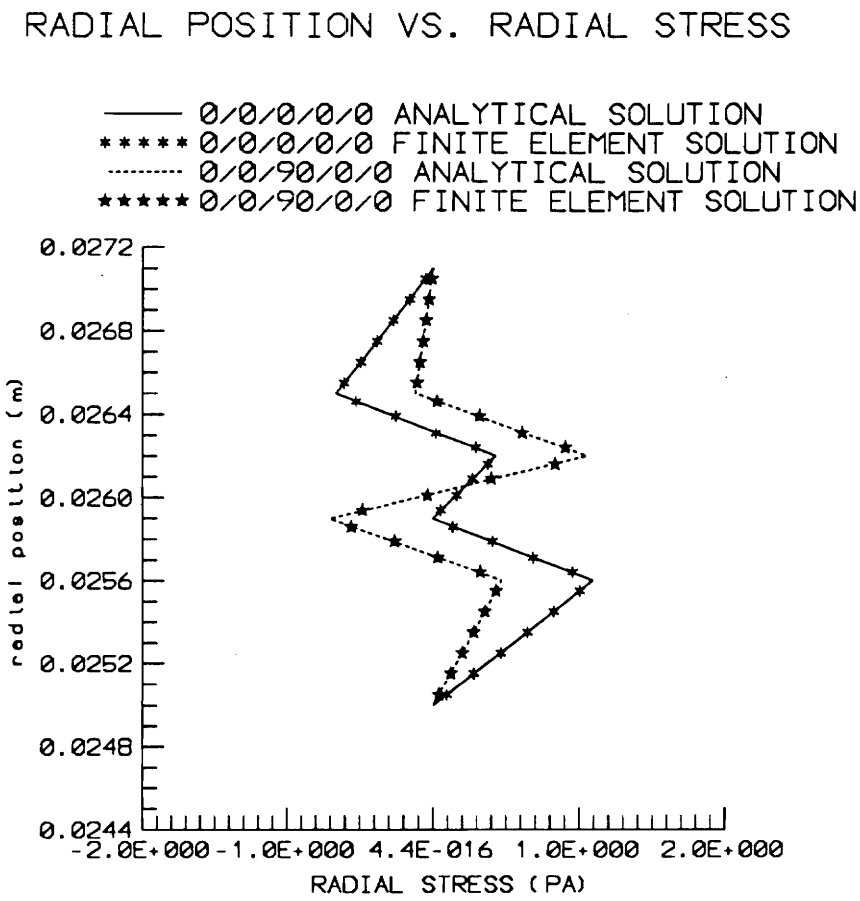
RADIAL POSITION VS. RADIAL STRESS
0/0/0/0/0 ANALYTICAL SOLUTION
0/0/0/0/0 FINITE ELEMENT SOLUTION
0/0/90/0/0 ANALYTICAL SOLUTION
0/0/90/0/0 FINITE ELEMENT SOLUTION
0.0272
0.0268
0.0264
0.0260
0.0256
0.0252
0.0248
0.0244
radial position (m)
-2.0E+000 -1.0E+000 4.4E-016 1.0E+000 2.0E+000
RADIAL STRESS (PA)

Figure 3.5

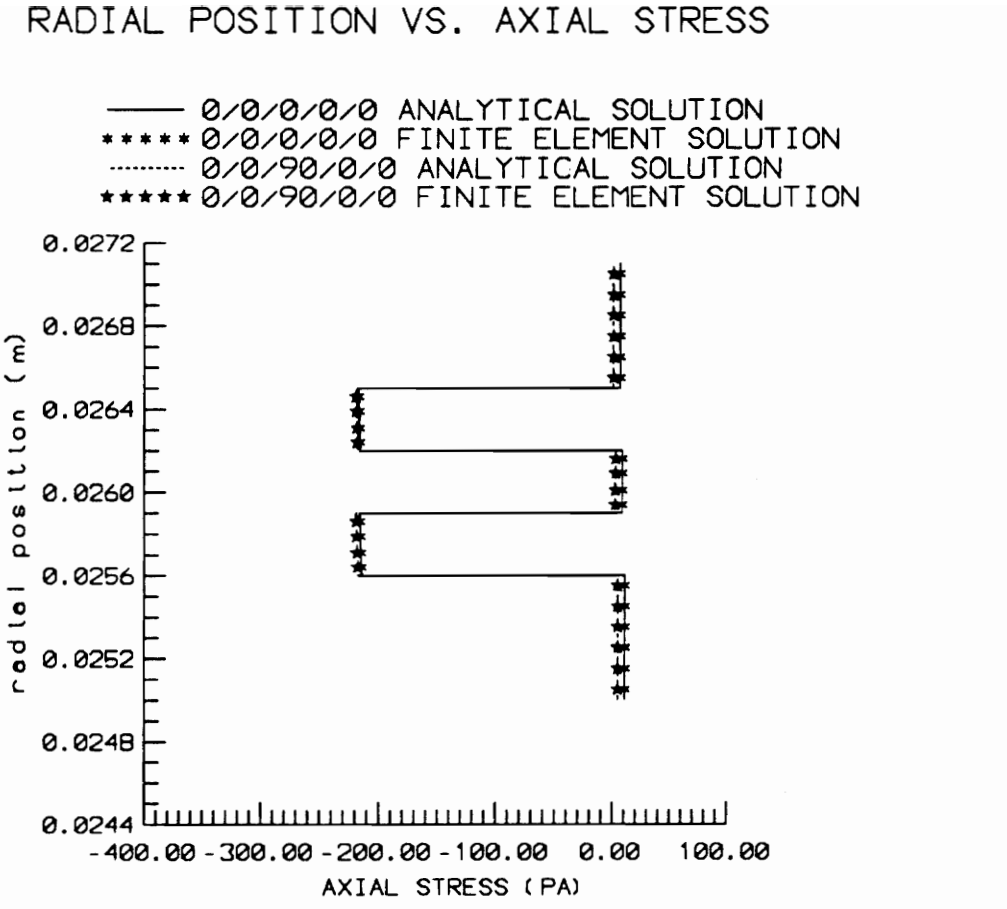
RADIAL POSITION VS. AXIAL STRESS
0/0/0/0/0 ANALYTICAL SOLUTION
0/0/0/0/0 FINITE ELEMENT SOLUTION
0/0/90/0/0 ANALYTICAL SOLUTION
0/0/90/0/0 FINITE ELEMENT SOLUTION
0.0272
0.0268
0.0264
0.0260
0.0256
0.0252
0.0248
0.0244
radial position (m)
-400.00
-300.00
-200.00
-100.00
0.00
100.00
AXIAL STRESS (PA)

Figure 3.6

3.6.2 Modal Actuator

One of the most widely used concepts in the control of flexible structures is called modal space control.[15] In this method, advantage is taken of the special form of the governing equations, namely that they satisfy certain types of boundary conditions and eigenvalue problems. Then it is possible to control the structure by controlling the modes and hence the name modal space control. In this section, it is demonstrated that modal space control, for a rod undergoing axial vibrations, can be achieved by spatially varying the polarization profile of piezoelectric layers. The modal actuator concept was originally proposed for plates and beams in Ref. [8].

To begin with, the equation of motion used here is given by

$$\rho \frac{\partial^2 w}{\partial t^2} = \frac{\partial \sigma_z}{\partial z} \tag{3.73}$$

where the constitutive relation between stresses and strains is

$$\sigma_z = c_{11} \frac{\partial w}{\partial z} - H_z E_r \tag{3.74}$$

Substituting (3.74) into (3.73) yields the following governing equation for a rod undergoing axial vibrations only. Shear deformations are assumed to be zero.

$$\rho \frac{\partial^2 w}{\partial t^2} = c_{11} \frac{\partial^2 w}{\partial z^2} - H_z \frac{\partial E_r}{\partial z} \tag{3.75}$$

The mass density ρ is assumed to be constant along the length of the rod and c_{11}, H_z and E_r are defined as in Chapter 2.

Equation (3.75) is subject to the following boundary conditions on axial displacements

$$\omega(0,t) = \omega\left(\frac{\ell}{2}, t\right) = 0 \tag{3.76}$$

Using standard modal analysis procedures,[16] a solution to Eqs. (3.75) and (3.76) is taken to be in the following form

$$\omega(x,t) = \sum_{r=1}^{\infty} X_r(z)\nu_r(t) \tag{3.77}$$

where $X_r(z)$ are eigenfunctions which satisfy the following eigenvalue problem.

$$-\rho\beta_r^2 X_r = c_{11}X_r'' \tag{3.78a}$$

$$X_r(0) = X_r\left(\frac{\ell}{2}\right) = 0 \tag{3.78b}$$

The eigenfunctions can be shown to be orthogonal and are normalized as follows

$$\int_0^{\frac{\ell}{2}} \rho X_s(z)X_r(z)dz = \delta_{rs} \tag{3.79a}$$

$$\int_0^{\frac{\ell}{2}} c_{11}X_s(z)X_r''(z)dz = -\beta_r^2\delta_{rs}. \tag{3.79b}$$

The eigenfunctions satisfying Eqs. (3.78) are given by

$$X_r(z) = \sin\lambda_r z. \tag{3.80}$$

where

$$\lambda_r = \frac{2r\pi}{\ell} = \beta_r\sqrt{\frac{\rho}{c_{11}}}$$

Proceeding with modal analysis, Eq. (3.77) is substituted into Eq. (3.75) and the result is multiplied by $X_r(z)$ and integrated over the domain. Writing this step out gives

$$\sum_{s=1}^{\infty}\left[\int_0^{\frac{\ell}{2}} \rho X_r(z)X_s(z)dz\right]\ddot{\nu}_s(t) = \sum_{s=1}^{\infty}\left[\int_0^{\frac{\ell}{2}} c_{11}X_r(z)X_s''(z)dz\right]\nu_s(t)$$
$$- H_z\int_0^{\frac{\ell}{2}} X_r(z)\frac{\partial E_r}{\partial z}dz \tag{3.81}$$

The orthogonality conditions in Eqs. (3.79) are now applied to Eq. (3.81) leaving

$$\ddot{\nu}_r + \beta_r^2 \nu_r = -H_z \int_0^{\frac{\ell}{2}} X_r(z) \frac{\partial E_r}{\partial z} dz \tag{3.82}$$

This is an independent modal equation governing the rth mode. It is possible to judicially select the forcing term on the right hand side so that modal space control is possible. Using the orthogonality conditions in Eqs. (3.79), the forcing term is taken as

$$\frac{\partial E_r}{\partial z} = X_r(z) \tag{3.83}$$

where the subscript r is not to be confused. E_r refers to the electric field applied in the radial direction of the cylinder and $X_r(z)$ is the rth eigenfunction.

If the forcing function is taken as defined in (3.83), only the rth mode is affected. This is a spatially distributed force which may be physically realized using PVDF. Specifically, the polarization profile E_r is taken to satisfy Eq. (3.83) and in this case is given by

$$E_r = A \cos \lambda_r z + B \tag{3.84}$$

where A and B are completely arbitrary. Any magnitude of electric field may be applied and therefore any mode of axial vibration may be controlled as long as the electric field follows according to Eq. (3.84). In addition, it is seen that the constant B does not appear in the governing equation, and because of the boundary conditions it does not affect the solution. However, for other types of boundary conditions, such as a free end at $z = \frac{\ell}{2}$, B could be taken as a boundary control parameter.

For an actual control problem, a physical realization of such a profile must be possible. While it is not possible to develop this profile and maintain the axisymmetry

assumption concerning the cylinder, a close approximation is proposed. Such a profile is developed in the processing of PVDF as indicated in Chapter 2.

Consider the sheet of PVDF to be wrapped around the cylinder. For a first mode actuator, the polarization profile indicated in Eq. (3.84) with B = 0, would look like that given in Figure 3.7a before it is wrapped about the cylinder. It is not difficult to see that using this profile the loads generated would be in strong violation of the axisymmetry assumption. Therefore, an equivalent pseudo-symmetric profile is proposed and indicated in Figure 3.7b. Of course, the shaded areas in each must be equivalently distributed along the length of the cylinder for which many combinations of varying numbers of fingers can be used. Using this profile, modal vibration control is possible.

For axial vibrations as described above, it is inherently assumed that displacements are uniform throughout the cross section of the cylinder. Then it is desirable that the actuator produce such displacements, otherwise it may produce excessive spillover into other modes and thus is not a modal actuator at all. When referring to displacements as uniform, the passive layers are indicated. Since the stiffness of PVDF is on the order of 50 times less than that of the composite material used here, it is desirable that the active layers induce a uniform displacement field in the passive layers, and therefore provide the best possible conditions for modal control of passive layers.

An actual vibration control problem is not given here. Instead, a static analysis of a cylinder, with piezoelectric layers having the above polarization profile is

a)

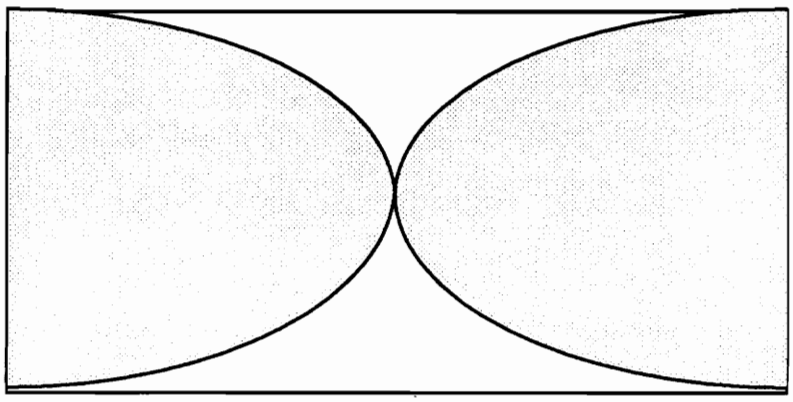

b)

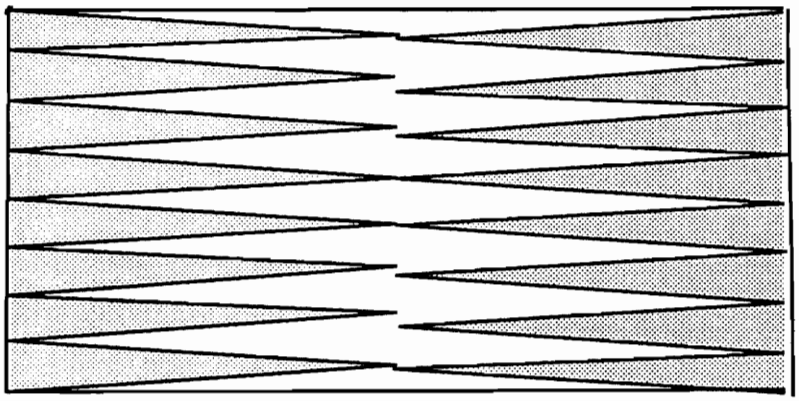

Figure 3.7 Polarization Profile for Modal Actuator

given. Based upon this analysis, it is possible to draw some conclusions concerning assumptions made for the modal actuator and to indicate why some laminae configurations are better than others for this use. Both the analytical and finite element solutions were used for a solution to this problem giving identical results. Therefore, results presented in this section are those from the analytical solution.

Results are given for a cylinder composed of five layers, two of which are PVDF. For this problem, the overall dimensions are fixed while layer configurations are varied. In the first configuration, laminae are oriented as $0°/0°/0°/0°/0°$, with the PVDF layers located in the 2nd and 4th positions. The radii used were: $r_o = 2.5 \times 10^{-3}$ m, $r_1 = 2.56 \times 10^{-3}$ m, $r_2 = 2.59 \times 10^{-3}$ m, $r_3 = 2.62 \times 10^{-3}$ m, $r_4 = 2.65 \times 10^{-3}$ m, and $r_5 = 2.71 \times 10^{-3}$ m. The length of the cylinder used was .5 m.

Using the analytical solution, axial displacements as a function of r and z are indicated in Figures 3.8 and 3.9. Figure 3.9 indicates at least part of the desired effect of the modal actuator. That is, the axial displacement comes in the form of the first mode. However, it varies with radial position as indicated in both figures.

As previously stated, it is best to produce a uniform axial displacement throughout the radial direction in the passive layers. Viewing the results above, it seems plausible to investigate the case where the PVDF layers are placed on the outside. Again, all layers are oriented $0°/0°/0°/0°/0°$. However, in this case, PVDF layers are placed on the inner and outer surfaces of the cylinder. The radii used were: $r_o = 2.5 \times 10^{-3}$ m, $r_1 = 2.53 \times 10^{-3}$ m, $r_2 = 2.59 \times 10^{-3}$ m, $r_3 = 2.62 \times 10^{-3}$ m,

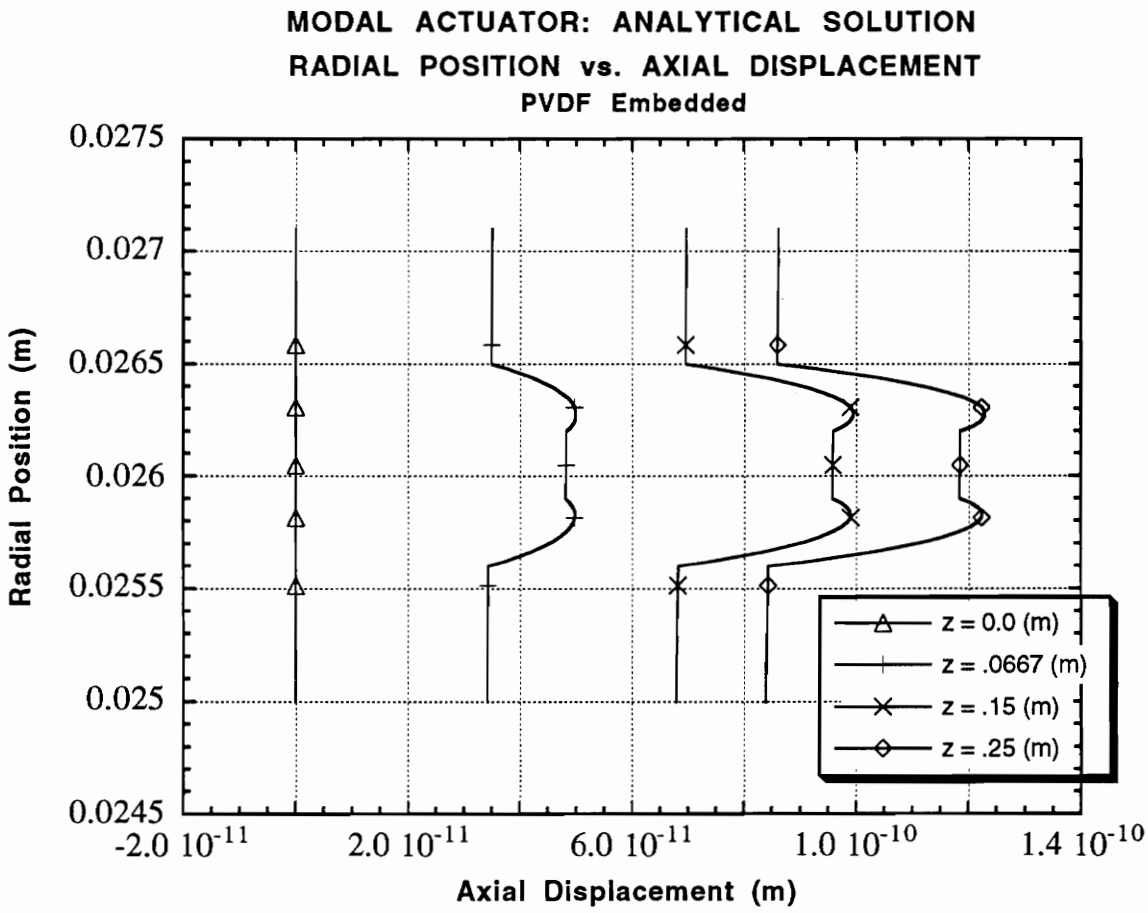
MODAL ACTUATOR: ANALYTICAL SOLUTION
RADIAL POSITION vs. AXIAL DISPLACEMENT
PVDF Embedded
Radial Position (m)
0.0275
0.027
0.0265
0.026
0.0255
0.025
0.0245
-2.0 10^-11
2.0 10^-11
6.0 10^-11
1.0 10^-10
1.4 10^-10
Axial Displacement (m)
z = 0.0 (m)
z = .0667 (m)
z = .15 (m)
z = .25 (m)

Figure 3.8

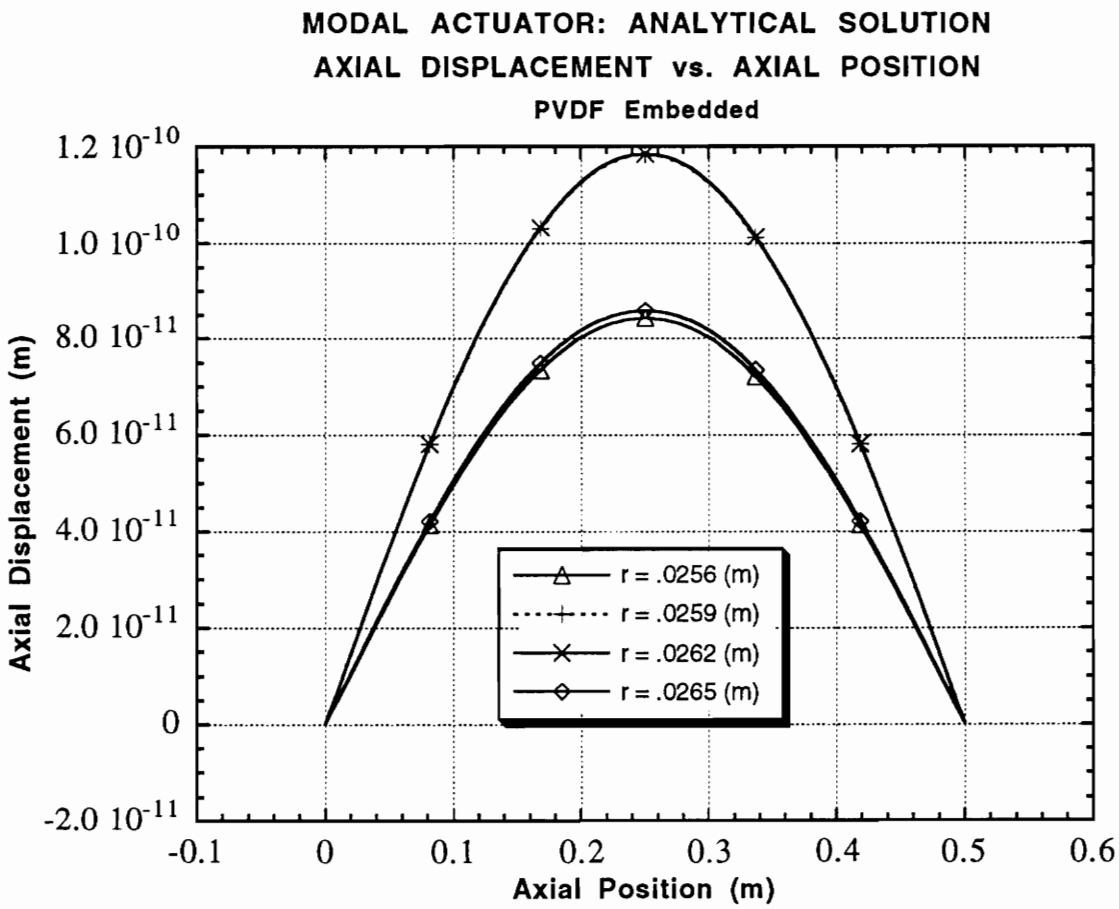
MODAL ACTUATOR: ANALYTICAL SOLUTION
AXIAL DISPLACEMENT vs. AXIAL POSITION
PVDF Embedded
Axial Displacement (m)
1.2 10-10
1.0 10-10
8.0 10-11
6.0 10-11
4.0 10-11
2.0 10-11
0
-2.0 10-11
-0.1
0
0.1
0.2
0.3
0.4
0.5
0.6
Axial Position (m)
r = .0256 (m)
r = .0259 (m)
r = .0262 (m)
r = .0265 (m)

Figure 3.9

$r_4 = 2.68 \times 10^{-3}$ m, and $r_5 = 2.71 \times 10^{-3}$ m. The results indicated in Figures 3.10 and 3.11 indicate the desired effects.

From Figure 3.12, it is seen that by placing PVDF on the inner and outer surfaces of the cylinder, axial stresses induced in passive layers are uniform throughout the thickness direction. Secondly, these stresses vary as $\cos(2 * PI * z/L)$ as indicated in Figure 3.13. Therefore the axial stress distributions satisfy the necessary requirements for a modal actuator. Another consideration is the relative magnitude of shear stresses induced due to the spatial variation of the piezoelectric effect. In magnitude, the interlaminae stresses given in Figure 3.14 are significantly smaller than the axial stresses present.

3.6.3 Polarization Patch

In this section, a polarization profile is taken in the form of a patch and modeled mathematically using Heaviside step functions $h(z)$ as

$$E_r(z) = h(z - z_o) - h(z - z_1) \tag{3.86}$$

This form for E_r is easily modeled using the FEM and can be incorporated into the analytical solution by expanding in a Fourier cosine series. The second equation in (3.3) requires a derivative for E_r with respect to z. This is given by

$$\frac{\partial E_r}{\partial z} = \delta(z - z_o) - \delta(z - z_o) \tag{3.87}$$

where $\delta(z)$ is the Dirac delta function. For the analytical solution, it is necessary that Eq. (3.87) be expressed in a Fourier sine series.

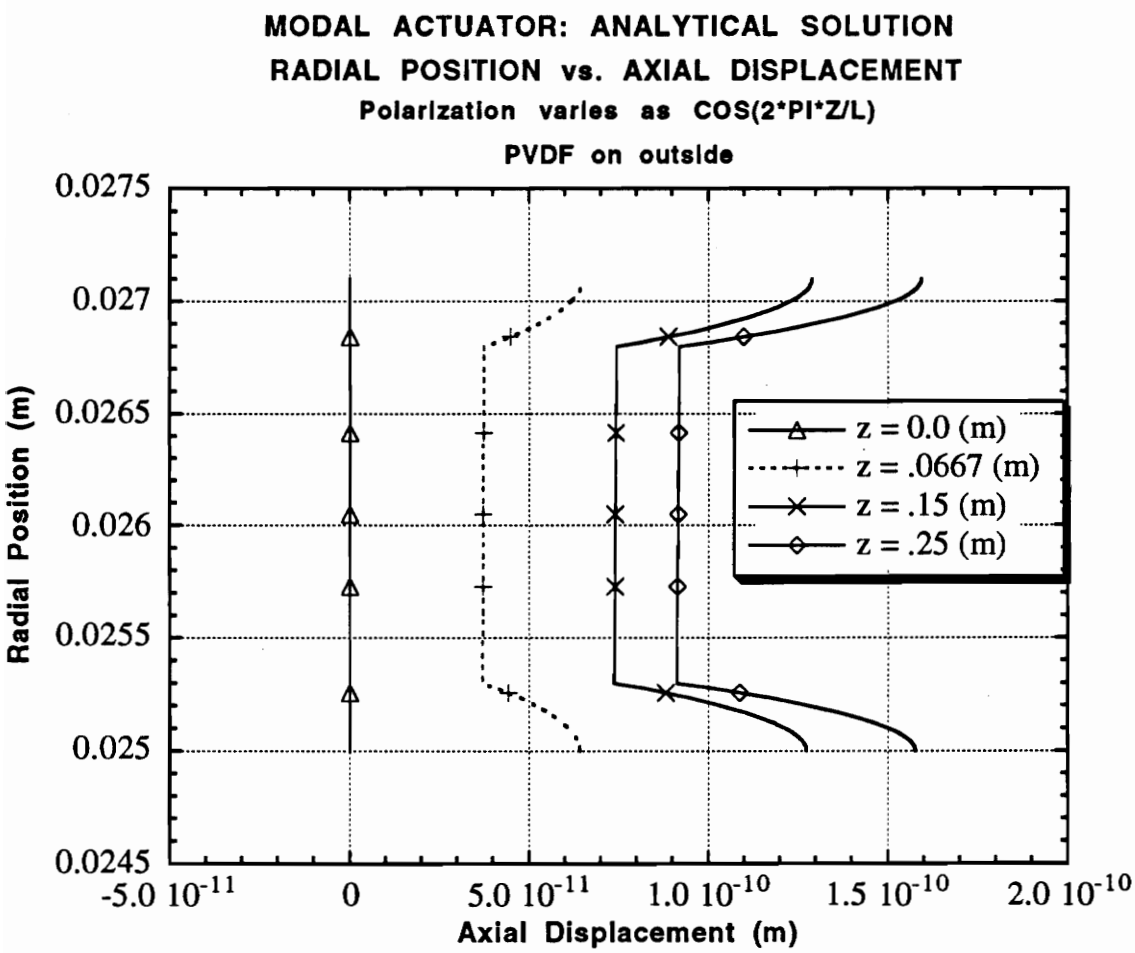
MODAL ACTUATOR: ANALYTICAL SOLUTION
RADIAL POSITION vs. AXIAL DISPLACEMENT
Polarization varies as COS(2*PI*Z/L)
PVDF on outside
Radial Position (m)
0.0275
0.027
0.0265
0.026
0.0255
0.025
0.0245
-5.0 10^-11
0
5.0 10^-11
1.0 10^-10
1.5 10^-10
2.0 10^-10
Axial Displacement (m)
z = 0.0 (m)
z = .0667 (m)
z = .15 (m)
z = .25 (m)

Figure 3.10

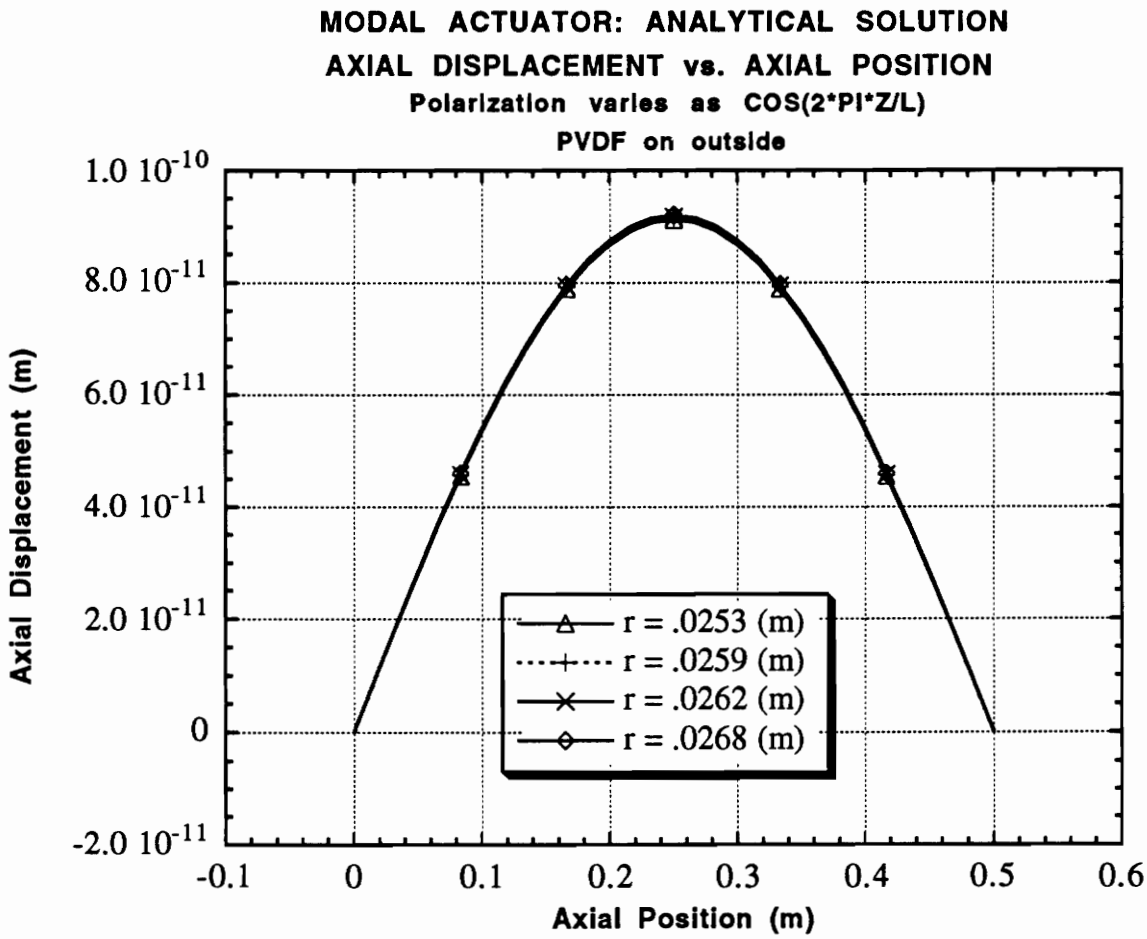
MODAL ACTUATOR: ANALYTICAL SOLUTION
AXIAL DISPLACEMENT vs. AXIAL POSITION
Polarization varies as COS(2*PI*Z/L)
PVDF on outside
1.0 10-10
8.0 10-11
6.0 10-11
4.0 10-11
2.0 10-11
0
-2.0 10-11
Axial Displacement (m)
-0.1
0
0.1
0.2
0.3
0.4
0.5
0.6
Axial Position (m)
r = .0253 (m)
r = .0259 (m)
r = .0262 (m)
r = .0268 (m)

Figure 3.11

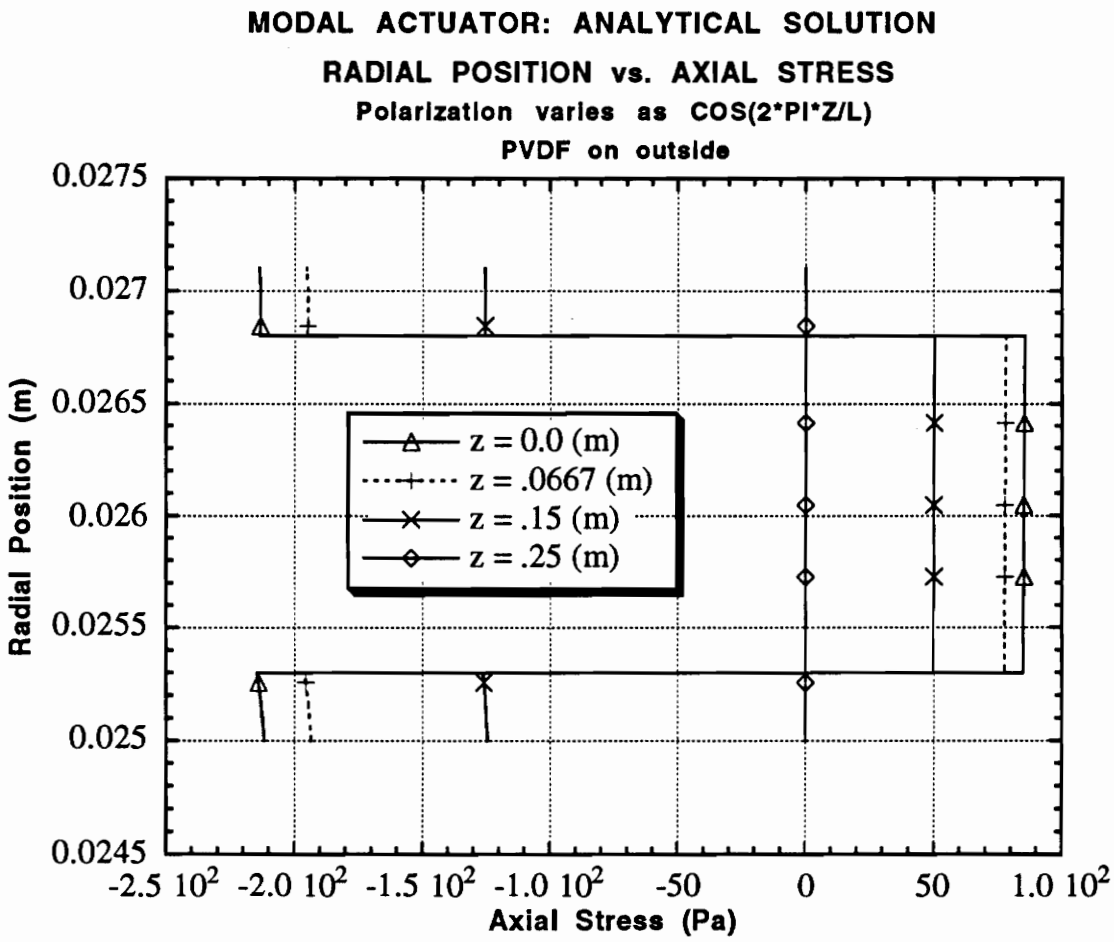
MODAL ACTUATOR: ANALYTICAL SOLUTION
RADIAL POSITION vs. AXIAL STRESS
Polarization varies as COS(2*PI*Z/L)
PVDF on outside
0.0275
0.027
0.0265
0.026
0.0255
0.025
0.0245
Radial Position (m)
z = 0.0 (m)
z = .0667 (m)
z = .15 (m)
z = .25 (m)
-2.5 10^2
-2.0 10^2
-1.5 10^2
-1.0 10^2
-50
0
50
1.0 10^2
Axial Stress (Pa)

Figure 3.12

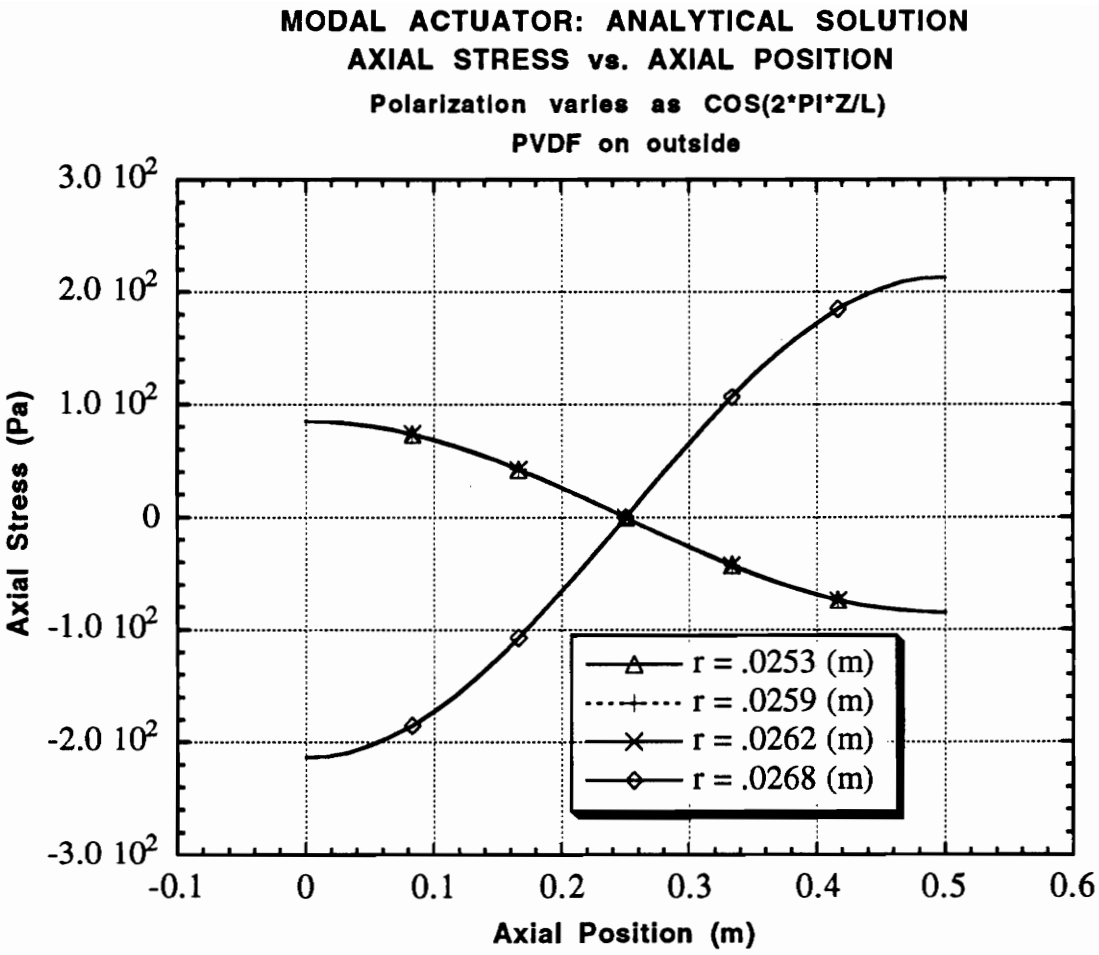
MODAL ACTUATOR: ANALYTICAL SOLUTION
AXIAL STRESS vs. AXIAL POSITION
Polarization varies as COS(2*PI*Z/L)
PVDF on outside
3.0 10^2
2.0 10^2
1.0 10^2
0
-1.0 10^2
-2.0 10^2
-3.0 10^2
Axial Stress (Pa)
-0.1
0
0.1
0.2
0.3
0.4
0.5
0.6
Axial Position (m)
r = .0253 (m)
r = .0259 (m)
r = .0262 (m)
r = .0268 (m)

Figure 3.13

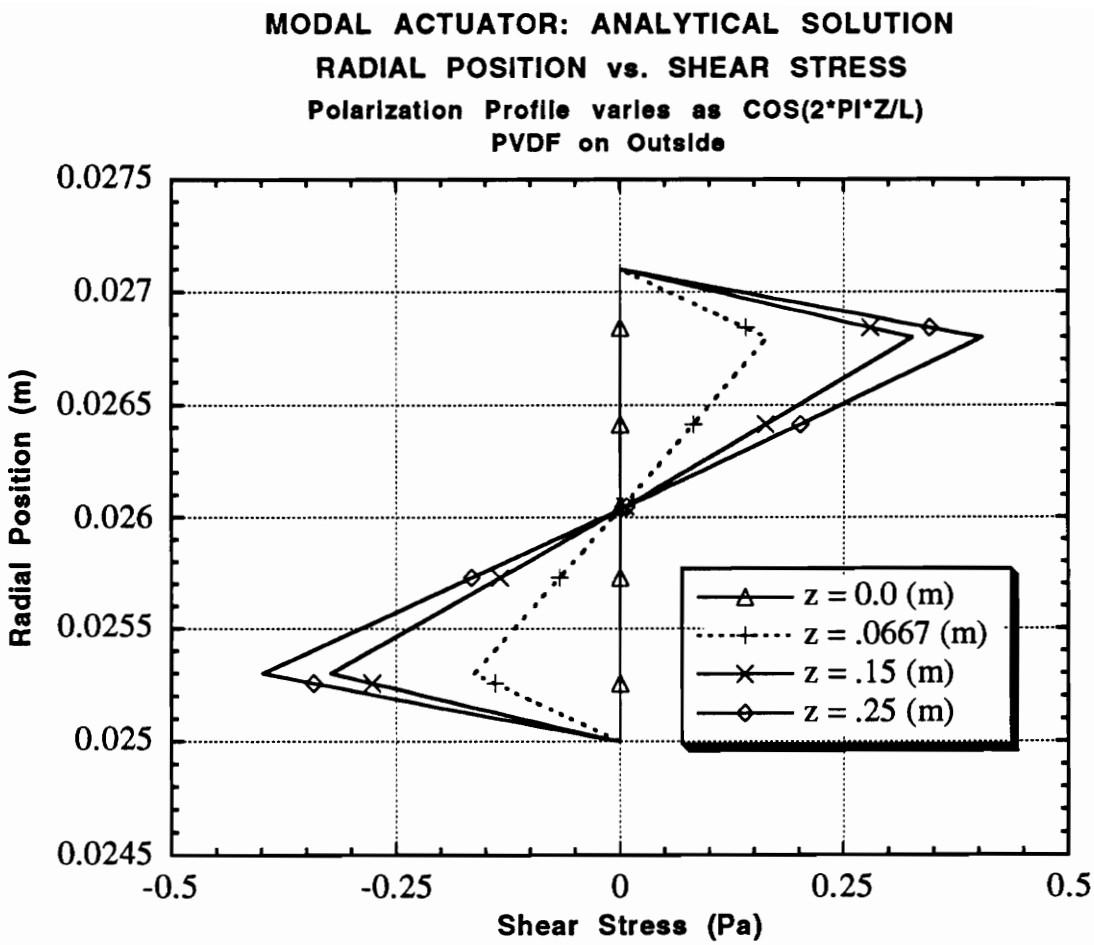
MODAL ACTUATOR: ANALYTICAL SOLUTION
RADIAL POSITION vs. SHEAR STRESS
Polarization Profile varies as COS(2*PI*Z/L)
PVDF on Outside
Radial Position (m)
0.0275
0.027
0.0265
0.026
0.0255
0.025
0.0245
-0.5
-0.25
0
0.25
0.5
Shear Stress (Pa)
z = 0.0 (m)
z = .0667 (m)
z = .15 (m)
z = .25 (m)

Figure 3.14

In the vicinity of sharp jumps in the polarization profile, several problems were encountered. In this area, very large displacement gradients are introduced due to the PVDF layers and this makes it difficult to calculate stresses using the FEM. Similarly, for the analytical solution, because the polarization profile was modeled with Fourier series, Gibbs phenomenon was introduced at the edges of the patch. These problems were reduced to some extent by increasing the number of elements in the FE mesh and by taking more terms in the Fourier series.

As might be expected, the number of terms taken in the power series is critical in obtaining good results. The rate of convergence depends upon λ_i to some extent. For the results presented here, the first 100 non-zero Fourier coefficients for $E_r(z)$ were used. Due to the patch location in this problem, centered at $z = .25m$, all odd modes were filtered out and it was necessary to use up to 130 terms in each associated power series based upon a stopping criteria requiring that the absolute value of additional terms be less than 1.0×10^{-45}. It is not possible to pre-calculate the power series coefficients for such high order terms because they exceed the largest value for which the computer can store. The highest order for which the power series coefficients could be pre-calculated was about 20. Therefore it was necessary to devise a scheme by which terms in the power series could be calculated based upon previous values much in the same way the coefficients may be calculated. Using this technique overflow was completely avoided. The method is described here.

The functions $f(r)$ and $g(r)$ are written as

$$f = \sum_{n=0}^{\infty} f_n \tag{3.88a}$$

$$g = \sum_{n=0}^{\infty} g_n \tag{3.88b}$$

where

$$f_n = a_n z^n.$$

$$g_n = b_n z^n.$$

Given the recursion relations for a_{n+2} and b_{n+2}, the value of f_{n+2} is calculated using f_{n-1}, f_n, f_{n-1}, g_{n+1} and g_n. The value for f_{n+2} is given by

$$f_{n+2} = a_{n+2} z^{n+2} \tag{3.89}$$

Substituting Eq. (3.21) into Eq. (3.89) yields

$$\begin{aligned} f_{n+2} = & \left[\frac{-(n+1)^2 a_{n+1} + p_5 r_o a_n + p_5 a_{n-1}}{r_o(n+2)(n+1)} \right] z^{n+2} \\ & + \left[\frac{(np_6 + p_7) b_n + p_6 r_o (n+1) b_{n+1}}{r_o(n+2)(n+1)} \right] z_{n+2} \end{aligned} \tag{3.90}$$

Recognizing the following terms in Eq. (3.90)

$$a_{n+1} z^{n+2} = (a_{n+1} z^{n+1}) z = f_{n+1} z \tag{3.91a}$$

$$a_n z^{n+2} = (a_n z^n) z^2 = f_n z^2 \tag{3.91b}$$

$$a_{n-1} z^{n+2} = (a_{n-1} z^{n-1}) z^3 = f_{n-1} z^3 \tag{3.91c}$$

$$b_n z^{n+2} = (b_n z^n) z^2 = g_n z^2 \tag{3.91d}$$

$$b_{n+1} z^{n+2} = (b_{n+1} z^{n+1}) z = g_{n+1} z \tag{3.91e}$$

a recursion relation for f_{n+2} is given as

$$\begin{aligned} f_{n+2} = & \frac{-(n+1)^2 f_{n+1} z + p_5 r_o f_n z^2 + p_5 f_{n-1} z^3}{r_o(n+2)(n+1)} \\ & + \frac{(np_6 + p_7) g_n z^2 + p_6 r_o (n+1) g_{n+1} z}{r_o(n+2)(n+1)} \end{aligned} \tag{3.92}$$

Similar relations hold for all the other power series and their derivatives.

Of course, overflow in the computer is only avoided if the power series converges to finite values to begin with. Using the method just described, a good convergence indicator is given by applying the ratio test[19] to successive terms in the series. While it is not possible to let $n \rightarrow \infty$ to check values of $|f_{n+2}/f_{n+1}|$ for convergence, trends are visible for values of n considered here. If a stopping criteria is not set on the power series, and, if it is convergent, underflow will likely occur before a true limit can be found using the ratio test.

Results for this problem are now discussed. The geometry and layer configurations studied here are the same as those for Case II in the section on the cylindrical truss element actuator.

As might be expected, the influence of the patch on displacements diminishes with points taken farther and farther away. This is easily seen in Figures 3.15 through 3.18. Since the patch has been placed at the center along the length of the cylinder, its effects result in some antisymmetric and symmetric phenomenon. For instance, the patch expands axially under the electric field and therefore points to the left of centerline ($z = .25m$) move left or have a negative displacement and points to the right of centerline move to the right. This is indicated in Figure 3.18. The radial displacement is primarily due to hoop expansion and is an example of a symmetric result with respect to z and is given in Figure 3.17. Due to this symmetry, and the fact that the axial displacement is zero at $z = .25m$, one fourth of the cylinder $z : [0, .25]$ was modeled using FEs. Both methods given nearly identical displacement

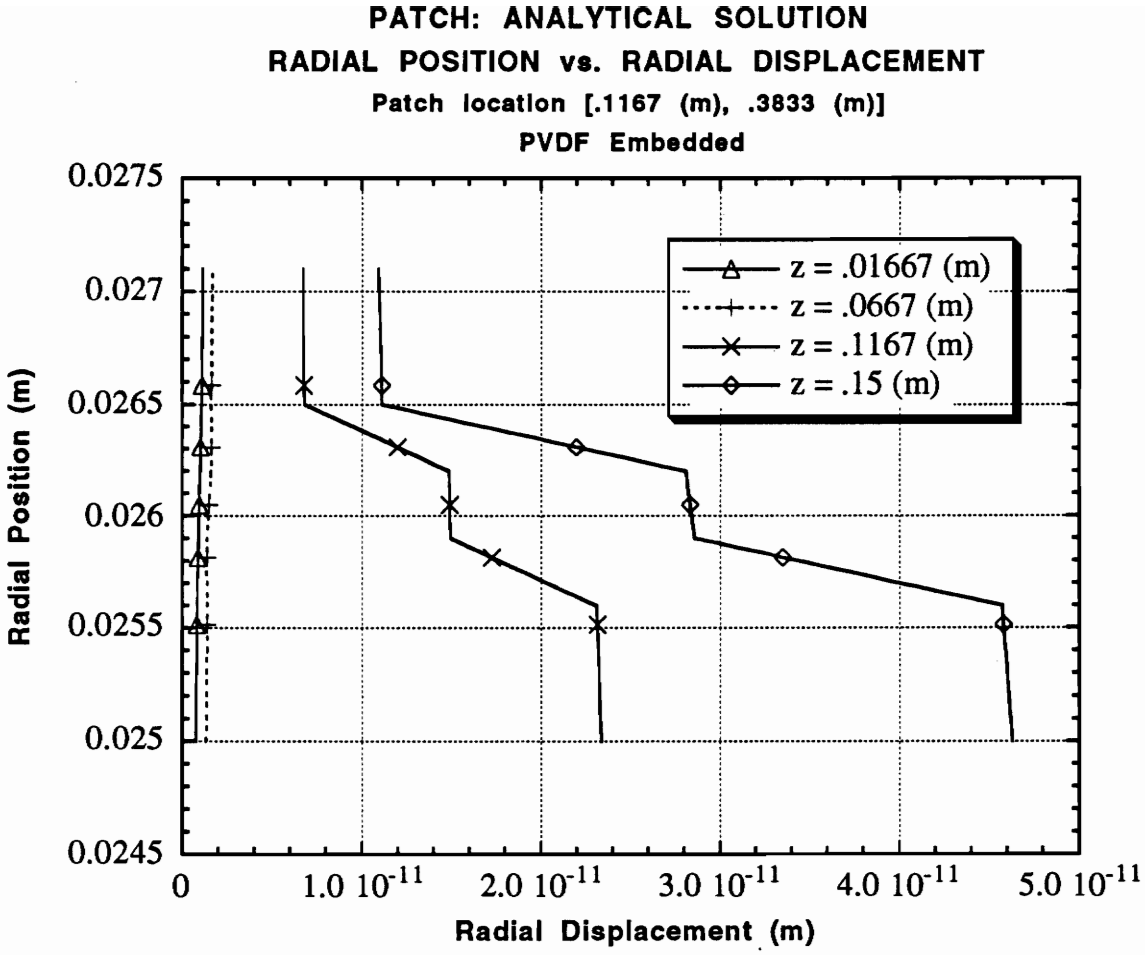
PATCH: ANALYTICAL SOLUTION
RADIAL POSITION vs. RADIAL DISPLACEMENT
Patch location [.1167 (m), .3833 (m)]
PVDF Embedded
z = .01667 (m)
z = .0667 (m)
z = .1167 (m)
z = .15 (m)
Radial Position (m)
0.0275
0.027
0.0265
0.026
0.0255
0.025
0.0245
0
1.0 10^-11
2.0 10^-11
3.0 10^-11
4.0 10^-11
5.0 10^-11
Radial Displacement (m)

Figure 3.15

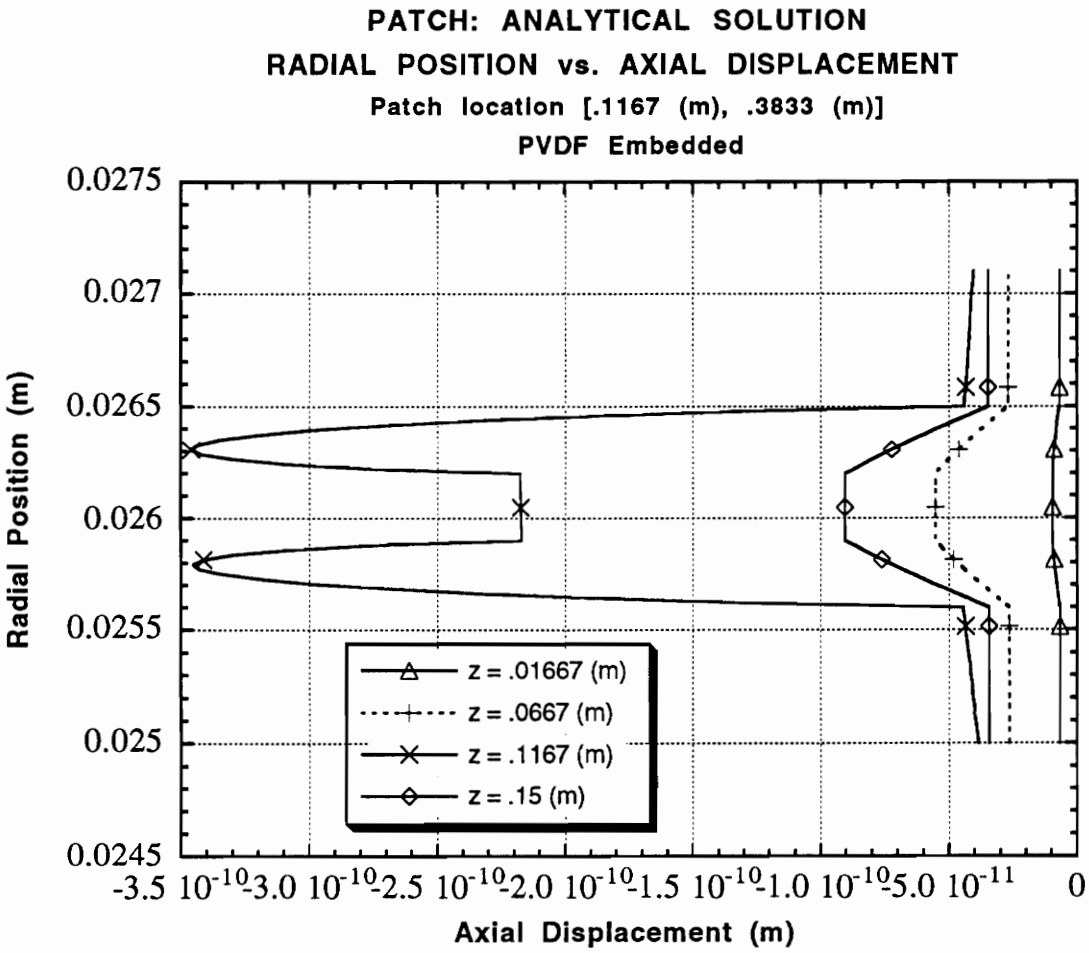
PATCH: ANALYTICAL SOLUTION
RADIAL POSITION vs. AXIAL DISPLACEMENT
Patch location [.1167 (m), .3833 (m)]
PVDF Embedded
Radial Position (m)
0.0275
0.027
0.0265
0.026
0.0255
0.025
0.0245
-3.5 10^-10 -3.0 10^-10 -2.5 10^-10 -2.0 10^-10 -1.5 10^-10 -1.0 10^-10 -5.0 10^-11 0
Axial Displacement (m)
z = .01667 (m)
z = .0667 (m)
z = .1167 (m)
z = .15 (m)

Figure 3.16

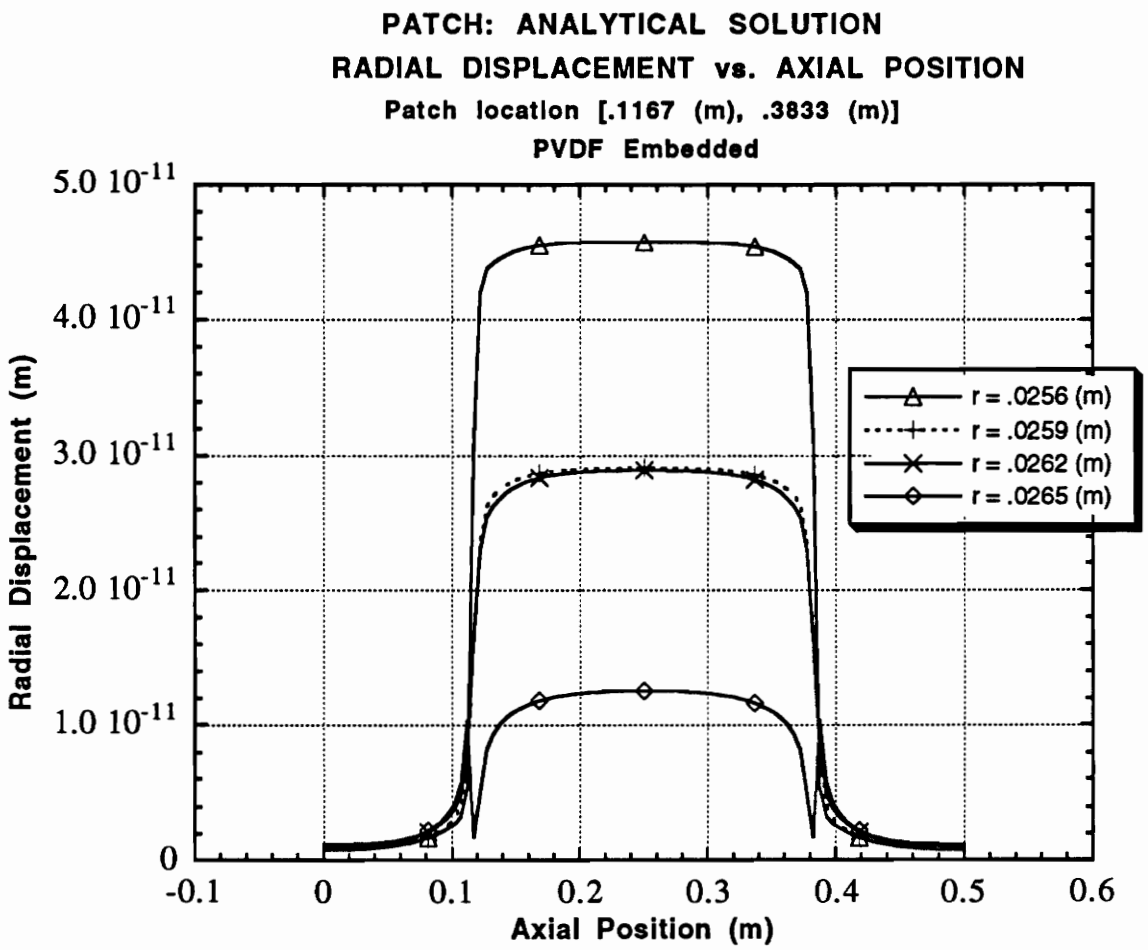
PATCH: ANALYTICAL SOLUTION
RADIAL DISPLACEMENT vs. AXIAL POSITION
Patch location [.1167 (m), .3833 (m)]
PVDF Embedded
5.0 10-11
4.0 10-11
3.0 10-11
2.0 10-11
1.0 10-11
0
Radial Displacement (m)
-0.1
0
0.1
0.2
0.3
0.4
0.5
0.6
Axial Position (m)
r = .0256 (m)
r = .0259 (m)
r = .0262 (m)
r = .0265 (m)

Figure 3.17

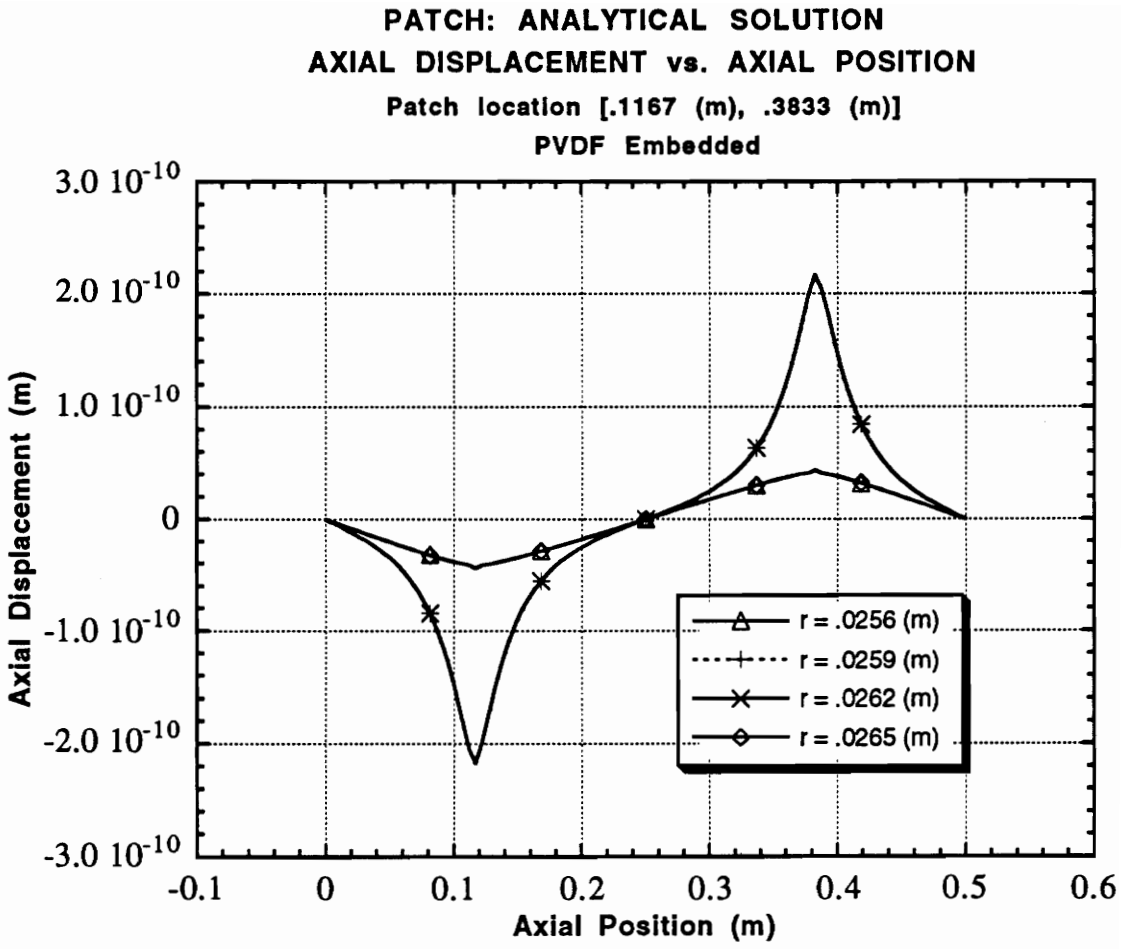
PATCH: ANALYTICAL SOLUTION
AXIAL DISPLACEMENT vs. AXIAL POSITION
Patch location [.1167 (m), .3833 (m)]
PVDF Embedded
3.0 10-10
2.0 10-10
1.0 10-10
0
-1.0 10-10
-2.0 10-10
-3.0 10-10
Axial Displacement (m)
-0.1
0
0.1
0.2
0.3
0.4
0.5
0.6
Axial Position (m)
r = .0256 (m)
r = .0259 (m)
r = .0262 (m)
r = .0265 (m)

Figure 3.18

fields with respect to r and z. It is also worth noting that displacements at the center of the cylinder are very close to those obtained when the polarization profile was taken as uniform. This was Case II in the section on the cylindrical truss element actuator presented in Figures 3.4 through 3.6.

The stress distributions calculated for this case contrast with those in Case II in several ways. Since there are sharp discontinuities in the polarization profile for the patch, shear stresses are introduced. Whereas in Case II, the polarization profile was uniform and therefore no shear stresses were induced. Due to this difference, the mechanism by which axial forces are transmitted to the boundaries is different for each.

In Case II of the cylindrical truss element actuator, the mechanism by which forces were generated at the ends was very simple. All compressive forces were transmitted to the boundaries via the PVDF layers themselves. This contrasts sharply with the present case. Compressive forces in PVDF layers are quickly transferred to adjacent passive laminae at the edges of the patch, and have zero axial stresses at the ends. Forces are then transmitted to the boundaries via passive laminae, and the net axial force transmitted is proportional to the length of the patch. A simple hand calculation using Figures 3.19 and 3.20 and the appropriate cross-sectional areas bears this out.

To understand the mechanism by which axial forces are transferred from PVDF laminae to passive laminae, a free body diagram of an outer laminae is given in Figure 3.21. The outer surface is stress free and therefore axial forces must be present if inter-laminae shear stresses are present. Using Figure 3.21, the following equilibrium

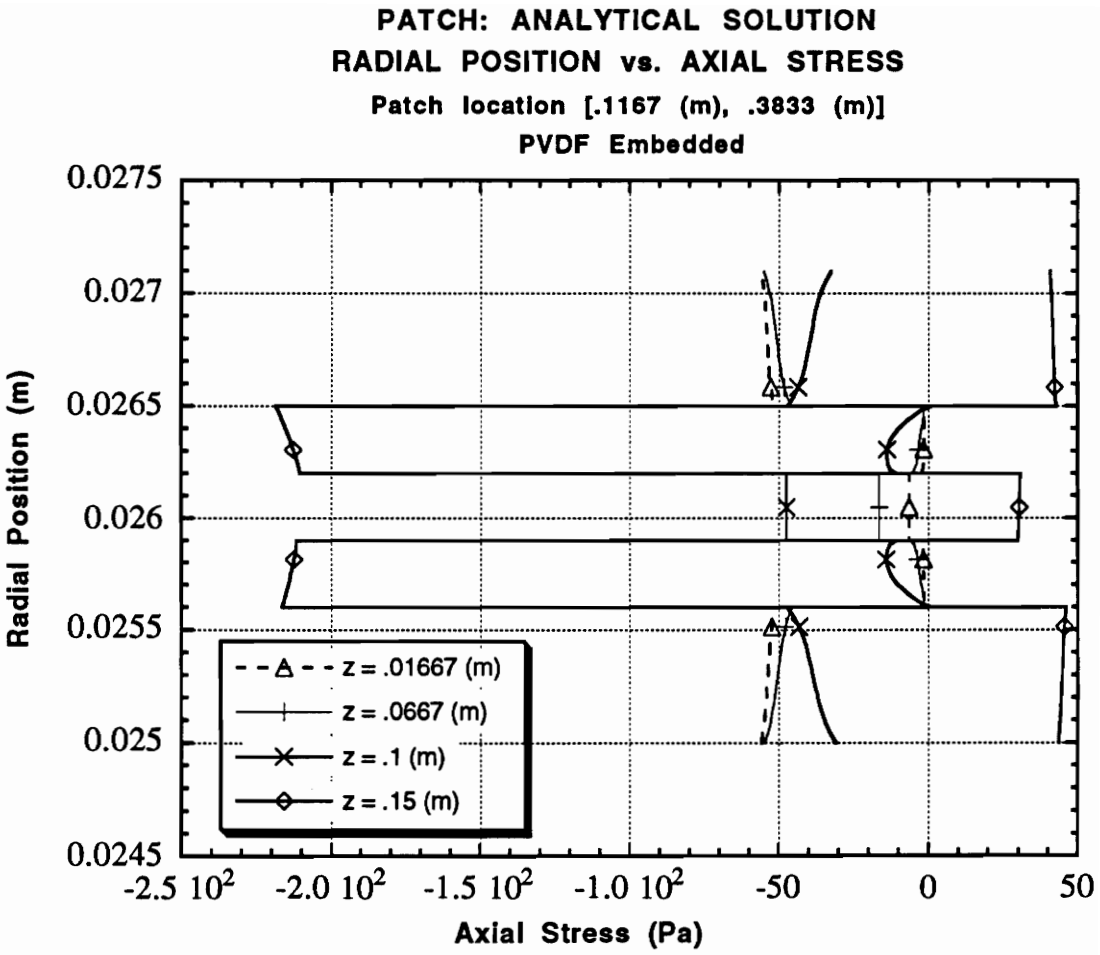
PATCH: ANALYTICAL SOLUTION
RADIAL POSITION vs. AXIAL STRESS
Patch location [.1167 (m), .3833 (m)]
PVDF Embedded
Radial Position (m)
0.0275
0.027
0.0265
0.026
0.0255
0.025
0.0245
-2.5 10^2
-2.0 10^2
-1.5 10^2
-1.0 10^2
-50
0
50
Axial Stress (Pa)
z = .01667 (m)
z = .0667 (m)
z = .1 (m)
z = .15 (m)

Figure 3.19

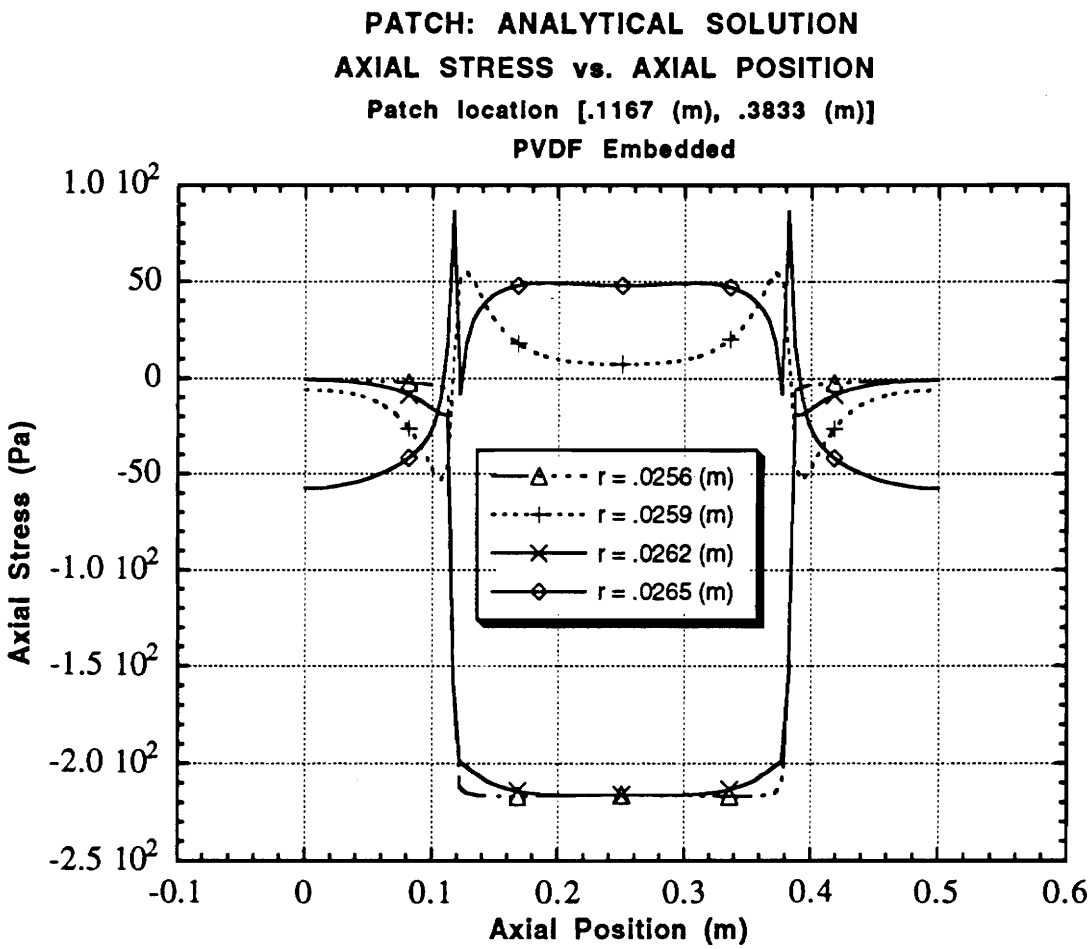
PATCH: ANALYTICAL SOLUTION
AXIAL STRESS vs. AXIAL POSITION
Patch location [.1167 (m), .3833 (m)]
PVDF Embedded
1.0 10^2
50
0
-50
-1.0 10^2
-1.5 10^2
-2.0 10^2
-2.5 10^2
Axial Stress (Pa)
-0.1
0
0.1
0.2
0.3
0.4
0.5
0.6
Axial Position (m)
r = .0256 (m)
r = .0259 (m)
r = .0262 (m)
r = .0265 (m)

Figure 3.20

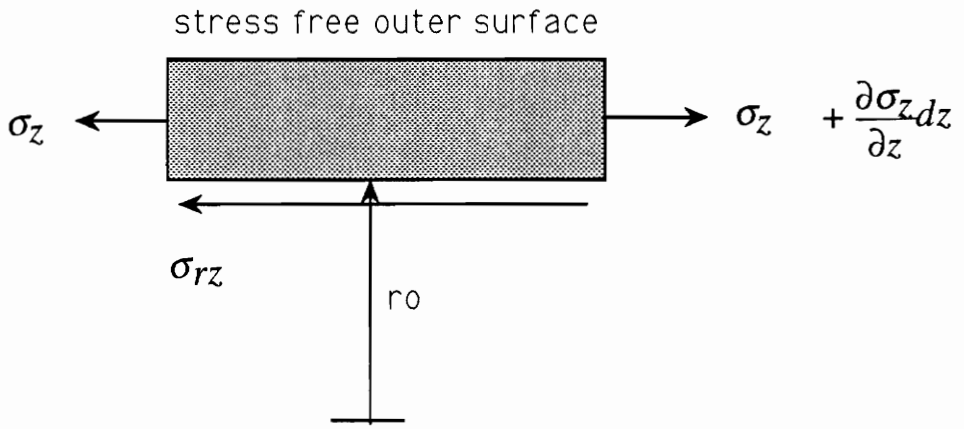

Figure 3.21 Free Body Diagram of Outer Lamina

equation is found.

$$\frac{\partial \sigma_z}{\partial z} r dr d\theta = r_o 2\pi \sigma_{rz} \tag{3.92}$$

Therefore, the rate of change of axial stress with respect to z depends upon shear stress. For example, using Figures 3.22 and 3.20, and considering a value of $r_o = .0265$ m in the figures, the axial stress variation with z follows according to the above equation except at the edges of the patch. At these points, Gibb's phenomenon affects the axial stress and a jag in the curve is present. However, because of the apparent insensitivity of interlaminae shear stresses to Gibb's phenomenon, the actual trace of the axial stress as the edge of the patch is crossed may be visualized and can be seen in results given by the FE solution shown in Figure 3.23. The FE solution did not suffer from this problem and the axial stresses follow exactly according to the above equation including the points at the edges of the patch. At all other values of r given in Figure 3.20, Gibb's phenomenon does not appear and both the analytical and FE results match identically. As a concluding note to this topic, it is interesting that at the edge of the patch, the FE solution gives better results for axial stresses than the analytical solution. However, with respect to the interlaminae shear stresses, the analytical solution gave good results as indicated in Figure 3.22, whereas the FE solution as presented here could not.

The distribution of shear stress is connected to another interesting result. As might be expected, the maximum shear levels occur at the edge of the patch, however, their location does not occur at interlaminate positions through the thickness. This suggests that the axial expansion near the edge of the patch is not the predominate

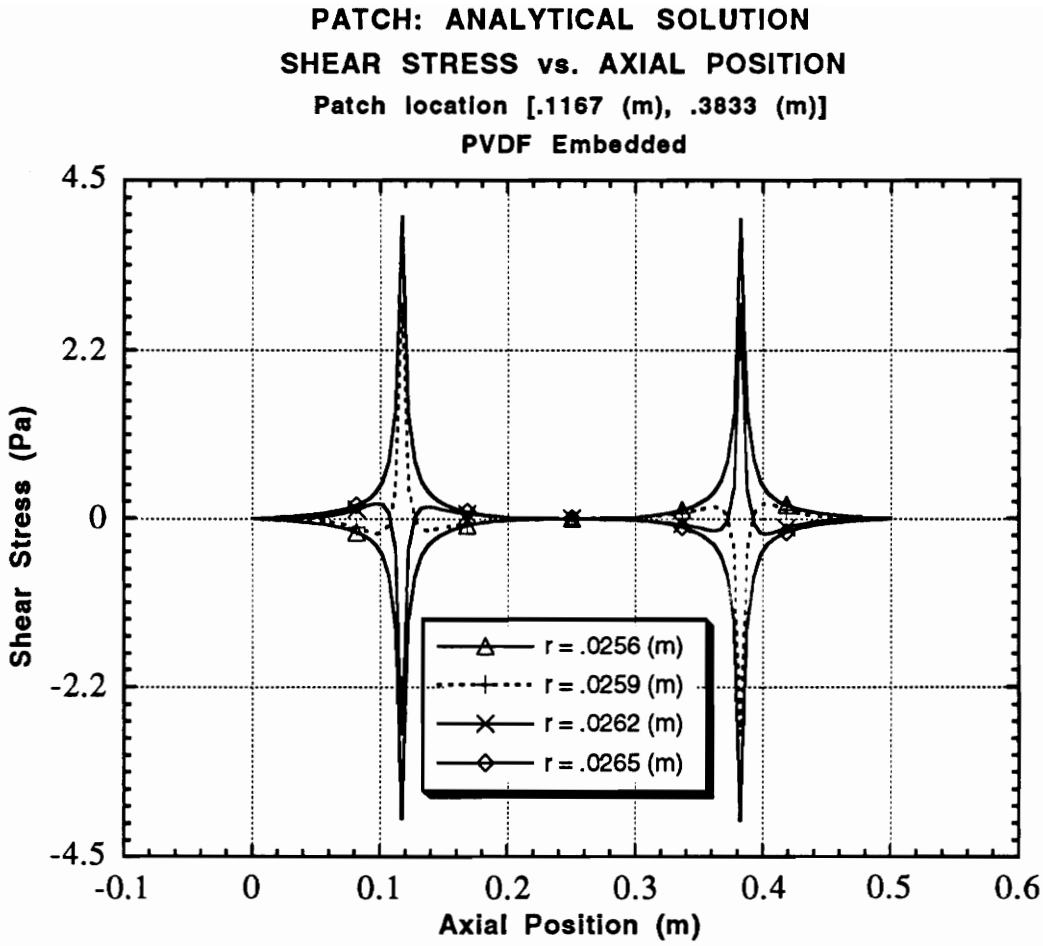
PATCH: ANALYTICAL SOLUTION
SHEAR STRESS vs. AXIAL POSITION
Patch location [.1167 (m), .3833 (m)]
PVDF Embedded
4.5
2.2
0
-2.2
-4.5
Shear Stress (Pa)
-0.1
0
0.1
0.2
0.3
0.4
0.5
0.6
Axial Position (m)
r = .0256 (m)
r = .0259 (m)
r = .0262 (m)
r = .0265 (m)

Figure 3.22

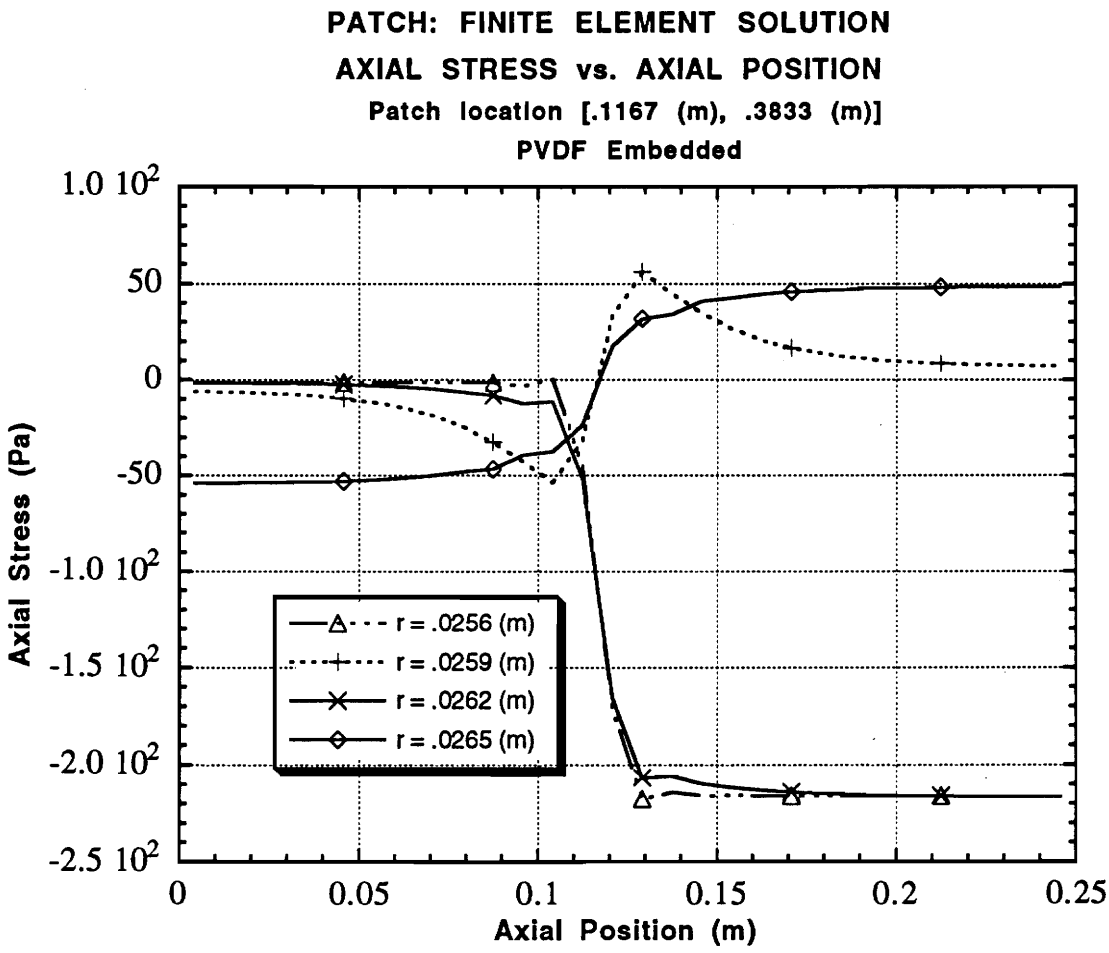
PATCH: FINITE ELEMENT SOLUTION
AXIAL STRESS vs. AXIAL POSITION
Patch location [.1167 (m), .3833 (m)]
PVDF Embedded
1.0 10^2
50
0
-50
-1.0 10^2
-1.5 10^2
-2.0 10^2
-2.5 10^2
Axial Stress (Pa)
0
0.05
0.1
0.15
0.2
0.25
Axial Position (m)
r = .0256 (m)
r = .0259 (m)
r = .0262 (m)
r = .0265 (m)

Figure 3.23

cause by which shear stresses are introduced. Antisymmetric, parabolic shear stress distributions are given in Figures 3.24 and 3.25. These curves suggest that local rather than global bending is present based upon their antisymmetric shapes. At this stage of the analysis, the exact mechanism by which this occurs has not been determined.

The last result discussed in this section is related to a convergence phenomenon encountered for radial stress calculations. Some results presented have had isolated appearances of Gibb's phenomenon. For example, Gibb's phenomenon appeared in the outer layer only, for axial stresses as a function of z given in Figure 3.20. It also appeared in the outer layer only for radial displacements as a function of z given in Figure 3.17. In these cases, it is not very bothersome because it is isolated and in the case of axial stresses it is possible to argue on other grounds to determine exactly what is happening at these points. In contrast with these two cases, radial stresses were found to be very sensitive to Gibb's phenomenon. They were also sensitive to the number of terms taken in the Fourier series. Figures 3.26 through 3.28 indicate the behavior obtained when using the first 50, 75 and 100 non-zero Fourier coefficients respectively in the solution. Beyond 100, this type of behavior appears to continue. The converged nature of Figure 3.28 explodes and behaves in a manner similar to that indicated in Figures 3.26 and 3.27. It may be that for this problem, a converged smooth curve is not possible for radial stresses. However, if the average values for the modulated curves inside the patch area are taken, the same results are given in all three figures. In spite of the modulations, the radial stress distribution inside the patch area is almost identical to that obtained for Case II. This is indicated

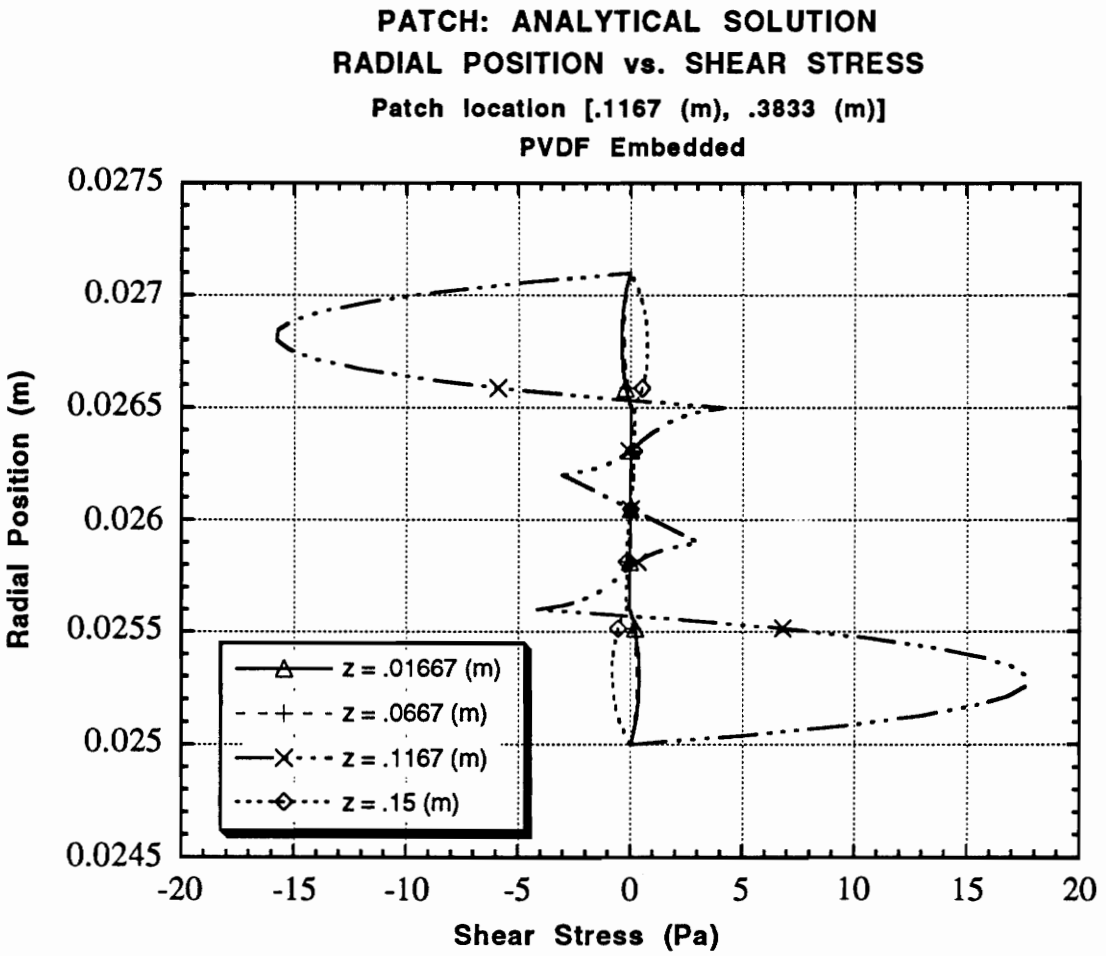
PATCH: ANALYTICAL SOLUTION
RADIAL POSITION vs. SHEAR STRESS
Patch location [.1167 (m), .3833 (m)]
PVDF Embedded
Radial Position (m)
0.0275
0.027
0.0265
0.026
0.0255
0.025
0.0245
-20
-15
-10
-5
0
5
10
15
20
Shear Stress (Pa)
z = .01667 (m)
z = .0667 (m)
z = .1167 (m)
z = .15 (m)

Figure 3.24

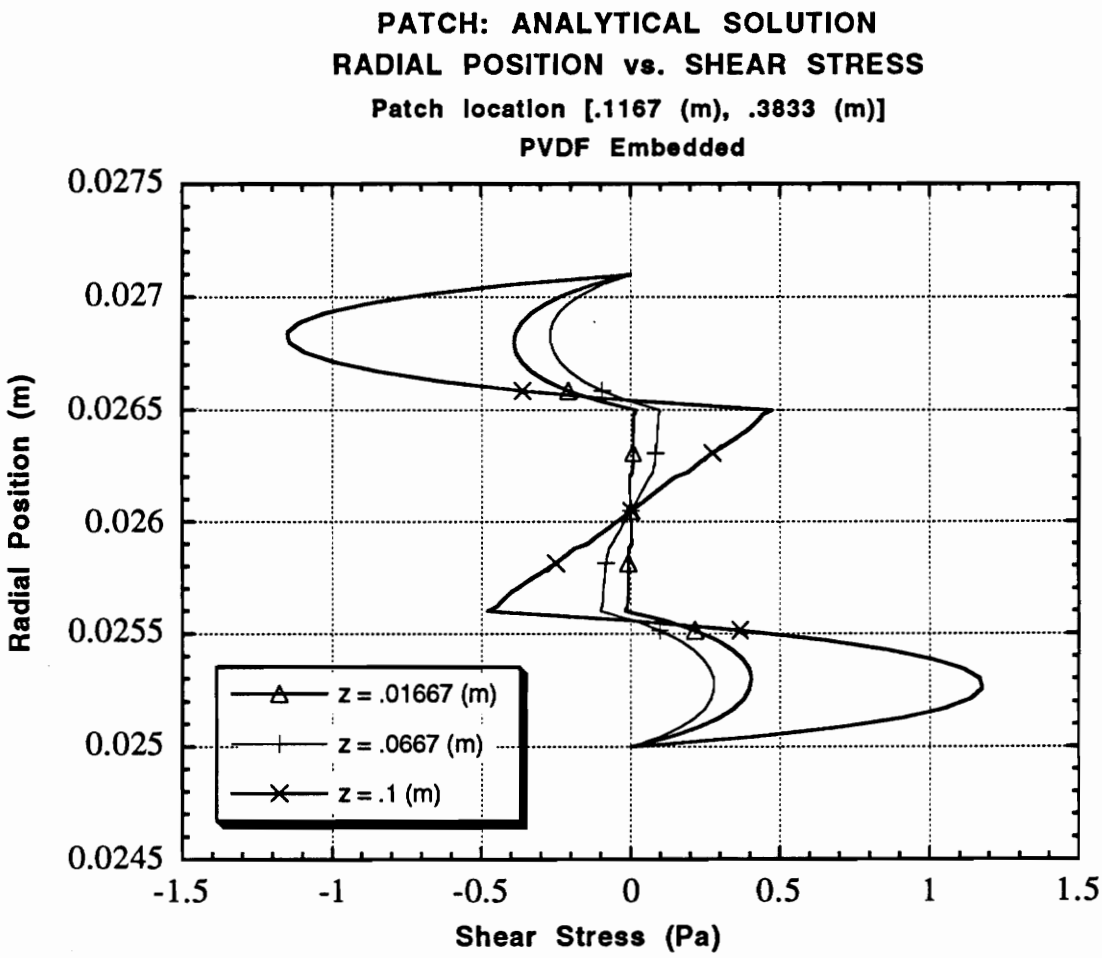
PATCH: ANALYTICAL SOLUTION
RADIAL POSITION vs. SHEAR STRESS
Patch location [.1167 (m), .3833 (m)]
PVDF Embedded
Radial Position (m)
0.0275
0.027
0.0265
0.026
0.0255
0.025
0.0245
-1.5
-1
-0.5
0
0.5
1
1.5
Shear Stress (Pa)
z = .01667 (m)
z = .0667 (m)
z = .1 (m)

Figure 3.25

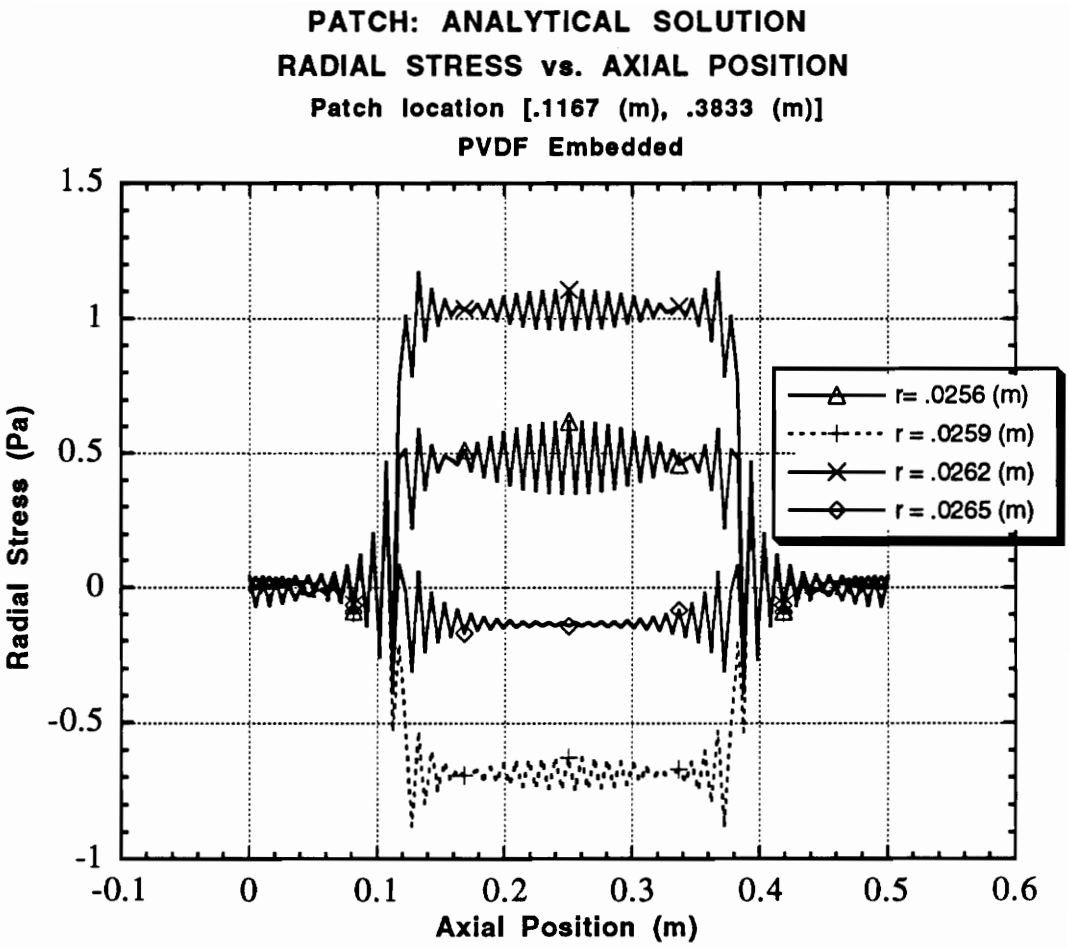
PATCH: ANALYTICAL SOLUTION
RADIAL STRESS vs. AXIAL POSITION
Patch location [.1167 (m), .3833 (m)]
PVDF Embedded
Radial Stress (Pa)
Axial Position (m)
1.5
1
0.5
0
-0.5
-1
-0.1
0
0.1
0.2
0.3
0.4
0.5
0.6
r= .0256 (m)
r = .0259 (m)
r = .0262 (m)
r = .0265 (m)

Figure 3.26

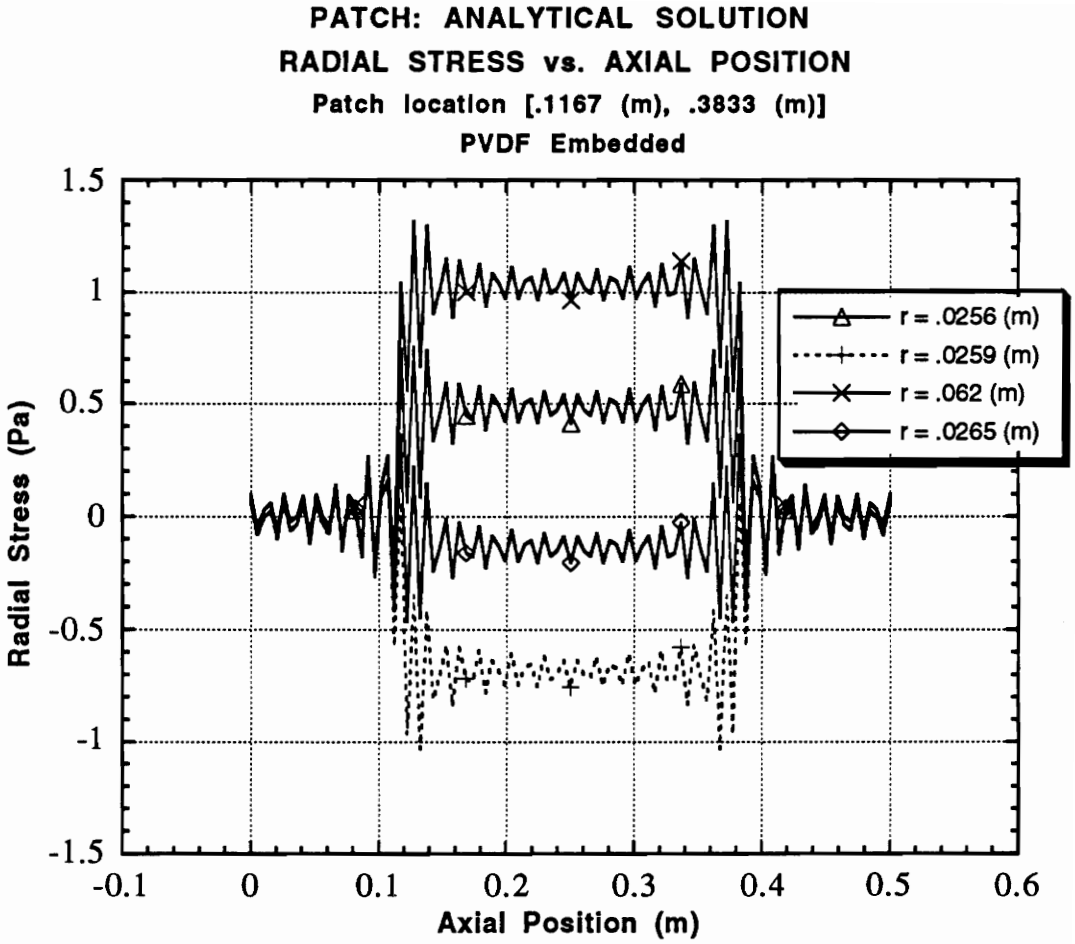
PATCH: ANALYTICAL SOLUTION
RADIAL STRESS vs. AXIAL POSITION
Patch location [.1167 (m), .3833 (m)]
PVDF Embedded
Radial Stress (Pa)
Axial Position (m)
1.5
1
0.5
0
-0.5
-1
-1.5
-0.1
0
0.1
0.2
0.3
0.4
0.5
0.6
r = .0256 (m)
r = .0259 (m)
r = .062 (m)
r = .0265 (m)

Figure 3.27

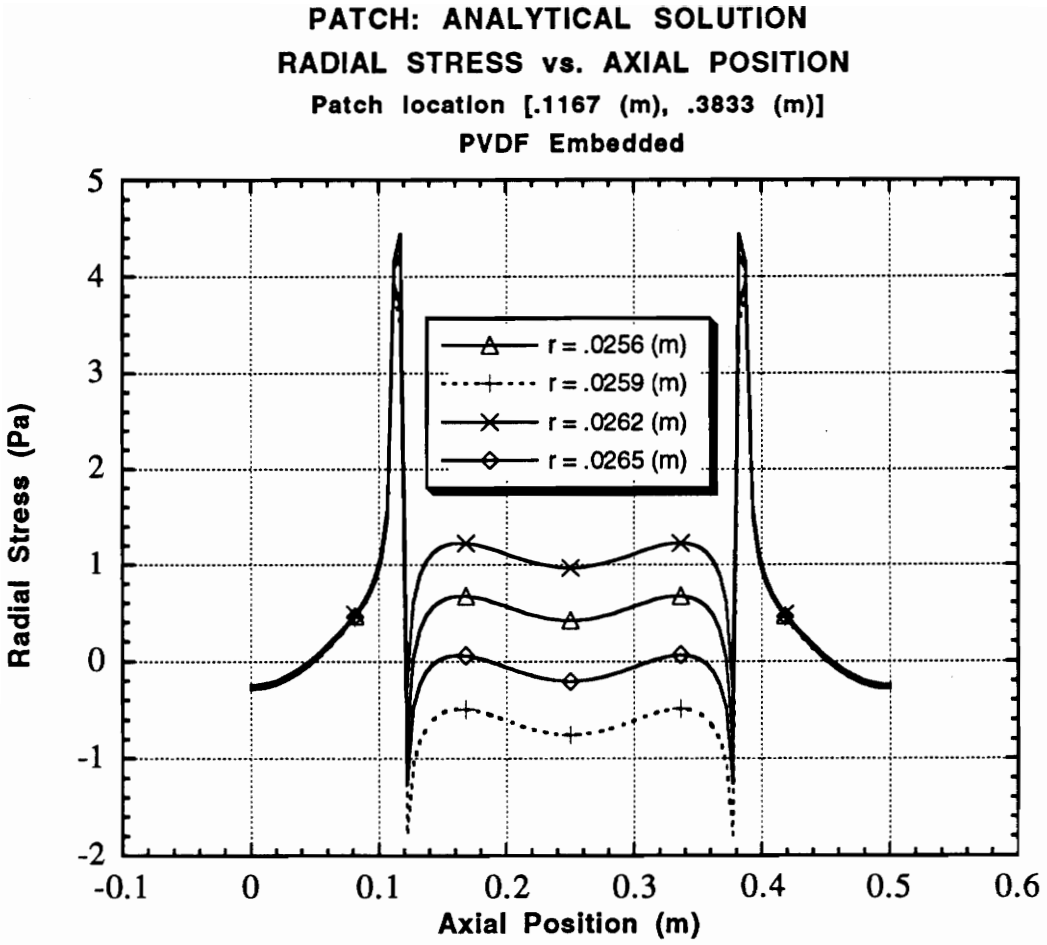
PATCH: ANALYTICAL SOLUTION
RADIAL STRESS vs. AXIAL POSITION
Patch location [.1167 (m), .3833 (m)]
PVDF Embedded
r = .0256 (m)
r = .0259 (m)
r = .0262 (m)
r = .0265 (m)
Radial Stress (Pa)
Axial Position (m)
5
4
3
2
1
0
-1
-2
-0.1
0
0.1
0.2
0.3
0.4
0.5
0.6

Figure 3.28

in Figure 3.29. The FE solution also had difficulties with radial stresses, although inside the patch area it converged to the same average values just described. At the edge of the patch, the FE solution did not give reasonable results. FE results are given in Figure 3.30.

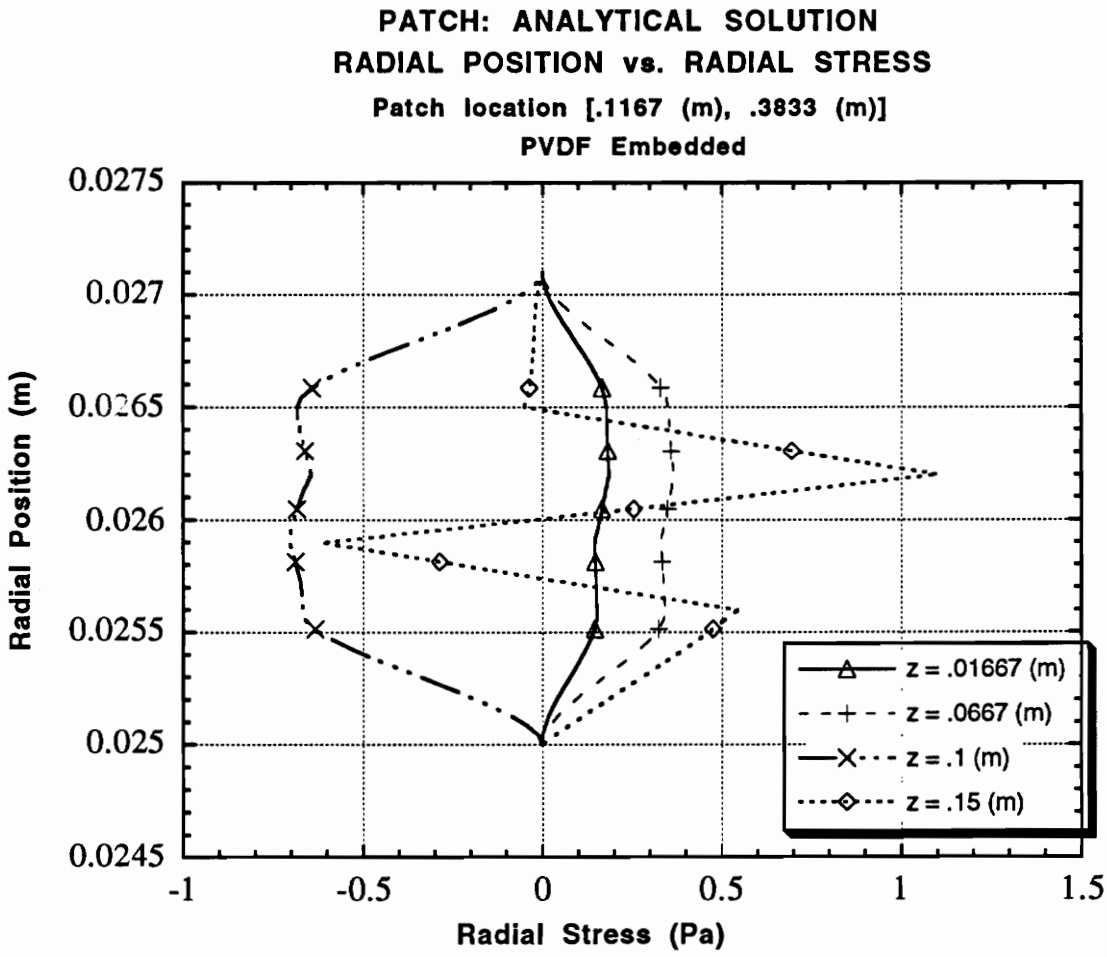
PATCH: ANALYTICAL SOLUTION
RADIAL POSITION vs. RADIAL STRESS
Patch location [.1167 (m), .3833 (m)]
PVDF Embedded
Radial Position (m)
0.0275
0.027
0.0265
0.026
0.0255
0.025
0.0245
-1
-0.5
0
0.5
1
1.5
Radial Stress (Pa)
z = .01667 (m)
z = .0667 (m)
z = .1 (m)
z = .15 (m)

Figure 3.29

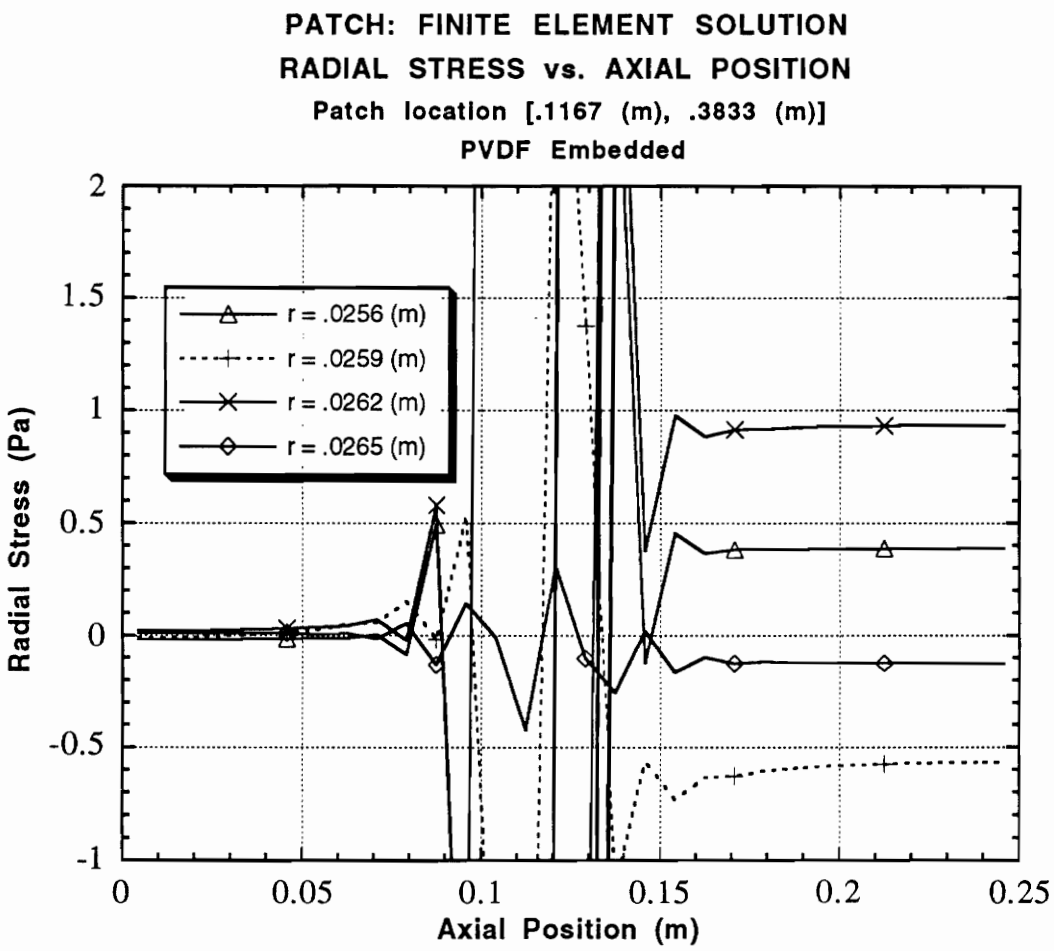
PATCH: FINITE ELEMENT SOLUTION
RADIAL STRESS vs. AXIAL POSITION
Patch location [.1167 (m), .3833 (m)]
PVDF Embedded
r = .0256 (m)
r = .0259 (m)
r = .0262 (m)
r = .0265 (m)
Radial Stress (Pa)
Axial Position (m)
2
1.5
1
0.5
0
-0.5
-1
0
0.05
0.1
0.15
0.2
0.25

Figure 3.30

CHAPTER 4

An Application of the Cylindrical Truss Element Actuator

4.1 Introduction

In this chapter, equations of motion for a 2D truss are derived. It is assumed that displacements are small and that each member undergoes axial deformations only. First the truss is discretized in space using the finite element method and the kinetic and potential energies are derived for each element. It follows that the kinetic and potential energy is a superposition of that from the elements. Using this and the fact that forces must be continuous throughout, global stiffness and mass matrices are assembled. Damping is added to the system via the cylindrical truss element actuator given in Chapter 3 and is modelled mathematically using Rayleigh's dissipation function. Using Lagrange's equations of motion, the governing equations for the vibration of the truss depicted in Figure 4.1 are derived. The truss is fixed at the base while the base is rotated with angular velocity and acceleration ω and $\dot{\omega}$ respectively. This rotation serves as a disturbance to the system and is a realistic representation of a truss structure being maneuvered in space. The resulting motions are calculated numerically using the Newmark method.

4.2 Equations of Motion

A position vector $\mathbf{R}$ defines a point in the truss.

$$\mathbf{R} = \mathbf{r} + \mathbf{u} \tag{4.1}$$

$\mathbf{r}$ represents the undeformed position expressed in terms of the rotating basis vectors $\mathbf{b_1}, \mathbf{b_2}, \mathbf{b_3}$ and $\mathbf{u}$ represents the elastic deformation relative to the undeformed position

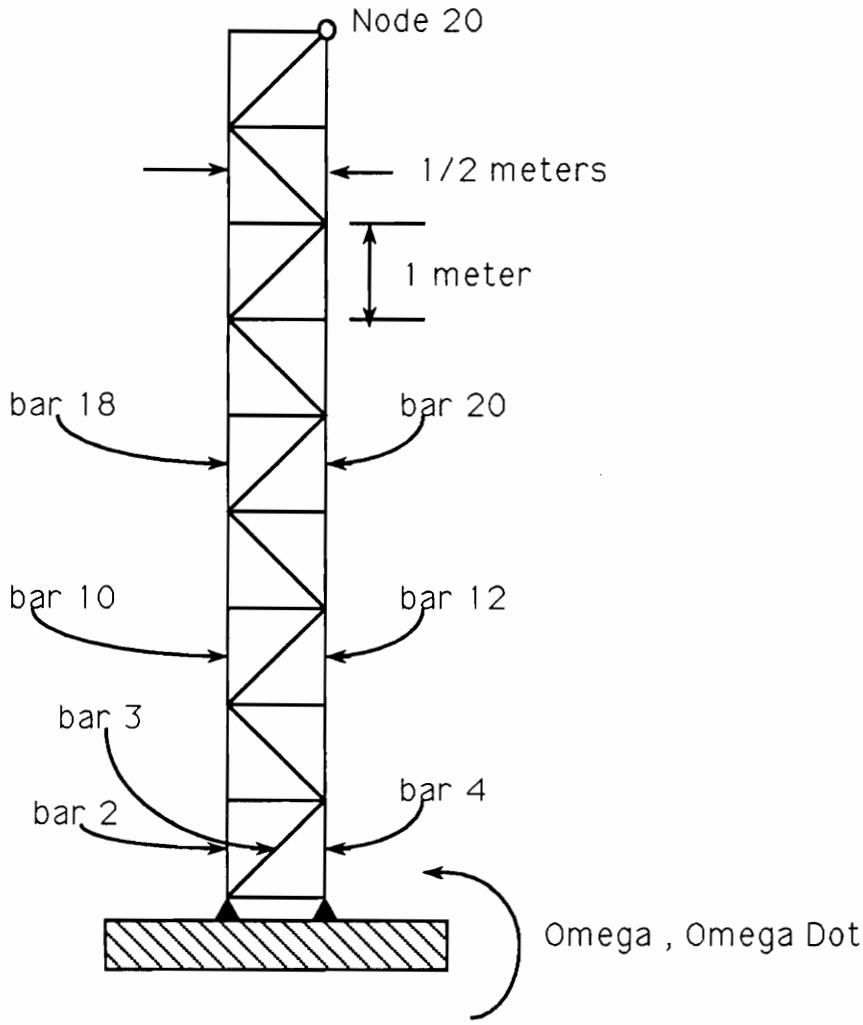

Figure 4.1 Truss Model

and expressed in a local rotating coordinate system $\mathbf{m_1}, \mathbf{m_2}, \mathbf{m_3}$. The velocity $\dot{\mathbf{R}}$ is given by

$$\dot{\mathbf{R}} = \boldsymbol{\omega} \times \mathbf{r} + \boldsymbol{\beta} \times \mathbf{u} + \dot{\mathbf{u}} \tag{4.2}$$

Where $\boldsymbol{\omega}$ and $\boldsymbol{\beta}$ are the absolute angular velocities of the $\{\mathbf{b}\}$ and $\{\mathbf{m}\}$ coordinate systems respectively. Using Eq. (4.2), the kinetic energy T is given by

$$T = \frac{1}{2}\int_D \dot{\mathbf{R}} \cdot \dot{\mathbf{R}} dm \tag{4.3}$$

Before proceeding, it is useful to compute $\dot{\mathbf{R}} \cdot \dot{\mathbf{R}}$ and simplify the expression based upon small displacements and the fact that the problem being considered is 2D. The following vector identity is helpful.

$$\mathbf{A} \times \mathbf{B} \times \mathbf{C} = \mathbf{B}(\mathbf{A} \cdot \mathbf{C}) - \mathbf{C}(\mathbf{A} \cdot \mathbf{B}) \tag{4.4}$$

Performing the dot product in (4.3) gives

$$\begin{aligned} \dot{\mathbf{R}} \cdot \dot{\mathbf{R}} =& (\boldsymbol{\omega} \times \mathbf{r}) \cdot (\boldsymbol{\omega} \times \mathbf{r}) + 2(\boldsymbol{\omega} \times \mathbf{r}) \cdot (\boldsymbol{\beta} \times \mathbf{u}) \\ &+ 2(\boldsymbol{\omega} \times \mathbf{r}) \cdot \dot{\mathbf{u}} + (\boldsymbol{\beta} \times \mathbf{u}) \cdot (\boldsymbol{\beta} \times \mathbf{u}) \\ &+ 2(\boldsymbol{\beta} \times \mathbf{u}) \cdot \dot{\mathbf{u}} + \dot{\mathbf{u}} \cdot \dot{\mathbf{u}} \end{aligned} \tag{4.5}$$

The second term can be written in the form of a scalar triple product

$$(\boldsymbol{\omega} \times \mathbf{r}) \cdot (\boldsymbol{\beta} \times \mathbf{u}) = \mathbf{u} \cdot (\boldsymbol{\omega} \times \mathbf{r}) \times \boldsymbol{\beta} = \boldsymbol{\beta} \cdot [\mathbf{u} \times (\boldsymbol{\omega} \times \mathbf{r})] \tag{4.6}$$

The vector identity in Eq. (4.4) can be applied to Eq. (4.6) giving

$$\boldsymbol{\beta} \cdot (\mathbf{u} \times (\boldsymbol{\omega} \times \mathbf{r})) = \boldsymbol{\beta} \cdot (\boldsymbol{\omega}(\mathbf{u} \cdot \mathbf{r}) - \mathbf{r}(\mathbf{u} \cdot \boldsymbol{\omega})) \tag{4.7}$$

Due to the fact that truss deflections $\mathbf{u}$ are in the plane perpendicular to rotations $\boldsymbol{\beta}$ and $\boldsymbol{\omega}$, (4.7) reduces to

$$\boldsymbol{\beta} \cdot (\mathbf{u} \times \boldsymbol{\omega} \times \mathbf{r}) = \beta \cdot \boldsymbol{\omega}(\mathbf{u} \cdot \mathbf{r}) \tag{4.8}$$

Using similar arguments for the remaining terms, Eq. (4.5) can be written for 2D motion as

$$\begin{aligned} \dot{\mathbf{R}} \cdot \dot{\mathbf{R}} =& \omega^2(\mathbf{r} \cdot \mathbf{r}) + 2\beta\omega(\mathbf{u} \cdot \mathbf{r}) + 2\omega \cdot (\mathbf{r} \times \dot{\mathbf{u}}) \\ &+ 2\beta^2(\mathbf{u} \cdot \mathbf{u}) + 2\beta \cdot (\mathbf{u} \times \dot{\mathbf{u}}) + \dot{\mathbf{u}} \cdot \dot{\mathbf{u}} \end{aligned} \tag{4.9}$$

The second simplifying assumption is based upon deformations of the truss. The elastic deformation $\mathbf{u}$ is expressed relative to a local bar coordinate system given in Figure 4.2. For this analysis it is assumed that the rotation of the local coordinate system is the same as that of the global coordinate system. The bar is assumed to translate only. Therefore $\boldsymbol{\beta}$ can be taken equivalent to ω and equation (4.9) becomes

$$\begin{aligned} \dot{\mathbf{R}} \cdot \dot{\mathbf{R}} =& \omega^2(\mathbf{r} \cdot \mathbf{r}) + 2\omega^2(\mathbf{u} \cdot \mathbf{r}) + 2\omega \cdot (\mathbf{r} \times \dot{\mathbf{u}}) \\ &+ 2\omega^2(\mathbf{u} \cdot \mathbf{u}) + 2\omega \cdot (\mathbf{u} \times \dot{\mathbf{u}}) + \dot{\mathbf{u}} \cdot \dot{\mathbf{u}} \end{aligned} \tag{4.10}$$

The next step is to discretize the domain. Using the finite element method, each bar is modeled as one element where the displacement of a point x along the bar is expressed in terms of nodal displacements and interpolation functions. Taking

$$\mathbf{u} = p(x,t)\mathbf{m}_1 + q(x,t)\mathbf{m}_2 \tag{4.11}$$

then the components of $\mathbf{u}$ can be expressed using linear interpolation functions $L_1(x)$

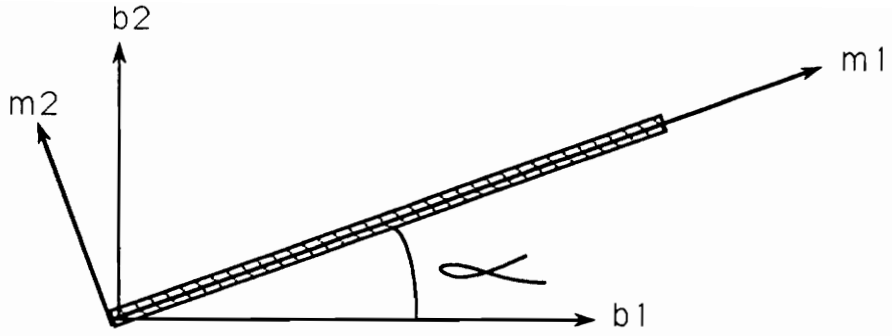

Figure 4.2 Local Bar Coordinate System

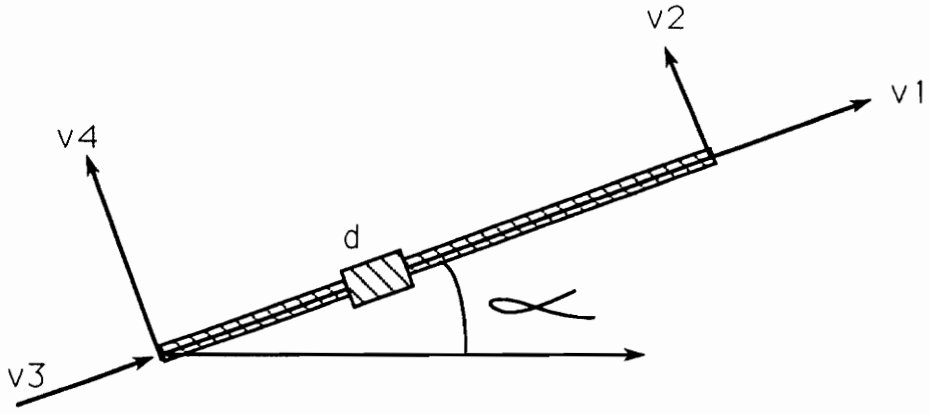

Figure 4.3 Nodal coordinates and Dashpot

and $L_2(x)$ as

$$\begin{Bmatrix} q(x,t) \\ q(x,t) \end{Bmatrix} = \begin{bmatrix} L_1 & 0 & L_2 & 0 \\ 0 & L_1 & 0 & L_2 \end{bmatrix} \begin{Bmatrix} v_1 \\ v_2 \\ v_3 \\ v_4 \end{Bmatrix} \tag{4.12}$$

where v_1, v_2, v_3 and v_4 are nodal displacements as given in Figure 4.3. Using Eqs. (4.3), (4.10) and (4.12), the kinetic energy of an element can be expressed in terms of nodal displacements and velocities. To this end, tensor notation is used to proceed with the vector operations in Eq. (4.10).

The position vector $\mathbf{r}$ is taken to be expressed in local coordinates as

$$\mathbf{r} = r_1\mathbf{m}_1 + r_2\mathbf{m}_2 \tag{4.13}$$

Components of $\mathbf{r}$ are given by

$$\mathbf{r} \rightarrow r_i \tag{4.14}$$

Equation 4.12 is written in tensor notation as

$$u_i = L_{ij}v_j \tag{4.15}$$

In addition, it is necessary to express nodal displacements in one coordinate system such that the equation of motion for the entire truss may be assembled. Therefore the following vector transformation is used

$$v_i = C_{ij}u_j^* \tag{4.16}$$

where C_{ij} are elements of the direction cosine matrix given by

$$C = \begin{bmatrix} \cos\alpha & \sin\alpha & 0 & 0 \\ -\sin\alpha & \cos\alpha & 0 & 0 \\ 0 & 0 & \cos\alpha & \sin\alpha \\ 0 & 0 & -\sin\alpha & \cos\alpha \end{bmatrix} \tag{4.17}$$

and $\mathbf{u}^*$ is a vector of global nodal displacements.

$$\mathbf{u}^* = \begin{Bmatrix} u_1^* \\ u_2^* \\ u_3^* \\ u_4^* \end{Bmatrix} \tag{4.18}$$

Equations (4.15) through (4.17) are now used in Eq. (4.10), which defines $\dot{\mathbf{R}} \cdot \dot{\mathbf{R}}$, and then Eq. (4.10) is substituted into Eq. (4.3) for the kinetic energy. Doing so gives

$$T = \omega^2 m_1 u^* + \omega m_2 \dot{u}^* + \omega^2 u^{*T} m_3 u^* + \omega u^{*T} m_4 \dot{u}^* + \frac{1}{2} \dot{u}^{*T} m_5 \dot{u}^* \tag{4.19}$$

where

$$\underset{(4 \times 1)}{m_1} = \int_0^\ell [\rho(x) r_i L_{i\ell} C_{\ell n}] dx \tag{4.20}$$

$$\underset{(4 \times 1)}{m_2} = \int_0^\ell \rho(x) [r_1 L_{2\ell} - r_2 L_{1\ell}] C_{\ell m} dx \tag{4.21}$$

$$\underset{(4 \times 4)}{m_3} = \int_0^\ell [\rho(x) L_{ij} L_{ik} C_{jn} C_{k\ell}] dx \tag{4.22}$$

$$\underset{4 \times 4}{m_4} = \int_0^\ell \rho(x) [L_{1\ell} L_{2n} - L_{2\ell} L_{1n}] C_{\ell p} C_{nm} dx \tag{4.23}$$

$$m_5 = m_3 \tag{4.24}$$

and $\rho(x)$ is the distribution of mass per unit length along the bar. In writing Eq. (4.19), the first term in Eq. (4.10) was dropped since it has no bearing on the equations of motion with respect to elastic deformations. The above matrices m_1, m_2, m_3, m_4 and m_5 have units length·mass, length·mass, mass, mass and mass respectively, and m_3 is symmetric while m_4 is skew-symmetric.

In a similar manner, the potential energy may be derived on an element basis. The potential energy V used here is that stored in the truss in the form of strain

energy and is given by[16]

$$V = \frac{1}{2}\int_o^\ell E(x)A(x)\left(\frac{\partial p}{\partial x}\right)^2 dx \tag{4.25}$$

Only the component of displacement along the axis of the bar contributes to the strain energy since transverse displacements are rigid body displacements. E and A are Young's modulus and the cross sectional area of the bar respectively and may vary along the length of the bar. The notation established for the kinetic energy is applied here.

$$\left(\frac{\partial p}{\partial x}\right)^2 = Q'_{ij}Q'_{ik}C_{jn}C_{k\ell}u^*_n u^*_\ell \tag{4.26}$$

where Q'_{ij} are components of a modified interpolation function matrix given as

$$Q' = \begin{bmatrix} \frac{dL_1}{dx} & 0 & \frac{dL_2}{dx} & 0 \\ 0 & 0 & 0 & 0 \end{bmatrix} \tag{4.27}$$

Then the potential energy can be written as

$$V = \frac{1}{2}u^{*T}ku^* \tag{4.28}$$

where

$$k_{n\ell} = \int_0^\ell [E(x)A(x)Q'_{ij}Q'_{ik}C_{jn}C_{k\ell}]dx$$

Rayleigh's dissapation function F is now given for an element with a viscous damper attached at its nodes as indicated in Figure 4.3. Damping is induced due to axial velocities only and the damping matrix D for an element is given by

$$D = d\begin{bmatrix} 1 & 0 & -1 & 0 \\ 0 & 0 & 0 & 0 \\ -1 & 0 & 1 & 0 \\ 0 & 0 & 0 & 0 \end{bmatrix} \tag{4.29}$$

where the magnitude of the damping is given by d. Rayleigh's dissipation function[16] is given as

$$F = \frac{1}{2} D_{rs} \dot{v}_r \dot{v}_s = \frac{1}{2} \dot{u}^T D^* \dot{u} \tag{4.30}$$

where $D^* = C^T D C$.

Now all the necessary ingredients have been calculated and Lagrange's equation of motion may be applied. This equation is given as[16]

$$\frac{d}{dt}\left[\frac{\partial T}{\partial \dot{u}^*}\right] - \frac{\partial T}{\partial u^*} + \frac{\partial V}{\partial u^*} + \frac{\partial F}{\partial \dot{u}^*} = 0 \tag{4.31}$$

Substituting T, V, and F into Eq. (4.31) gives the following element equations of motion for the elastic deformation of the truss.

$$m_5 \ddot{u}^* + [\omega(m_4^T - m_4) + D^*]\dot{u}^* + [\dot{\omega} m_4^T - 2\omega^2 m_3 + k]u^* = \omega^2 m_1 - \dot{\omega} m_2 \tag{4.32}$$

As mentioned in the previous section, it is necessary to assemble the element mass, damping and stiffness matrices. This was done using FEM1D.[14] In addition, the equations of motion were solved numerically using the Newmark method[21] in conjunction with FEM1D.

The Newmark method gives approximations for u and its first time derivative $\dot{u}$ at the $(s+1)^{th}$ time step as

$$u_{s+1} = u_s + \Delta t \dot{u}_s + \frac{(\Delta t)^2}{2} \ddot{u}_{s+\gamma} \tag{4.33a}$$

$$\dot{u}_{s+1} = \dot{u}_s + \ddot{u}_{s+\alpha} \Delta t \tag{4.33b}$$

Equation (4.32) is written for the $(s+1)^{th}$ time step as

$$m_{s+1} \ddot{u}_{s+1} + c_{s+1} \dot{u}_{s+1} + k_{s+1} u_{s+1} = f_{s+1} \tag{4.34}$$

Substituting Eqs. (4.33) into (4.34) yields a linear algebraic equation in u_{s+1}. This equation is given as

$$A_{s+1}u_{s+1} = B_{s+1} \tag{4.35}$$

where

$$A_{s+1} = \frac{2}{(\Delta t)^2}\frac{m_{s+1}}{\gamma} + \frac{2\alpha}{\gamma\Delta t}c_{s+1} + k_{s+1} \tag{4.35a}$$

$$\begin{aligned} B_{s+1} =& f_{s+1} + \left[\frac{2}{(\Delta t)^2}\frac{u_s}{\gamma} + \frac{2}{\Delta t}\frac{\dot{u}_s}{\gamma} + \frac{(\gamma-1)}{\gamma}\ddot{u}_s\right] m_{s+1} \\ & - c_{s+1}\left[-\frac{2\alpha}{\gamma\Delta t}u_s + \left(1-\frac{2\alpha}{\gamma}\right)\dot{u}_s + \left(1-\frac{\alpha}{\gamma}\right)\Delta t\ddot{u}_s\right] \end{aligned} \tag{4.35b}$$

α and γ are parameters which determine the stability of the scheme.[21]

For this problem, $\alpha = \frac{1}{2}$ and $\gamma = \frac{1}{2}$ were used. In solving Eq. (4.35) it is necessary to use a full banded solver because the matrix m_4 in Eq. (4.32) is skew-symmetric. Using the Newmark method, the full non-autonomous nature of Eq. (4.32) may be accounted for in the solution.

4.3 Example

The problem chosen here demonstrates the usefulness of the cylindrical truss element acutator as an active damping member. A full study of Eq. (4.32) is not intended although it is possible using the numerical techniques described at the end of the previous section. However, it is worth mentioning the physical interpretation of the forcing terms on the right hand side of Eq. (4.32). The $\omega^2 m_1$ component represents a force generated normal to the path of motion of the truss, as it is rotated, and is the so called centrifugal force. The $\dot{\omega} m_2$ term is the force generated tangential to the path of motion and is due to the angular acceleration.

Time traces for ω and $\dot{\omega}$ used in the sample problem are given in Figure 4.4. The shape of these functions is realistic although the duration is not. It is likely that the rotation rate ω would be ramped up to some speed and then remain constant for sometime until the desired rotation is achieved and then ω would be ramped down. However because of the short duration taken here, no appreciable rotation takes place and the event merely serves as an initial disturbance to the truss.

Member properties for the truss were taken from Case II in the section on the cylindrical truss element actuator. The effects of PVDF layers on axial stiffness are negligible. For mass calculations, $\rho(x) = .3371\ kg/m$ for passive members and $\rho(x) = .5159\ kg/m$ for active members was used.

Figure 4.5 indicates the transverse displacement of node 20, as given in Figure 4.1, with and without active dampers present. Active damping members were placed in bars 2, 3, 4, 10, 12, 18, and 20 and are specially marked in Figure 4.1. Due to the geometry of the truss, response was very similar to what might be expected of a cantilevered beam. Due to the nature of the disturbance, only the first mode was excited. Points below node 20 responded in phase and with the same frequency as node 20 but with different amplitudes depending on position.

The response is indicative of what might be expected based upon physical intuition. Due to the magnitude of ω, ω^2 terms have negligible effect on the response and the forcing term with $\dot{\omega}$ dominates. In the ramp up, the truss responds by oscillating about a static equilibrium position of approximately $5 \times 10^{-5} m$. This corresponds to the constant angular acceleration. When the rotation reaches the

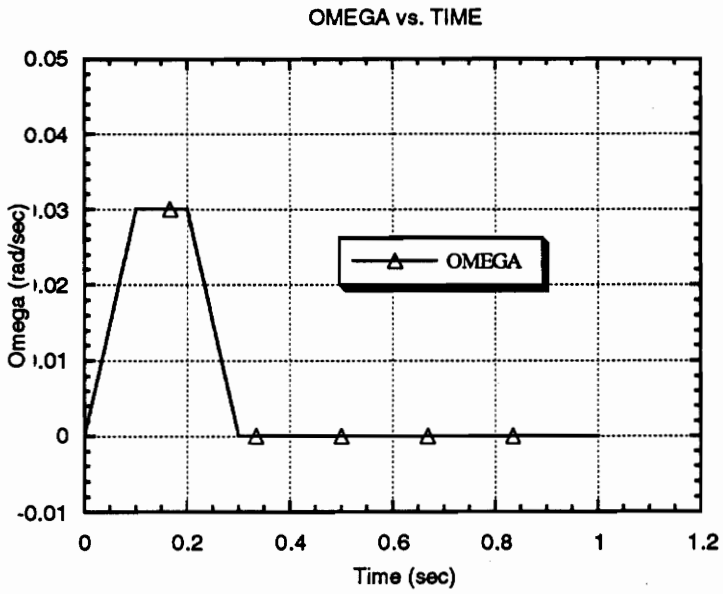
OMEGA vs. TIME
0.05
0.04
0.03
0.02
0.01
0
-0.01
Omega (rad/sec)
OMEGA
0
0.2
0.4
0.6
0.8
1
1.2
Time (sec)

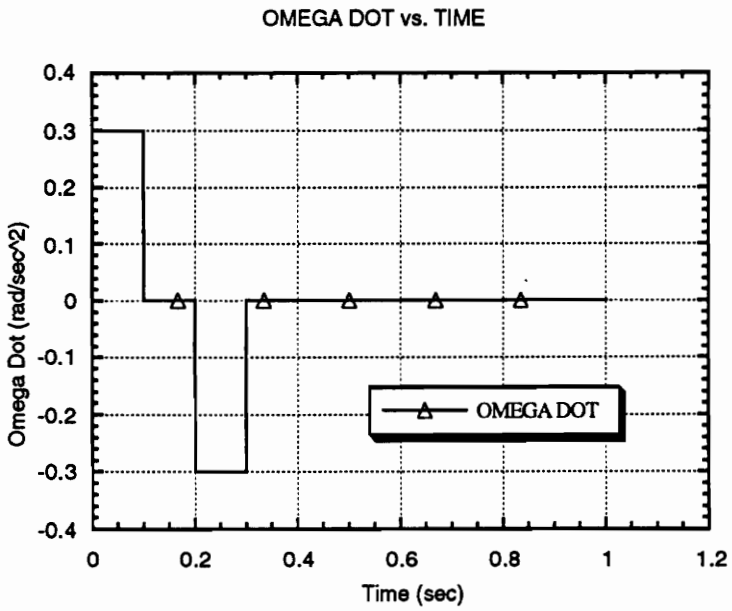
OMEGA DOT vs. TIME
0.4
0.3
0.2
0.1
0
-0.1
-0.2
-0.3
-0.4
Omega Dot (rad/sec^2)
OMEGA DOT
0
0.2
0.4
0.6
0.8
1
1.2
Time (sec)

Figure 4.4

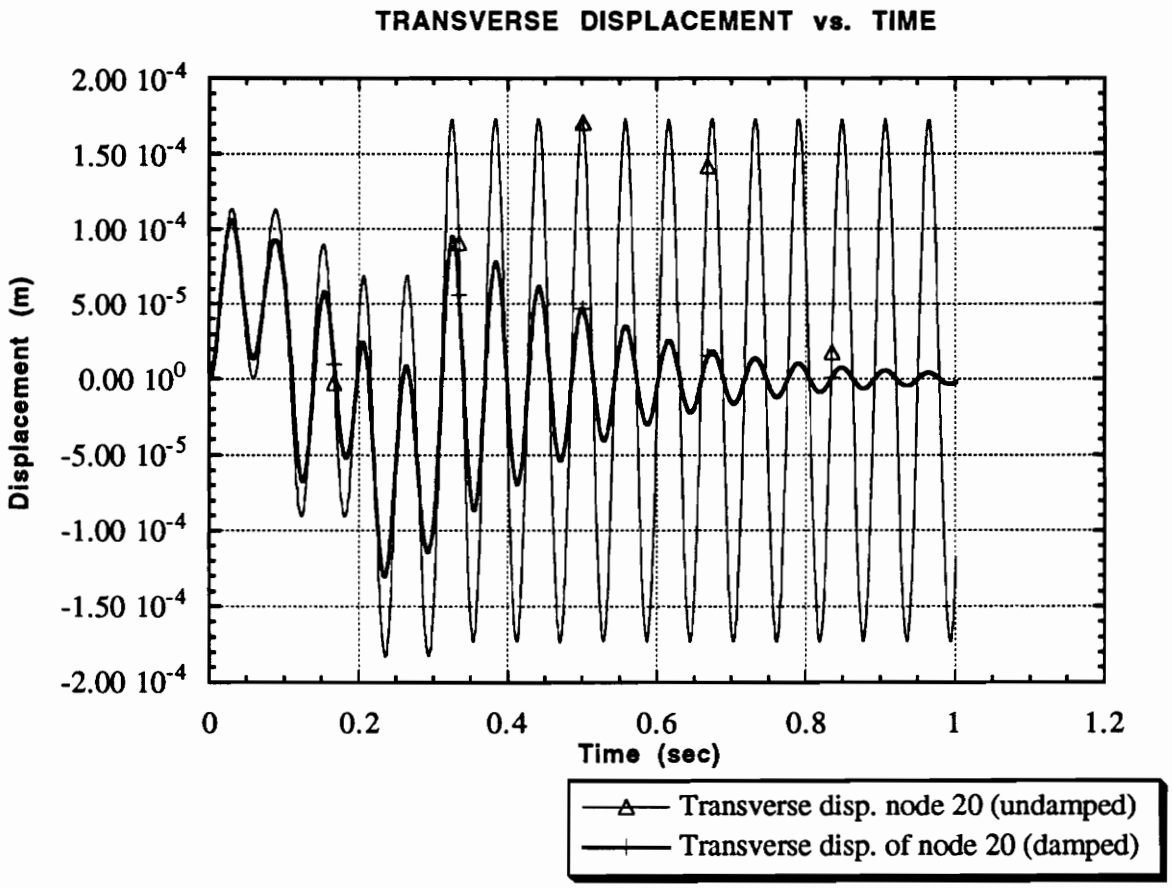
TRANSVERSE DISPLACEMENT vs. TIME
2.00 10-4
1.50 10-4
1.00 10-4
5.00 10-5
0.00 100
-5.00 10-5
-1.00 10-4
-1.50 10-4
-2.00 10-4
Displacement (m)
0
0.2
0.4
0.6
0.8
1
1.2
Time (sec)
Transverse disp. node 20 (undamped)
Transverse disp. of node 20 (damped)

Figure 4.5

plateau at .1 seconds, the truss oscillates about an equilibrium position which is nearly zero. Here, the angular acceleration is zero. Finally, on the ramp down, the truss sways to the opposite side and oscillates about a position on the negative side. This corresponds to the constant angular acceleration in the negative direction. Then when the disturbance is turned off, the truss undergoes free vibrations. In each stage of the process of the undamped case, the amplitude of vibration increases. This is because, in the various stages, strain energy is stored in the truss. Finally when all the external loads are removed, all the strain energy is free to be exchanged with the kinetic energy during oscillation. This effect is present but to a less extent when active members are present.

The active dampers effectively do two things. The first is that the maximum amplitude of oscillations during both the loading and free vibration stages are significantly reduced. The second and obvious result is that the vibrations decay to zero.

It is necessary to mention that for damping to be applied as indicated here, the nodal velocities must be known so that a feedback voltage may be applied. While the derivation was not given in this study, the active members may also be used to sense nodal velocities and therefore this is not a drawback.

Time traces of the damping forces generated in the various bars are given in Figures 4.6 through 4.9. The forces generated are based upon a maximum available voltage of 200 V. When the damping force was computed to be higher than what was achievable with the actuators using 200 V, then it was set to this maximum value.

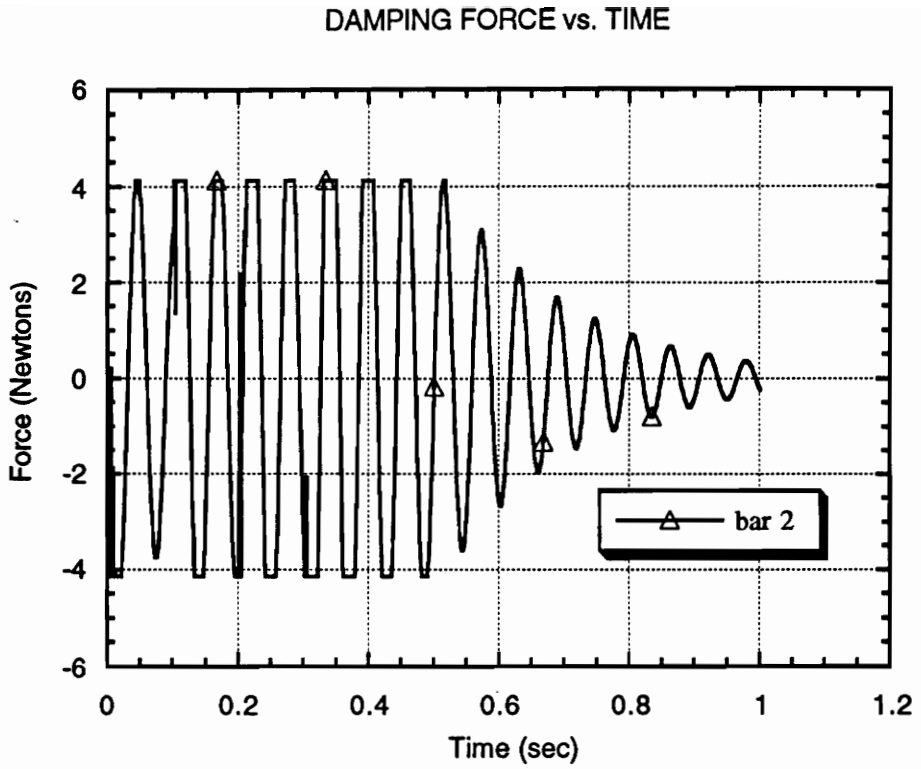
DAMPING FORCE vs. TIME
Force (Newtons)
6
4
2
0
-2
-4
-6
0
0.2
0.4
0.6
0.8
1
1.2
Time (sec)
bar 2

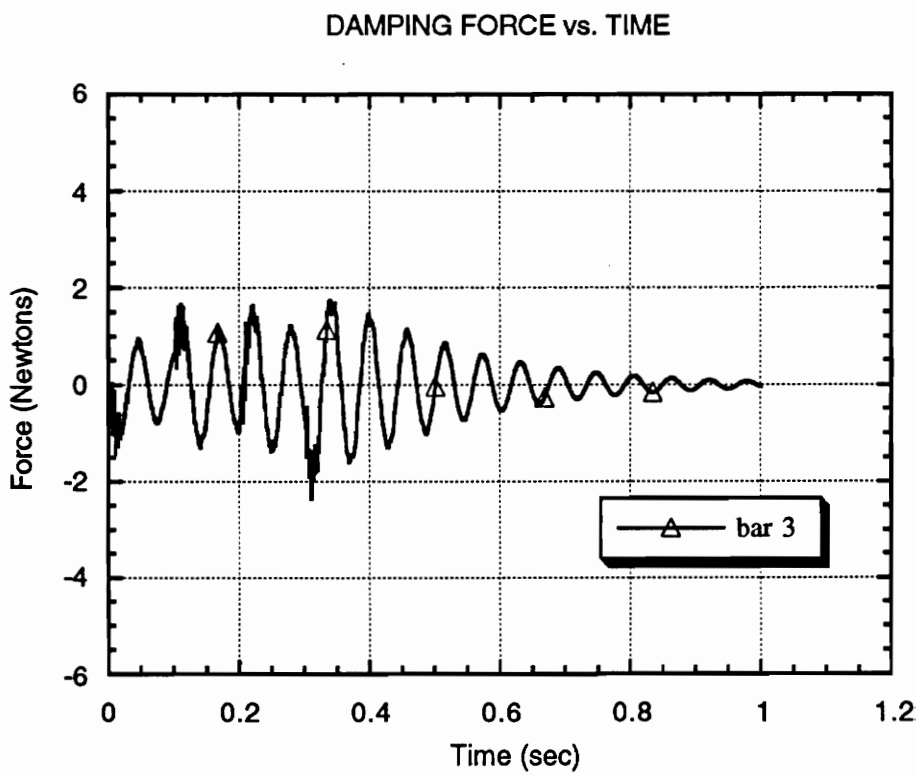
DAMPING FORCE vs. TIME
Force (Newtons)
6
4
2
0
-2
-4
-6
0
0.2
0.4
0.6
0.8
1
1.2
Time (sec)
bar 3

Figure 4.6

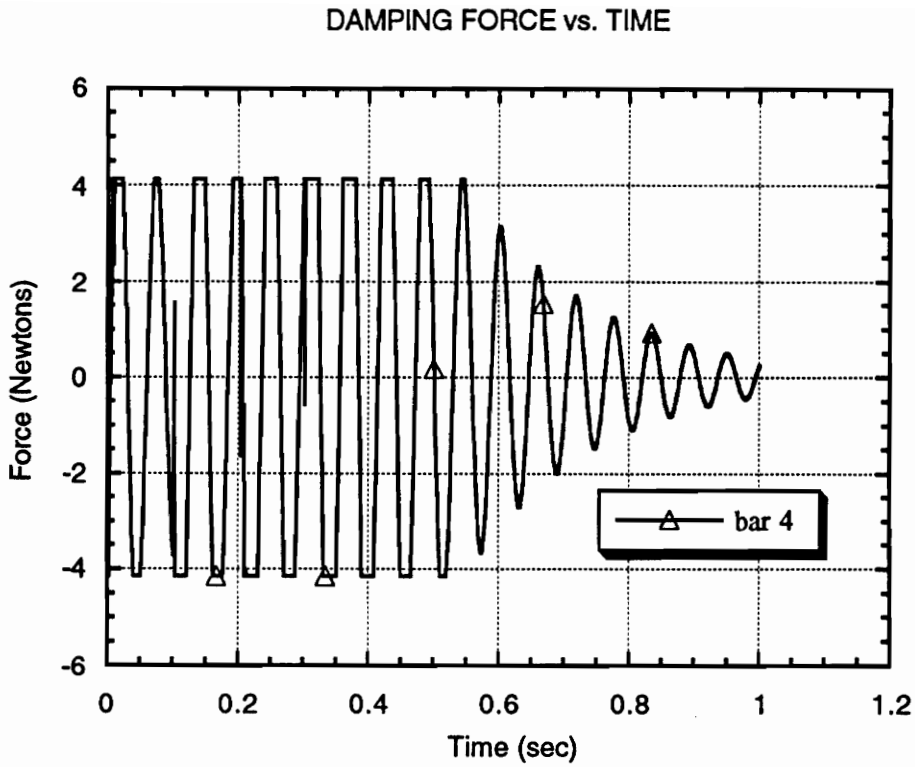
DAMPING FORCE vs. TIME
Force (Newtons)
6
4
2
0
-2
-4
-6
0
0.2
0.4
0.6
0.8
1
1.2
Time (sec)
bar 4

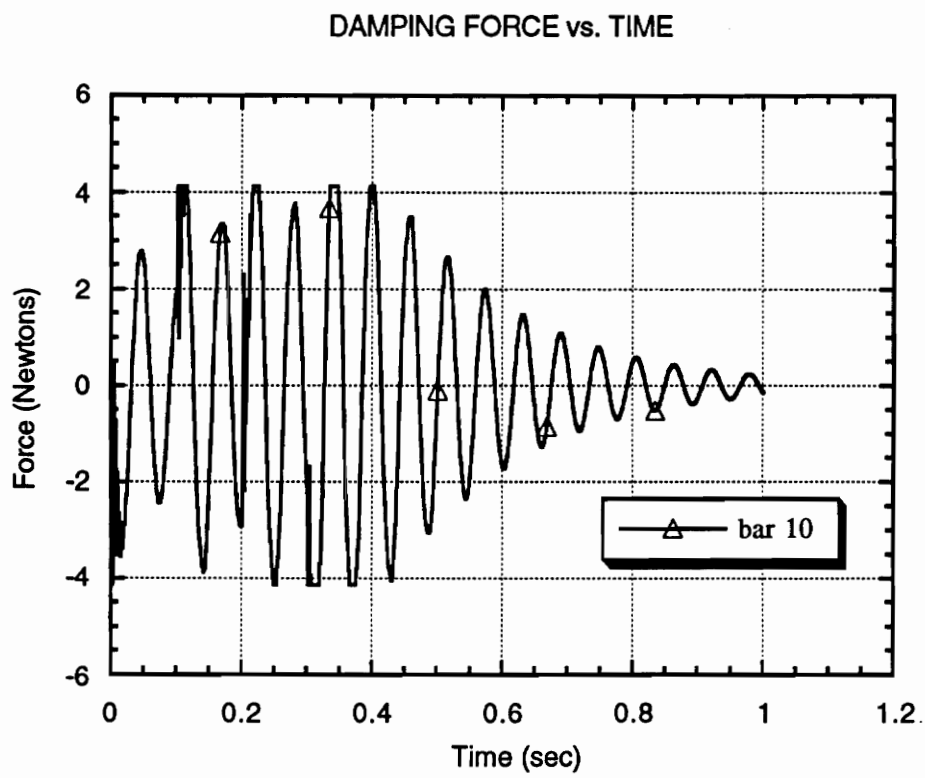
DAMPING FORCE vs. TIME
Force (Newtons)
6
4
2
0
-2
-4
-6
0
0.2
0.4
0.6
0.8
1
1.2
Time (sec)
bar 10

Figure 4.7

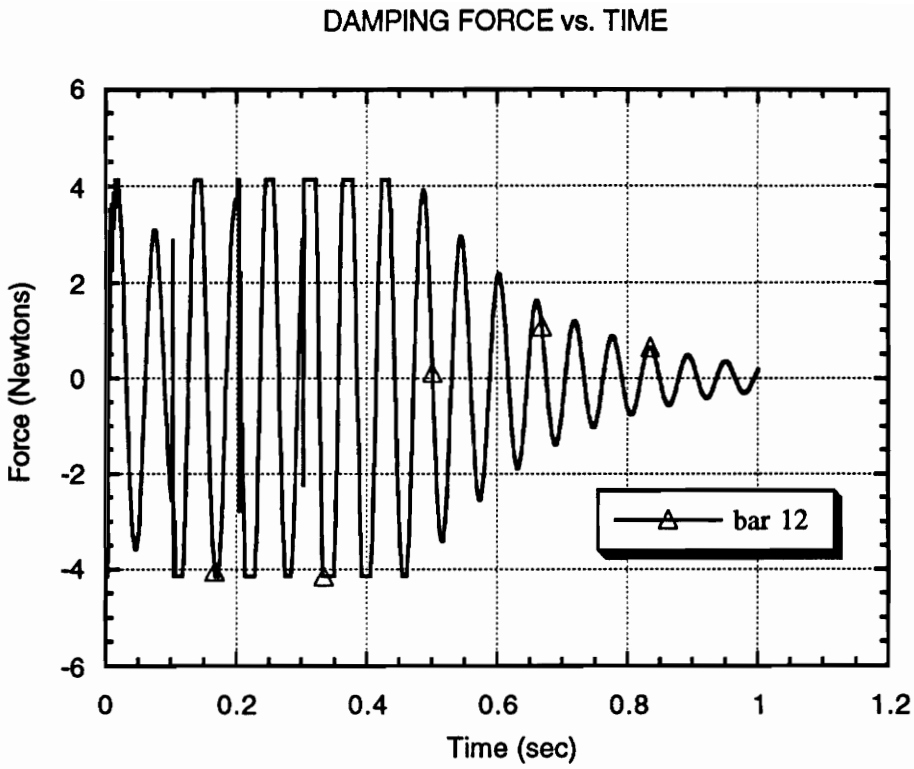
DAMPING FORCE vs. TIME
Force (Newtons)
6
4
2
0
-2
-4
-6
0
0.2
0.4
0.6
0.8
1
1.2
Time (sec)
bar 12

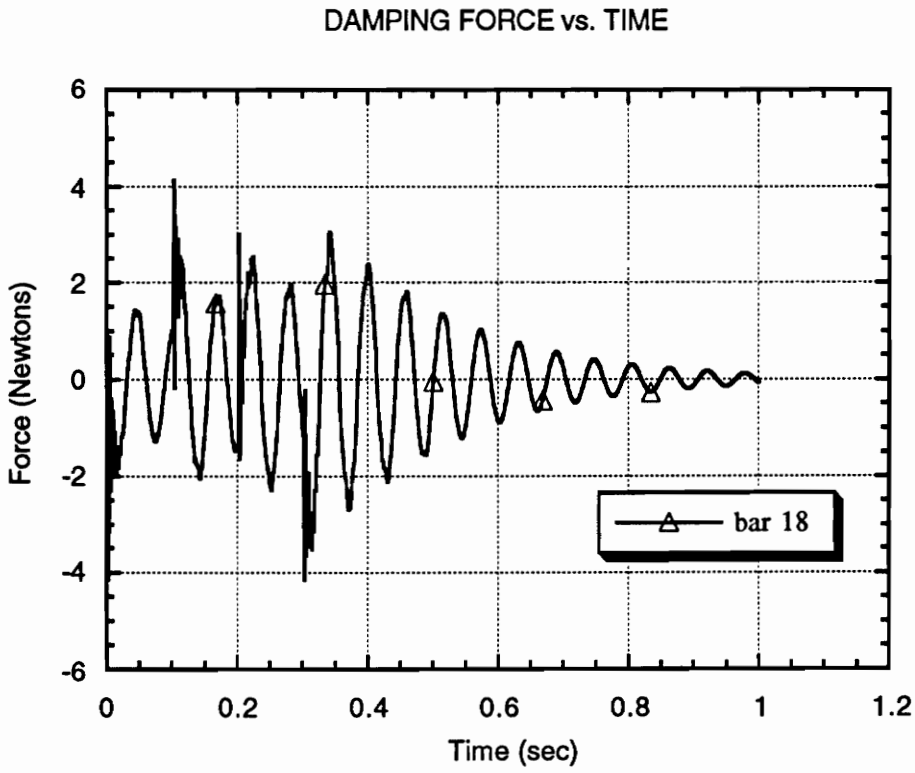
DAMPING FORCE vs. TIME
Force (Newtons)
6
4
2
0
-2
-4
-6
0
0.2
0.4
0.6
0.8
1
1.2
Time (sec)
bar 18

Figure 4.8

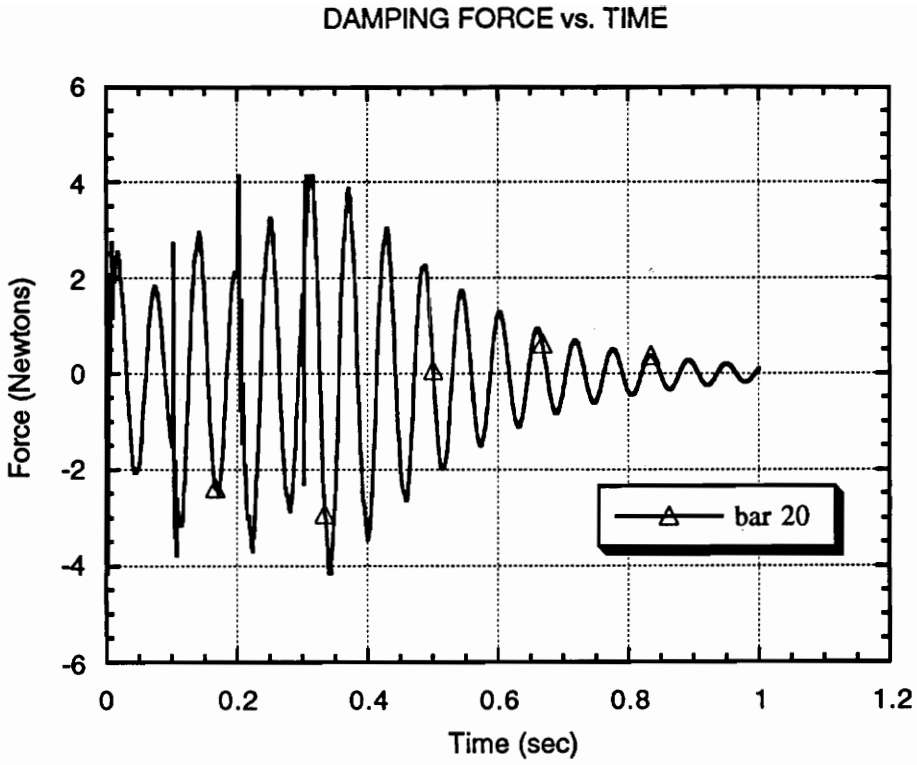
DAMPING FORCE vs. TIME
Force (Newtons)
6
4
2
0
-2
-4
-6
0
0.2
0.4
0.6
0.8
1
1.2
Time (sec)
bar 20

Figure 4.9

This is evident in the figures. It is also worth noting that the actuators were utilized based upon location. For example, the forces generated by bar 3 are on the whole much smaller in magnitude than those generated in other bars. Excluding bar 3, which is a diagonal, the bars at the base generated higher damping forces than the bars above. This makes sense because for the first mode of vibration, strains are largest at the base and this particular type of actuator is most effectively placed in such areas since it responds according to a change in length of the member. For this reason, damping forces generated in bar 3 are much smaller than those generated in other bars. Dampers placed in horizontal positions would produce zero damping.

CHAPTER 5

Conclusions

5.1 Main Results from Thesis

The subject matter for this thesis can be given under two main headings. First, the development of analytical and finite element solutions by which a thorough static analysis is given of an axisymmetric composite cylinder under loadings due to embedded piezoelectric laminae; and second, applications.

In the development portion of this study, piezoelectric concepts have been given in such a way that they may be applied for any problem type. Using these concepts, a thorough formulation of the analytical and finite element solutions have been presented. The analytical solution includes shear deformations and may also be applied to problems for which non-uniform thermal gradients are present along the axis of the cylinder. It may also be used for cases in which external shear and normal stresses are applied on inner and outer cylinder surfaces. The finite element formulation may also be applied to all these cases.

Several applications of the aforementioned analytical tools were given. A cylindrical truss element actuator was developed and various cases were studied to determine optimal ply orientations. This actuator was shown to transmit axial forces to the boundaries via PVDF layers themselves. It was then applied to dampen the vibrations of a truss structure under realistic loading conditions and shown to be very effective for this use. From this analysis, it was indicated that this type of actuator works more efficiently in certain locations of the truss and not only damps transient

vibrations, but also reduces the maximum amplitude of motion during transient loadings.

Another type of actuator was also developed. It was shown that by spatially varying the piezoelectric effect, modal actuators, capable of exciting modes of axial vibrations in a bar could be made. A suitable polarization profile for such an actuator was proposed for the first mode.

The final application for the analysis tools was a study of the effects of a polarization patch. The mechanism by which axial forces are transmitted to the boundaries was investigated and shown to be different from that for the cylindrical truss element actuator. In the case of the polarization patch, forces are transmitted to the boundaries via passive laminae and are proportional to the length of patch. This was investigated and shown to be attributable to the non-uniformity of the piezoelectric effect. From this non-uniformity, it follows that shear stresses must be introduced. A formula was given based upon the equilibrium conditions for an outer laminae and used to show why axial forces must be present when interlaminae shear stresses are present. For cases such as this, the analytical solution indicates that displacements through the thickness of piezoelectric layers are of quadratic and higher orders.

5.2 Continuation of Research

The research presented in this thesis may be extended by including more general loadings and by more extensive studies using the analysis tools developed.

The analytical solution presented for the composite cylinder may be used to solve combined problems for which there are mechanical, thermal and piezoelectric loadings present. It may also be extended to include thermal gradients which vary in the radial direction, in which case, a different power series solution for the right hand side of the governing equations would be obtained. A larger extension would be to attempt a power series solution for cylinders which are not axisymmetric. This would involve solving the fully 3D elasticity equations.

Another extension to this work would involve using a reciprocal relationship that exists between sensors and actuators. In this case, strains and strain rates may be sensed by measuring charge built up on piezoelectric laminae. Based upon this information, practical applications of the actuators developed here would be physically realizable. In this case, so called collocated sensors and actuators would be possible, yielding very attractive properties for vibration control. Another possibility for such sensors would be in monitoring a system for damages.

The equations of motion developed for the truss also represent a rich source for continued research. Similar equations may be derived for a 3D space truss and the non-autonomous nature of these equations could be investigated to determine the influence of angular velocity and acceleration on the response. Control algorithms and optimal placement of actuators could be studied. Very large space structures could be studied and additional effects could be included such as: thermal loadings, low earth orbits for which additional terms in the potential energy would be required,

mechanical loadings due to motion of attached rigid bodies, and nonlinear terms due to large motions.

Bibliography

1. W. P. Mason, "Piezoelectricity, its history and applications," *J. Acoust. Soc. Am.*, 70(6), Dec. 1981, pp. 1561-1566.

2. H. Kawai, "The Piezoelectricity of Poly (Vinylidene Fluoride)," *Jpn. J. Appl. Phys.*, 8, pp. 975-976, 1979.

3. G. M. Sessler, "Piezoelectricity in polyvinylidenefluoride," *J. Acoust. Soc. Am.*, 70(6), Dec. 1981, pp. 1596-1608.

4. D. Frederick, T. S. Chang, *Continuum Mechanics*, Cambridge, Mass., 1965.

5. Robert M. Jones, *Mechanics of Composite Materials*, Hemisphere Publishing Corporation, 1975.

6. J. F. Nye, *Physical Properties of Crystals*, Oxford University Press, 1985.

7. C. K. Lee, "Theory of laminated piezoelectric plates for the design of distributed sensors/actuators, Part I: governing equations and reciprocal relationships," *J. Acoust. Soc. Am.*, 87(3), March 1990, pp. 1144-1158.

8. C. K. Lee, and F. C. Moon, "Modal sensors and actuators," *Transactions of the ASME*, Vol. 57, June 1990, pp. 434-441.

9. T. Baily and J. E. Hubbard Jr., "Distributed Piezoelectric-Polymer Active Vibration Control of a Cantilever Beam," *J. Guid. Control*, 8(5), 1985, pp. 605-611.

10. R. G. Kepler and R. A. Anderson, "Piezoelectricity and pyroelectricity in polyvinylidene fluoride," *J. Appl. Phys.*, 49(8), August 1978, pp. 4490-4494.

11. M. Tamura, S. Hagiwara, and S. Matsumoto, "Some aspects of piezoelectricity and pryoelectricity in uniaxially stretched poly(vinylidene flouride)," *Journal of Applied Physics*, Vol. 48, No. 2, Feb. 1977, pp. 513-521.

12. S. P. Timoshenko and J. N. Goodier, *Theory of Elasticity*, Third Edition, McGraw-Hill, 1951.

13. W. E. Boyce and R. C. Diprima, *Elementary Differential Equations and Boundary Value Problems*, Fourth Edition, John Wiley & Sons, 1986.

14. J. N. Reddy, *An Introduction to the Finite Element Method*, McGraw-Hill Book Company, 1984.

15. Leonard Meirovitch, "Control of Distributed Structures,"Springer Series in Computational Mechanics, Large Space Structures: Dynamics and Control, Springer-Verlag Berlin Heidelberg, 1988.

16. Leonard Meirovitch, *Elements of Vibration Analysis*, McGraw Hill Book Company, 1986.

17. J. L. Fanson, and J. A. Garba, "Experimental Studies of Active Members in Control of Large Space Structures," AIAA Paper No. 88-2207, 1988.

18. Mark S. Derstine, Marek-Jerzy Pindera, and David E. Bowles, "Combined Mechanical Loading of Composite Tubes," *Center for Composite Materials and Structures*, CCMS-88-11, Virginia Tech, June, 1988.

19. Peter V. O'Neil, *Advanced Engineering Mathematics*, Second Edition, Wadsworth Publishing Company, 1987.

20. A. W. Babister, *Transcendental Functions Satisfying Nonhomogeneous Linear Differential Equations*, The Macmillan Company, 1967, pp. 16-17.

21. J. N. Reddy, *An Introduction to the Finite Element Method*, McGraw-Hill Book Company, New York, Second Edition, 1992.

22. E. F. Crawley, and J. de Luis, "Use of Piezoelectric Actuators as Elements of Intelligent Structures," *AIAA Journal*, Vol. 25, No. 10, October, 1987, pp. 1373-1385.

Vita

John Anthony Mitchell was born in California on April 16, 1963. He grew up in Alaska and graduated from High School there in 1981. After working for two years, he went to Texas A & M University for undergraduate studies. He graduated from Texas A & M University with a Bachelor of Science degree in Ocean Engineering in December 1987. Then Mr. Mitchell worked in Houston, Texas for two years, for Noble, Denton and Associates Inc., an offshore engineering consulting firm. In January 1990, Mr. Mitchell came to Virginia Polytechnic Institute and State University, to pursue graduate studies. He graduated in July 1992, with a Master of Science degree in Engineering Mechanics. His areas of research were smart structures, dynamics and control. In September 1992, he plans to continue his research at Texas A & M University and pursue studies towards a Doctor of Philosophy degree in Mechanical Engineering.